HAL
open science

Interactive chemistry in the Laboratoire de Météorologie Dynamique general circulation model: model description and impact analysis of biogenic hydrocarbons on tropospheric chemistry

G. A. Folberth, D. A. Hauglustaine, J. Lathière, F. Brocheton

To cite this version:

G. A. Folberth, D. A. Hauglustaine, J. Lathière, F. Brocheton. Interactive chemistry in the Laboratoire de Météorologie Dynamique general circulation model: model description and impact analysis of biogenic hydrocarbons on tropospheric chemistry. Atmospheric Chemistry and Physics, 2006, 6 (8), pp.2273-2319. 10.5194/acp-6-2273-2006 . hal-00328444

HAL Id: hal-00328444

https://hal.science/hal-00328444v1

Submitted on 18 Jun 2008

HAL is a multi-disciplinary open access archive for the deposit and dissemination of scientific research documents, whether they are published or not. The documents may come from teaching and research institutions in France or abroad, or from public or private research centers.

L'archive ouverte pluridisciplinaire **HAL**, est destinée au dépôt et à la diffusion de documents scientifiques de niveau recherche, publiés ou non, émanant des établissements d'enseignement et de recherche français ou étrangers, des laboratoires publics ou privés.

Atmos. Chem. Phys., 6, 2273–2319, 2006
www.atmos-chem-phys.net/6/2273/2006/
© Author(s) 2006. This work is licensed
under a Creative Commons License.

Atmospheric Chemistry and Physics

Interactive chemistry in the Laboratoire de Météorologie Dynamique general circulation model: model description and impact analysis of biogenic hydrocarbons on tropospheric chemistry

G. A. Folberth[1,*], D. A. Hauglustaine[1], J. Lathière[1], and F. Brocheton[2]

[1]Laboratoire des Sciences du Climat et de l'Environnement (LSCE), Gif-sur-Yvette, France
[2]Centre National de Recherches Météorologiques (CNRM), Météo France, Toulouse, France
[*]now at: School of Earth and Ocean Science (SEOS), University of Victoria, Victoria, Canada

Received: 8 July 2005 – Published in Atmos. Chem. Phys. Discuss.: 25 October 2005
Revised: 10 February 2006 – Accepted: 28 February 2006 – Published: 21 June 2006

Abstract. We present a description and evaluation of LMDz-INCA, a global three-dimensional chemistry-climate model, pertaining to its recently developed NMHC version. In this substantially extended version of the model a comprehensive representation of the photochemistry of non-methane hydrocarbons (NMHC) and volatile organic compounds (VOC) from biogenic, anthropogenic, and biomass-burning sources has been included. The tropospheric annual mean methane (9.2 years) and methylchloroform (5.5 years) chemical lifetimes are well within the range of previous modelling studies and are in excellent agreement with estimates established by means of global observations. The model provides a reasonable simulation of the horizontal and vertical distribution and seasonal cycle of CO and key non-methane VOC, such as acetone, methanol, and formaldehyde as compared to observational data from several ground stations and aircraft campaigns. LMDz-INCA in the NMHC version reproduces tropospheric ozone concentrations fairly well throughout most of the troposphere. The model is applied in several sensitivity studies of the biosphere-atmosphere photochemical feedback. The impact of surface emissions of isoprene, acetone, and methanol is studied. These experiments show a substantial impact of isoprene on tropospheric ozone and carbon monoxide concentrations revealing an increase in surface O_3 and CO levels of up to 30 ppbv and 60 ppbv, respectively. Isoprene also appears to significantly impact the global OH distribution resulting in a decrease of the global mean tropospheric OH concentration by approximately 0.7×10^5 molecules cm^{-3} or roughly 8% and an increase in the global mean tropospheric methane lifetime by approximately seven months. A global mean ozone net radiative forcing due to the isoprene induced increase in the tropospheric ozone burden of 0.09 W m^{-2} is found. The key role of isoprene photooxidation in the global tropospheric redistribution of NO_x is demonstrated. LMDz-INCA calculates an increase of PAN surface mixing ratios ranging from 75 to 750 pptv and 10 to 250 pptv during northern hemispheric summer and winter, respectively. Acetone and methanol are found to play a significant role in the upper troposphere/lower stratosphere (UT/LS) budget of peroxy radicals. Calculations with LMDz-INCA show an increase in HO_x concentrations region of 8 to 15% and 10 to 15% due to methanol and acetone biogenic surface emissions, respectively. The model has been used to estimate the global tropospheric CO budget. A global CO source of 3019 Tg CO yr^{-1} is estimated. This source divides into a primary source of 1533 Tg CO yr^{-1} and secondary source of 1489 Tg CO yr^{-1} deriving from VOC photooxidation. Global VOC-to-CO conversion efficiencies of 90% for methane and between 20 and 45% for individual VOC are calculated by LMDz-INCA.

Correspondence to: G. A. Folberth
(gerd.folberth@ec.gc.ca)

1 Introduction

Non-Methane volatile organic compounds (NMVOC) are known to affect the chemical composition of the atmosphere decisively. NMVOC play a key role in the sequestration of nitrogen oxides (NO_x) via the formation of organic nitrates (e.g., PAN and analogs), can directly or indirectly increase the acidity of precipitation, and provide the starting material for much of the natural atmospheric aerosols. They have been found to significantly contribute to the production of pollutants and are of major concern in the assessment and controlling strategies of present-day and future air quality (e.g. Graedel, 1979; Brasseur and Chatfield, 1991; Crutzen and Zimmermann, 1991; Fehsenfeld et al., 1992; Andreae,

1995; Crutzen, 1995; Andreae and Crutzen, 1997; Berntsen et al., 1997; Levy II et al., 1997; Wang et al., 1998c; Granier et al., 2000; Hauglustaine and Brasseur, 2001). But most important, NMVOC play a central role in tropospheric ozone formation.

Ozone is a key component in the atmosphere. It is an effective oxidant and greenhouse gas, especially in the upper troposphere (Lacis et al., 1990; Hauglustaine et al., 1994). In addition, near the surface ozone can have detrimental effects on the vegetation and on human health (Fishman, 1991; Finlaysonpitts and Pitts, 1993; Taylor, 2001; Bernard et al., 2001). Ozone photolysis by ultraviolet radiation is the primary source of hydroxyl radicals in the troposphere. Photochemical oxidation of NMVOC, on the other hand, is primarily initiated and, hence, controlled by reaction with OH. This reaction determines the magnitude and distribution of hydroxyl radical concentrations, thereby altering the oxidative capacity of the troposphere (Houweling et al., 1998; Wang et al., 1998c; Poisson et al., 2000).

The direct radiative forcing due to NMVOC has been found to be negligibly small. An upper limit to the global mean anthropogenic forcing of 0.015 $W\,m^{-2}$ has been established by Highwood et al. (1999). Collins et al. (2002), on the other hand, have presented a study, which convincingly demonstrates that NMVOC are able to exert a substantial indirect effect on greenhouse warming by affecting ozone formation and the methane lifetime toward reaction with OH. Moreover, the formation of secondary organic aerosols (SOA) in the course of photochemical NMVOC oxidation is believed to have a direct and indirect effect on the radiative flux of the lower atmosphere (Kanakidou et al., 2000; Tsigaridis and Kanakidou, 2003).

NMVOC primarily originate from three principle sources: anthropogenic activities, biomass burning, and the biosphere. The biosphere acts as the largest source of reactive trace gases in the troposphere. It has been suggested that the biogenic source on the global scale surpasses several times the combined NMVOC emission flux originating from anthropogenic and biomass burning sources. State-of-the-art emission estimates include an annual global BVOC source of approximately 750 $Tg\,C\,yr^{-1}$ (Guenther et al., 1995) whereas the anthropogenic and biomass burning sources together amount to roughly 90 $Tg\,C\,yr^{-1}$ of NMVOC (Hao and Liu, 1994; Olivier et al., 1996; Olivier and Berdowski, 2001; Olivier et al., 2001; Van der Werf et al., 2003).

Biogenic volatile organic compounds (BVOC) include isoprene and isoprenoid compounds (such as monoterpenes and higher terpenes) as well as a large number of other species from the groups of alkanes, non-isoprenoid alkenes, carbonyls, alcohols, and organic acids. They are emitted into the atmosphere from natural sources in terrestrial and marine ecosystems. In terms of abundance and importance the predominant BVOC are isoprene and terpenes, methanol, and acetone (Bonsang et al., 1992; MacDonald and Fall, 1993; Sharkey and Singsaas, 1995; Kirstine et al., 1998; Bonsang and Boissard, 1999; Doskey and Gao, 1999; Guenther et al., 2000; Singh et al., 2000; Galbally and Kirstine, 2002; Jacob et al., 2002).

An increasing importance of isoprene (Shallcross and Monks, 2000; Sanderson et al., 2003) and other BVOC (Guenther et al., 1999; Kellomaki et al., 2001; Lathière et al., 2005a; Hauglustaine et al., 2005) in the future has been hypothesized due to an increasing net primary production associated with a warmer climate (Constable et al., 1999). If global patterns and magnitudes of biogenic VOC emissions change in correlation with climate-related alterations in temperature, precipitation, and solar insolation, in turn a feed back upon the climate via changes in the accumulation rate of atmospheric greenhouse gases seems very likely.

Hauglustaine et al. (2004) recently presented the global climate-chemistry model LMDz-INCA, which takes into account the CH_4–NO_x–CO–O_3 chemistry of the background troposphere. This model has been supplemented by a detailed non-methane hydrocarbon scheme in order to investigate biosphere-atmosphere interactions. This work represents a further step in the framework of several ongoing studies (Boucher et al., 2002; Hauglustaine et al., 2004; Bauer et al., 2004), which eventually will converge toward a modelling system that takes into account the "complete" chemistry of the troposphere and stratosphere, including the different types of aerosols, in a fully interactive Earth System Model.

In this work we present the non-methane hydrocarbon version of INCA (version NMHC.1.0). A description and general evaluation of this new model version is provided. The more general application abilities are than used to investigate various aspects of biosphere NMVOC emissions and tropospheric chemical composition including ozone formation, tropospheric HO_x, and possible impacts on future climate.

2 Model description

2.1 The LMDz General Circulation Model

LMDz (**L**aboratoire de **M**étéorologie **D**ynamique, **z**oom) is a grid point General Circulation Model (GCM) developed initially for climate studies by Sadourny and Laval (1984). As part of the IPSL Earth System Model, the GCM lately has undergone a major recoding and has been applied in climate feedback studies by Friedlingstein et al. (2001) and Dufresne et al. (2002).

In LMDz the finite volume transport scheme of Van Leer (1977) as described in Hourdin and Armengaud (1999) is used to calculate large-scale advection of tracers. The parameterization of deep convection is based on the scheme of Tiedtke (1989); a local second-order closure formalism is used to describe turbulent mixing in the planetary boundary layer (PBL).

Table 1. Chemical species in LMDz-INCA.

#	tracer	family[a]	description	ch.[b]	a/c[c]	em.[d]	d.d.[e]	w.s.[f]	τ[g]
1	O_x	O_3+O(^{1}D)+O(^{3}P)	odd oxygen (ozone and atomic oxygen)	•	•	–	•	–	s
2	O_3I	single	inert ozone[h]	–	•	–	•	–	l
3	O_3S	single	stratospheric ozone[i]	–	•	–	•	–	l
4	N	single	nitrogen radical	•	–	–	–	–	s
5	N_2O	single	nitrous oxide	•	•	•	–	–	l
6	NO	single	nitric oxide	•	•	•[j]	•	–	s
7	NO_2	single	nitrogen dioxide	•	•	–	•	–	s
8	NO_3	single	nitrate radical	•	•	–	•	–	s
9	N_2O_5	single	nitrogen pentoxide	•	•	–	•	–	s
10	HNO_2	single	nitrous acid	•	•	–	•	•	s
11	HNO_3	single	nitric acid	•	•	–	•	•	s
12	HNO_4	single	peroxynitric acid	•	•	–	•	•	s
13	H	single	hydrogen radical	•	–	–	–	–	s
14	H_2	single	molecular hydrogen	•	•	•	•	–	l
15	H_2O	single	water vapor	•	•	–	–	–	s
16	OH	single	hydroxyl radical	•	–	–	•	–	s
17	HO_2	single	hydroperoxy radical	•	–	–	•	–	s
18	H_2O_2	single	hydrogen peroxide	•	•	–	•	•	s
19	CH_4	single	methane	•	•	•	–	–	l
20	CH_3O_2	single	methyl peroxy radical	•	–	–	–	–	s
21	CH_3O	single	methoxy radical	•	–	–	–	–	s
22	CH_3OOH	single	methyl hydroperoxide	•	•	–	•	•	s
23	CH_3OH	single	methanol	•	•	•	•	•	s
24	CH_2O	single	formaldehyde	•	•	–	•	•	s
25	CO	single	carbon oxide	•	•	•	•	–	l
26	CO2FF	single	carbon dioxide[k] (inert tracer)	–	•	•	–	–	l
27	C_2H_6	single	ethane	•	•	•	•	–	s
28	$C_2H_5O_2$	single	ethyl peroxy radical	•	–	–	–	–	s
29	C_2H_5OH	single	ethanol and higher alcohols	•	•	–	•	•	s
30	C_2H_5OOH	single	ethyl hydroperoxide	•	•	–	•	•	s
31	CH_3CHO	single	acetaldehyde	•	•	–	•	•	s
32	CH_3CO_3	single	peroxy acetyl radical	•	–	–	–	–	s
33	CH_3COOH	single	acetic acid and higher organic acids	•	•	–	•	•	s
34	$CH_3C(O)OOH$	single	paracetic acid	•	•	–	•	•	s
35	C_3H_8	single	propane	•	•	•	•	–	s
36	$C_3H_7O_2$	single	propyl peroxy radical	•	–	–	–	–	s
37	C_3H_7OOH	single	propyl hydroperoxide	•	•	–	•	•	s
38	CH_3COCH_3	single	acetone	•	•	•	•	•	s
39	PROPAO2	single	$CH_3COCH_2O_2$	•	–	–	–	–	s
40	PROPAOOH	single	CH_3COCH_2OOH	•	•	–	•	•	s
41	CH_3COCHO	single	methylglyoxal	•	•	–	•	•	s
42	ALKAN	single	C_4- and higher alkanes	•	•	•	–	–	s
43	ALKANO2	single	C_4- and higher alkanyl peroxy radicals	•	•	–	–	–	s
44	ALKANOOH	single	C_4- and higher alkanyl hydroperoxides	•	•	–	•	•	s
45	MEK	single	methyl ethyl ketone ($CH_3CH_2COCH_3$)	•	•	•	•	•	s
46	MEKO2	single	peroxy radical from MEK	•	–	–	–	–	s
47	MEKOOH	single	hydroperoxide from MEK	•	•	–	•	•	s
48	C_2H_4	single	ethene	•	•	•	•	–	s
49	C_3H_6	single	propene	•	•	•	•	–	s
50	PROPEO2	single	hydroxy propyl peroxy radical	•	–	–	–	–	s
51	PROPEOOH	single	hydroxy propyl hydroperoxide	•	•	–	•	•	s
52	C_2H_2	single	ethine	•	•	•	•	–	s
53	ALKEN	single	C_4- and higher alkenes	•	•	•	–	–	s
54	ALKENO2	single	C_4- and higher alkenyl peroxy radicals	•	–	–	–	–	s
55	ALKENOOH	single	C_4- and higher alkenyl hydroperoxides	•	•	–	•	•	s
56	AROM	single	aromatic compounds	•	•	•	–	–	s
57	AROMO2	single	peroxy radicals from AROM	•	–	–	–	–	s
58	AROMOOH	single	hydroperoxides from AROM	•	•	–	•	•	s

Table 1. Continued.

#	tracer	family[a]	description	ch.[b]	a/c[c]	em.[d]	d.d.[e]	w.s.[f]	τ[g]
59	ISOP	single	isoprene	•	•	•	•	–	s
60	ISOPO2	single	peroxy radical from isoprene	•	–	–	–	–	s
61	ISOPNO3	single	nitrate radical adduction to isoprene	•	–	–	–	–	s
62	MVK	single	methyl vinyl ketone ($CH_2CHCOCH_3$)	•	•	•	•	•	s
63	MACR	single	methacrolein (CH_2CCH_3CHO)	•	•	–	•	–	s
64	MACRO2	single	peroxy radical from methacrolein	•	–	–	–	–	s
65	MACROOH	single	hydroperoxide from methacrolein	•	•	–	•	•	s
66	MACO3	single	carboxy radical from methacrolein	•	–	–	–	–	s
67	APIN	single	α-pinene and other terpenes	•	•	•	•	–	s
68	APINO2	single	peroxy radicals from APIN	•	–	–	–	–	s
69	APINO3	single	ozone adduction to terpenes	•	–	–	–	–	s
70	PCHO	single	aldehydes from APIN	•	•	–	•	•	s
71	PCO3	single	carboxy radicals from APIN	•	–	–	–	–	s
72	ONITU	single	unreactive organic nitrates	•	•	–	•	•	s
73	ONITUO2	single	peroxy radicals from ONITU + OH	•	–	–	–	–	s
74	ONITR	single	reactive organic nitrates	•	•	–	•	•	s
75	PAN	single	peroxy acetyl nitrate	•	•	–	•	•	s
76	MPAN	single	PAN analog from MACR	•	•	–	•	–	s
77	APINPAN	single	PAN analog from APIN	•	•	–	•	–	s
78	PCO3PAN	single	PAN analog from PCHO	•	•	–	•	–	s
79	XO2	single	counter for organic peroxy radicals	•	–	–	–	–	s
80	XOOH	single	counter for organic hydroperoxides	•	•	–	•	•	s
81	MCF	single	methyl chloroform (CH_3CCl_3)	•	•	•	–	–	l
82	^{222}Rn	single	radon	•	•	•	–	–	l
83	^{210}Pb	single	lead	•	•	–	•	•	l

[a] used only in transport [b] Species is subject to chemistry [c] Species is subject to advection/convection [d] Species has a surface source [e] Species is subject to dry deposition [f] Species is subject to wet scavenging [g] s: short-lived, l: long-lived [h] not subject to O_3 photochemistry [i] marker for stratospheric O_3 intrusion [j] NO_x is emitted as NO [k] Fossil fuel combustion

Table 2. Photolysis reactions in LMDz-INCA.

#	reaction			refs.
j1	$O_2 + h\nu$	$\rightarrow$	$2 * O(^3P)$	1
j2	$O_3 + h\nu$	$\rightarrow$	$O(^1D) + O_2$	1
j3	$O_3 + h\nu$	$\rightarrow$	$O(^3P) + O_2$	1
j4	$H_2 + h\nu$	$\rightarrow$	$OH + H$	1
j5	$HO_2 + h\nu$	$\rightarrow$	$2 * OH$	1
j6	$NO + h\nu$	$\rightarrow$	$O(^3P) + N$	2
j7	$NO_2 + h\nu$	$\rightarrow$	$NO + O(^3P)$	1
j8	$NO_3 + h\nu$	$\rightarrow$	$NO + O_2$	1
j9	$NO_3 + h\nu$	$\rightarrow$	$NO_2 + O(^3P)$	1
j10	$N_2O + h\nu$	$\rightarrow$	$O(^1D) + N_2$	1
j11	$N_2O_5 + h\nu$	$\rightarrow$	$NO_2 + NO_3$	1
j12	$HNO_2 + h\nu$	$\rightarrow$	$NO + OH$	1
j13	$HNO_3 + h\nu$	$\rightarrow$	$NO_2 + OH$	1
j14	$HNO_4 + h\nu$	$\rightarrow$	$NO_2 + HO_2$	1
j15	$CH_3OOH + h\nu$	$\rightarrow$	$CH_2O + OH + H$	1
j16	$CH_2O + h\nu$	$\rightarrow$	$CO + 2 * H$	1
j17	$CH_2O + h\nu$	$\rightarrow$	$CO + H_2$	1
j18	$CH_3CHO + h\nu$	$\rightarrow$	$CH_3O_2 + CO + HO_2$	1
j19	$MACR + h\nu$	$\rightarrow$	$0.67 * HO_2 + 0.33 * MCO3 + 0.67 * CH_2O + 0.67 * CO + 0.67 * CH_3CO_3 + 0.33 * OH$	1
j20	$PCHO + h\nu$	$\rightarrow$	$HO_2 + CO + XO2$	3
j21	$CH_3COCH_3 + h\nu$	$\rightarrow$	$CH_3CO_3 + CH_3O_2$	1
j22	$CH_3COCHO + h\nu$	$\rightarrow$	$CH_3CO_3 + CO + HO_2$	1
j23	$MEK + h\nu$	$\rightarrow$	$CH_3CO_3 + C_2H_5O_2$	4
j24	$MVK + h\nu$	$\rightarrow$	$0.3 * CH_3CO_3 + 0.7 * C_3H_6 + 0.7 * CO + 0.3 * CH_3O_2$	1
j25	$ONITU + h\nu$	$\rightarrow$	$NO_2 + 0.512 * MEK + 0.33 * CH_3COCH_3 + 0.346 * C_2H_5O_2 + 0.653 * HO_2$	8
j26	$ONITR + h\nu$	$\rightarrow$	$HO_2 + CO + NO_2 + CH_2O$	3
j27	$PAN + h\nu$	$\rightarrow$	$CH_3CO_3 + NO_2$	1
j28	$MPAN + h\nu$	$\rightarrow$	$MCO2 + NO_2$	5
j29	$APINPAN + h\nu$	$\rightarrow$	$APINO3 + NO_2$	5
j30	$PCO3PAN + h\nu$	$\rightarrow$	$PCO3 + NO_2$	5
j31	$CH_3C(O)OOH + h\nu$	$\rightarrow$	$CH_3O_2 + OH + CO_2$	7
j32	$C_2H_5OOH + h\nu$	$\rightarrow$	$CH_3CHO + HO_2 + OH$	6
j33	$C_3H_7OOH + h\nu$	$\rightarrow$	$0.218 * CH_3CHO + OH + HO_2 + 0.782 * CH_3COCH_3$	6
j34	$PROPAOOH + h\nu$	$\rightarrow$	$CH_2O + CH_3CO_3 + OH$	6
j35	$PROPEOOH + h\nu$	$\rightarrow$	$CH_3CHO + CH_2O + HO_2 + OH$	6
j36	$ALKANOOH + h\nu$	$\rightarrow$	$0.562 * HO_2 + 0.334 * XO2 + 0.358 * CH_3COCH_2 + OH + 0.514 * MEK + 0.006 * CH_2O + 0.454 * CH_3CHO + 0.1 * CH_3O_2$	6
j37	$ALKENOOH + h\nu$	$\rightarrow$	$OH + HO_2 + 0.165 * CH_2O + 0.68 * CH_3CHO + 0.155 * CH_3COCH_3$	6
j38	$AROMOOH + h\nu$	$\rightarrow$	$OH + 0.423 * CH_3COCH_3 + 1.658 * HO_2 + 0.658 * CO + 0.658 * CH_3CO_3$	6
j39	$MACROOH + h\nu$	$\rightarrow$	$OH + 0.84 * CO + HO_2 + 0.16 * CH_2O + CH_3COCHO$	6
j40	$MACROOH + h\nu$	$\rightarrow$	$1.16 + HO_2 + CO + 0.84 * OH + 0.84 * CH_3COCHO + 0.16 * PROPAOOH$	3
j41	$MEKOOH + h\nu$	$\rightarrow$	$OH + 0.93 * CH_3CHO + 0.6 * CH_3CO_3 + 0.07 * CH_2O + 0.2 * MEK$	6
j42	$XOOH + h\nu$	$\rightarrow$	OH	6
j43	$MCF + h\nu$	$\rightarrow$	(no products considered)	1

references:
1, Madronich and Flocke (1998); 2, Brasseur and Solomon (1987)
3, J=J(CH_3CHO); 4, J=1.7×J(CH_3COCH_3)
5, J=J(PAN); 6, J=J(CH_3OOH); 7, J=0.28×J(H_2O_2)
8, J(ONITU)=J(CH_3ONO_2)

Table 3. Heterogenous reactions included in LMDz-INCA.

#	Reaction	Reaction probability
h1	$N_2O_5 \rightarrow 2\ HNO_3$	$\gamma_{200K} = 0.185$, $\gamma_{300K} = 0.03$
h2	$NO_3 \rightarrow HNO_3$	$\gamma = 0.1$
h3	$NO_2 \rightarrow 0.5\ HNO_3 + 0.5\ HNO_2$	$\gamma = 0.1$
h4	$HO_2 \rightarrow 0.5\ H_2O_2 + 0.5\ O_2$	$\gamma = 1.0\times 10^{-3}$

Table 4. Thermochemical reactions in LMDz-INCA.

#	reaction			rate coefficient	refs.
k1	$O(^3P)+O_2+M$	→	O_3+M	6.0×10^{-34} $(300/T)^{2.3}$	2
k2	$O(^3P)+O(^3P)+M$	→	O_2+M	4.23×10^{-28} $T^{-2.0}$	14,15
k3	$O(^3P)+O_3$	→	$2\ O_2$	8.0×10^{-12} exp(-2060/T)	1
k4	$O(^1D)+O_3$	→	$2\ O_2$	1.2×10^{-10}	2
k5	$O(^1D)+N_2$	→	$O(^3P)+N_2$	1.8×10^{-11} exp(107/T)	1
k6	$O(^1D)+O_2$	→	$O(^3P)+O_2$	3.2×10^{-11} exp(67/T)	1
k7	$O(^1D)+H_2O$	→	2 OH	2.2×10^{-10}	2
k8	$O(^1D)+H_2$	→	OH+H	1.1×10^{-10}	1,2
k9	$O(^1D)+N_2O$	→	2 NO	6.7×10^{-11}	2
k10	$O(^1D)+N_2O$	→	N_2+O_2	4.4×10^{-11}	1
k11	O_2+N	→	$NO+O(^3P)$	1.5×10^{-11} exp(-3600/T)	2
k12	O_2+H+M	→	HO_2+M	$k_0=5.69\times10^{-32}$ $(T/298)^{-1.6}$ $k_\infty=7.5\times10^{-11}$ $F_c=0.6$	2
k13	O_3+H	→	$OH+O_2$	1.0×10^{-10} exp(-367/T)	5
k14	$OH+O(^3P)$	→	$H+O_2$	2.2×10^{-11} exp(120/T)	2
k15	$OH+O_3$	→	HO_2+O_2	1.9×10^{-12} exp(-1000/T)	1
k16	$OH+H_2$	→	H_2O+H	5.5×10^{-12} exp(-2000/T)	2
k17	OH+OH	→	$H_2O+O(^3P)$	4.2×10^{-12} exp(-240/T)	2
k18	$OH+HO_2$	→	H_2O+O_2	4.8×10^{-11} exp(250/T)	1,2
k19	$OH+H_2O_2$	→	H_2O+HO_2	2.9×10^{-12} exp(-160/T)	1,2
k20	$OH+HNO_2$	→	H_2O+NO_2	1.8×10^{-11} exp(-390/T)	2
k21	$OH+HNO_3$	→	H_2O+NO_3	$k_1=7.2\times10^{-15}$ exp(785/T) $k_2=4.1\times10^{-16}$ exp(1440/T) $k_3=1.9\times10^{-33}$ exp(725/T) [M] $k = k_1 + \frac{k_3}{1+\frac{k_3}{k_2}}$	13
k22	$OH+HNO_4$	→	$H_2O+NO_2+O_2$	1.3×10^{-12} exp(380/T)	2
k23	$HO_2+O(^3P)$	→	$OH+O_2$	3.0×10^{-11} exp(200/T)	2
k24	HO_2+O_3	→	$OH+2\ O_2$	1.1×10^{-14} exp(-500/T)	2
k25	HO_2+H	→	2 OH	7.2×10^{-11}	1
k26	HO_2+H	→	H_2+O_2	5.6×10^{-12}	1
k27	HO_2+H	→	$H_2O+O(^3P)$	2.4×10^{-12}	1
k28	HO_2+HO_2	→	$H_2O_2+O_2$	$k_0=2.3\times10^{-13}$ (600/T) $k_\infty=1.7\times10^{-33}$ [M] exp(1000/T) $F_c=1.0+1.4\times10^{-21}$ $[H_2O]$ exp(2200/T) $k = (k_0 + k_\infty)\ F_c$	14,15
k29	$NO+O_3$	→	NO_2+O_2	1.8×10^{-12} exp(-1370/T)	1
k30	NO+OH+M	→	HNO_2+M	$k_0=7.01\times10^{-31}$ $(T/298)^{-2.6}$ $k_\infty=3.6\times10^{-11}$ $(T/298)^{-0.1}$ $F_c=0.6$	2
k31	$NO+HO_2$	→	NO_2+OH	3.5×10^{-12} exp(250/T)	2
k32	NO+N	→	$N_2+O(^3P)$	2.1×10^{-11} exp(100/T)	2
k33	$NO_2+O(^3P)$	→	$NO+O_2$	6.5×10^{-12} exp(120/T)	1,2
k34	$NO_2+O(^3P)+M$	→	NO_3+M	$k_0=9.0\times10^{-32}$ $(T/298)^{-2.0}$ $k_\infty=2.2\times10^{-11}$ $F_c=0.6$	2
k35	NO_2+O_3	→	NO_3+O_2	1.2×10^{-13} exp(-2450/T)	2
k36	NO_2+H	→	OH+NO	4.0×10^{-10} exp(-340/T)	2
k37	NO_2+OH+M	→	HNO_3+M	$k_0=2.6\times10^{-30}$ $(T/298)^{-2.9}$ $k_\infty=7.5\times10^{-11}$ $(T/298)^{-0.6}$ $F_c=0.6$	1
k38	NO_2+HO_2+M	→	HNO_4+M	$k_0=1.8\times10^{-31}$ $(T/298)^{-3.2}$ $k_\infty=4.7\times10^{-12}$ $(T/298)^{-1.4}$ $F_c=0.6$	13

Table 4. Continued.

#	reaction			rate coefficient	refs.
k39	HNO_4+M	→	NO_2+HO_2+M	k_0=1.8×10^{-31} (T/298)$^{-3.2}$ k_∞=4.7×10^{-12} (T/298)$^{-1.4}$ k_{inv}=2.1×10^{-27} exp(10900/T) F_c=0.6	13
k40	NO_2+NO_3+M	→	N_2O_5+M	k_0=2.0×10^{-30} (T/298)$^{-4.4}$ k_∞=1.4×10^{-12} (T/298)$^{-0.7}$ F_c=0.6	14,15
k41	N_2O_5+M	→	NO_2+NO_3+M	k_0=2.0×10^{-30} (T/298)$^{-4.4}$ k_∞=1.4×10^{-12} (T/298)$^{-0.7}$ k_{inv}=3.0×10^{-27} exp(10991/T) F_c=0.6	14,15
k42	NO_3+NO	→	2NO_2	1.8×10^{-11} exp(110/T)	1
k43	NO_3+HO_2	→	0.4HNO_3+0.6 OH+0.6NO_2	2.3×10^{-12} exp(170/T)	6
k44	CH_3CCl_3+OH	→	H_2O	1.8×10^{-12} exp(-1550/T)	2
k45	CH_4+OH	→	CH_3O_2+H_2O	2.45×10^{-12} exp(-1775/T)	2
k46	CH_4+O(^{1}D)	→	CH_3O_2+OH	2.25×10^{-10}	7
k47	CH_4+O(^{1}D)	→	CH_2O+H_2	1.65×10^{-11}	1,2,8
k48	CH_4+O(^{1}D)	→	CH3OH	4.98×10^{-11}	9
k49	CH_3O_2+NO	→	CH_3O+NO_2	3.0×10^{-12} exp(280/T)	2
k50	CH_3O_2+NO_3	→	CH_3O+NO_2+O_2	3.1×10^{-12}	10
k51	CH_3O_2+HO_2	→	CH_3OOH+O_2	3.8×10^{-13} exp(800/T)	1,2
k52	CH_3O_2+CH_3O_2	→	CH_3OH+CH_2O+O_2	1.5×10^{-13} exp(190/T)	2,11
k53	CH_3O_2+CH_3O_2	→	2CH_3O+O_2	1.0×10^{-13} exp(190/T)	2,11
k54	CH_3O+O_2	→	CH_2O+HO_2	3.9×10^{-14} exp(-900/T)	2
k55	CH_3O+NO_2	→	CH_2O+HNO_2	1.1×10^{-11} exp(-1200/T)	2
k56	CH_3OH+OH	→	CH_2O+HO_2+H_2O	3.1×10^{-12} exp(-360/T)	1
k57	CH_3OOH+OH	→	CH_2O+OH+H_2O	1.0×10^{-12} exp(190/T)	1
k58	CH_3OOH+OH	→	CH_3O_2+H_2O	1.9×10^{-12} exp(190/T)	1
k59	CH_2O+OH	→	CO+HO_2+H_2O	8.59×10^{-12} exp(20/T)	1
k60	CH_2O+NO_3	→	CO+HO_2+HNO_3	5.8×10^{-16}	1
k61	CH_2O+O(^{3}P)	→	CO+HO_2+OH	3.4×10^{-11} exp(-1600/T)	2,12
k62	CO+OH	→	CO_2+H	1.57×10^{-13}+3.54×10^{-33} [M]	16
k63	C_2H_6+OH	→	$C_2H_5O_2$+H_2O	1.52×10^{-17} exp(-498/T) T^2	13
k64	$C_2H_5O_2$+NO	→	CH_3CHO+HO_2+NO_2	2.7×10^{-12} exp(360/T)	13
k65	$C_2H_5O_2$+NO_3	→	CH_3CHO+HO_2+NO_2+O_2	2.4×10^{-12}	13
k66	$C_2H_5O_2$+HO_2	→	C_2H_5OOH+O_2	4.4×10^{-13} exp(900/T)	13
k67	$C_2H_5O_2$+CH_3O_2	→	0.74CH_2O+0.74CH_3CHO+ 0.96HO_2+0.26CH_3OH+0.26C_2H_5OH	2.0×10^{-13}	13
k68	$C_2H_5O_2$+$C_2H_5O_2$	→	1.63CH_3CHO+1.26HO_2+ 0.37C_2H_5OH	9.8×10^{-14} exp(100/T)	13
k69	C_2H_5OOH+OH	→	$C_2H_5O_2$+HO_2	1.9×10^{-12} exp(190/T)	13
k70	C_2H_5OOH+OH	→	CH_3CHO+OH+H_2O	7.69×10^{-17} exp(253/T) T^2	13
k71	C_2H_5OH+OH	→	CH_3CHO+HO_2+H_2O	6.18×10^{-18} exp(532/T) T^2	13
k72	C_3H_8+OH	→	$C_3H_7O_2$+H_2O	1.55×10^{-17} exp(-61/T) T^2	13
k73	$C_3H_7O_2$+NO	→	0.72CH_3COCH_3+0.94NO_2+ 0.22CH_3CHO+0.94HO_2+0.06ONITU	2.7×10^{-12} exp(360/T)	13
k74	$C_3H_7O_2$+NO_3	→	0.234CH_3CHO+NO_2+HO_2+ 0.766CH_3COCH_3	2.4×10^{-12}	13
k75	$C_3H_7O_2$+HO_2	→	C_3H_7OOH+O_2	1.9×10^{-13}exp(1300/T)	13
k76	$C_3H_7O_2$+CH_3O_2	→	0.128CH_3COCH_3+0.78HO_2+ 0.695CH_2O+0.305CH_3OH+ 0.567CH_3CHO	5.18×10^{-12}	13
k77	C_3H_7OOH+OH	→	$C_3H_7O_2$+H_2O	1.9×10^{-12}exp(190/T)	13
k78	C_3H_7OOH+OH	→	CH_3CHO+OH+H_2O	1.67×10^{-17}exp(253/T)T^2	13
k79	CH_3COCH_3+OH	→	PROPAO2+H_2O	2.81×10^{-12}exp(-760/T)	1
k80	PROPAO2+NO	→	CH_3CO_3+CH_2O+NO_2	2.7×10^{-12}exp(360/T)	13
k81	PROPAO2+NO_3	→	CH_3CO_3+CH_2O+NO_2+O_2	2.4×10^{-12}	13
k82	PROPAO2+HO_2	→	PROPAOOH+O_2	1.9×10^{-13}exp(1300/T)	13
k83	PROPAO2+CH_3O_2	→	1.31CH_2O+0.23CH_3OH+ 0.23CH_3COCHO+0.54HO_2+ 0.54CH_3CO_3	3.8×10^{-12}	13

Table 4. Continued.

#	reaction			rate coefficient	refs.
k84	PROPAOOH+OH	→	PROPAO2+H_2O	1.9×10^{-12}exp(190/T)	13
k85	PROPAOOH+OH	→	CH_3COCHO+OH+H_2O	4.69×10^{-17}exp(253/T)T^2	13
k86	C_2H_4+OH+M	→	0.667PROPEO2+M	$k_0=1.0\times10^{-28}(T/298)^{-0.8}$ $k_\infty=8.79\times10^{-12}$ $F_c=0.7$	2
k87	C_2H_4+O_3	→	CH_2O+0.46CO+0.16HO_2+ 0.08OH+0.17CO_2	1.2×10^{-14}exp(-2630/T)	2
k88	C_3H_6+OH+M	→	PROPEO2+M	$k_0=2.94\times10^{-27}(T/298)^{-3.0}$ $k_\infty=2.775\times10^{-11}(T/298)^{-1.3}$ $F_c=0.5$	13
k89	C_3H_6+O_3	→	0.63248CH_2O+0.341CH_3O_2+ 0.0868CH_4+0.4166CO+ 0.0124CH_3OH+0.2096HO_2+ 0.2474OH+0.38CH_3CHO+0.2754CO_2	6.51×10^{-15}exp(-1900/T)	2
k90	PROPEO2+NO	→	CH_3CHO+CH_2O+HO_2+NO_2	2.7×10^{-12}exp(360/T)	13
k91	PROPEO2+NO_3	→	CH_3CHO+CH_2O+ HO_2+NO_2+O_2	2.4×10^{-12}	13
k92	PROPEO2+HO_2	→	PROPEOOH+O_2	1.9×10^{-13}exp(1300/T)	13
k93	PROPEO2+CH_3O_2	→	0.305CH_3OH+0.78HO_2+ 1.085CH_2O+0.39CH_3CHO+ 0.305CH_3COCHO	7.583×10^{-13}	13
k94	PROPEOOH+OH	→	PROPEO2+H_2O	1.9×10^{-12}exp(190/T)	13
k95	PROPEOOH+OH	→	CH_3COCHO+OH+H_2O	2.35×10^{-17}exp(696/T)T^2	13
k96	PROPEOOH+OH	→	CH_3COCHO+OH+H_2O	2.69×10^{-17}exp(253/T)T^2	13
k97	PROPEOOH+OH	→	CH_3CHO+HO_2+H_2O	1.26×10^{-17}exp(253/T)T^2	13
k98	PROPEOOH+OH	→	PROPAOOH+HO_2+H_2O	3.19×10^{-18}exp(696/T)T^2	13
k99	CH_3CHO+OH	→	CH_3CO_3+H_2O	5.6×10^{-12}exp(270/T)	2
k100	CH_3CHO+NO_3	→	CH_3CO_3+HNO_3	1.4×10^{-12}exp(-1860/T)	13
k101	CH_3CO_3+NO	→	CH_3O_2+NO_2+CO_2	5.3×10^{-12}exp(360/T)	13
k102	CH_3CO_3+NO_2+M	→	PAN+M	$k_0=2.7\times10^{-28}(T/298)^{-7.1}$ $k_\infty=1.2\times10^{-11}(T/298)^{-0.9}$ $F_c=0.3$	13
k103	PAN+M	→	CH_3CO_3+NO_2+M	$k_0=5.0\times10^{-2}$exp(-12875/T) $k_\infty=2.2\times10^{+16}$exp(-13435/T) $F_c=0.27$	13
k104	CH_3CO_3+NO_3	→	CH_3O_2+NO_2+CO_2+O_2	5.0×10^{-12}	13
k105	CH_3CO_3+HO_2	→	0.3O_3+0.3CH_3OOH+ 0.7O_2+0.7$CH_3C(O)OOH$	4.3×10^{-13}exp(1040/T)	13
k106	CH_3CO_3+CH_3O_2	→	CH_2O+0.86CH_3O_2+ 0.86HO_2+0.86CO_2+O_2+ 0.14CH_3COOH	1.3×10^{-12}exp(640/T)	13
k107	CH_3CO_3+CH_3CO_3	→	2CH_3O_2+2CO_2	2.3×10^{-12}exp(530/T)	13
k108	$CH_3C(O)OOH$+OH	→	CH_3CO_3+H_2O	1.9×10^{-12}exp(190/T)	13
k109	C_2H_2+OH+M	→	0.36CO+0.64CH_3COCHO+ 0.36HO_2+0.65OH+M	$k_0=5.01\times10^{-30}(T/298)^{-1.5}$ $k_\infty=9.0\times10^{-13}(T/298)^{2.0}$ $F_c=0.62$	1
k110	ISOP+OH	→	ISOPO2	2.89×10^{-11}exp(335/T)	1,2
k111	ISOP+O_3	→	0.42MACR+0.16MVK+ 0.05C_3H_6+0.18OH+ 0.09HO_2+0.42CH_2O+ 0.27CO+0.07H_2+0.15CO_2	9.36×10^{-15}exp(-1913/T)	13
k112	ISOP+NO_3	→	ISOPNO3	3.03×10^{-12}exp(-446/T)	13
k113	ISOPO2+NO	→	0.12ONITR+0.88NO_2+ 0.76HO_2+0.608CH_2O+ 0.404MACR+0.354MVK+0.12XO2	2.7×10^{-12}exp(360/T)	13
k114	ISOPO2+NO_3	→	0.864HO_2+NO_2+0.69CH_2O+ 0.46MACR+0.403MVK+0.136XO2	2.4×10^{-12}	13
k115	ISOPO2+HO_2	→	0.867HO_2+0.739CH_2O+ 0.506MACR+0.429MVK+ 0.133XO2+XOOH	1.9×10^{-13}exp(1300/T)	13

Table 4. Continued.

#	reaction			rate coefficient	refs.
k116	ISOPO2+CH_3O_2	→	0.305CH_3OH+0.703HO_2+ 0.91CH_2O+0.137XO2+ 0.351MACR+0.205MVK	1.33×10^{-12}	13
k117	ISOPO2+CH_3CO_3	→	0.275CH_3COOH+0.58HO_2+ 0.725CO+0.725CH_3O_2+ 0.198XO+20.397CH_2O+ 0.504MACR+0.296MVK	7.96×10^{-12}	13
k118	ISOPNO3+NO	→	1.206NO_2+0.794HO_2+ 0.072CH_2O+0.167MACR+ 0.039MVK+0.794ONITR	2.7×10^{-12}exp(360/T)	13
k119	ISOPNO3+NO_3	→	1.206NO_2+0.794HO_2+ 0.072CH_2O+0.167MACR+ 0.039MVK+0.794ONITR	2.4×10^{-12}	13
k120	ISOPNO3+HO_2	→	0.206NO_2+0.794HO_2+ 0.008CH_2O+0.167MACR+ 0.039MVK+0.794ONITR+XOOH	1.9×10^{-13}exp(1300/T)	13
k121	ISOPNO3+CH_3O_2	→	0.305CH_3OH+0.711HO_2+ 0.697CH_2O+0.06NO_2+ 0.059MACR+0.001MVK+ 0.635ONITR	1.749×10^{-12}	13
k122	APIN+OH	→	APINO2	1.08×10^{-11}exp(444/T)	13
k123	APIN+O_3	→	0.56OH+0.56APINO3	1.1615×10^{-15}exp(-732/T)	13
k124	APIN+NO_3	→	APINO2+NO_2	1.19×10^{-12} exp(490/T)	13
k125	APINO2+NO	→	PCHO+NO_2+HO_2	2.7×10^{-12}exp(360/T)	13
k126	APINO2+NO_3	→	PCHO+NO_2+HO_2+O_2	2.4×10^{-12}	13
k127	APINO2+HO_2	→	PCHO+HO_2+XOOH	1.9×10^{-13}exp(1300/T)	13
k128	APINO2+CH_3O_2	→	0.305CH_3OH+0.695APINO3+HO_2	1.22×10^{-13}	13
k129	APINO2+CH_3CO_3	→	0.725CO_2+0.725CH_3O_2+ 0.725PCHO+0.725HO_2+ 0.275CH_3COOH	7.37×10^{-13}	13
k130	APINO3+NO	→	NO_2+CO_2+CH_3COCH_3+ 2PROPEO2	5.3×10^{-12}exp(360/T)	13
k131	APINO3+NO_2+M	→	APINPAN+M	k_0=2.7×10^{-28}(T/298)$^{-7.1}$ k_∞=1.2×10^{-11}(T/298)$^{-0.9}$ F_c=0.3	13
k132	APINPAN+M	→	APINO3+NO_2+M	k_0=4.0×10^{-3}exp(-12100/T) k_∞=$5.4\times10^{+16}$exp(-13830/T) F_c=0.3	14,15
k133	APINO3+NO_3	→	NO_2+CO_2+CH_3COCH_3+ 2PROPEO2+O_2	5.0×10^{-12}	13
k134	APINO3+HO_2	→	0.3O_3+0.3CH_3COOH+ 0.7O_2+0.7$CH_3C(O)OOH$	4.3×10^{-13}exp(1040/T)	13
k135	APINO3+CH_3O_2	→	0.335CH_2O+0.665CH_2O+ 0.665HO_2+0.665CH_3COCH_3+ 1.33PROPEO2+CO_2	4.52×10^{-12}	13
k136	APINO3+CH_3CO_3	→	2CO_2+CH_3O_2+ CH_3COCH_3+2PROPEO2	4.6×10^{-12}exp(530/T)	13
k137	APINO3+APINO3	→	2CO_2+2CH_3COCH_3+4PROPEO2	2.3×10^{-12}exp(530/T)	13
k138	MACR+OH	→	0.5MACRO2+0.5HO_2+0.5MCO3	1.86×10^{-11}exp(175/T)	13
k139	MACR+O_3	→	0.8CH_3COCHO+0.13HO_2+ 0.37CO+0.1H_2+0.2OH+ 0.34CH_2O+0.14CO_2	1.359×10^{-15}exp(-2112/T)	13
k140	MVK+OH	→	MACRO2	2.67×10^{-12}exp(452/T)	13
k141	MVK+O3	→	0.05CH_2O+0.95CH_3COCHO+ 0.08OH+0.15HO_2+0.12H_2+ 0.16CO_2+0.44CO	7.51×10^{-16}exp(-1521/T)	13
k142	MACRO2+NO	→	0.015ONITR+0.985NO_2+ 0.985HO_2+0.158CH_2O+ 0.158CH_3COCHO+0.828CO+ 0.828CH_3COCHO	2.7×10^{-12}exp(360/T)	13

Table 4. Continued.

#	reaction			rate coefficient	refs.
k143	MACRO2+NO_3	→	NO_2+HO_2+0.16CH_2O+ 0.16CH_3COCHO+0.84CO+ 0.84CH_3COCHO	2.4×10^{-12}	13
k144	MACRO2+HO_2	→	MACROOH	1.9×10^{-13}exp(1300/T)	13
k145	MACRO2+CH_3O_2	→	0.916HO_2+1.064CH_2O+ 0.458CO+0.458CH_3COCHO+ 0.229CH_3OH+0.458CH_3CHO+	4.1288×10^{-13}	13
k146	MACRO2+CH_3CO_3	→	0.794CO_2+0.794CH_3O_2+ 0.412CH_3CHO+0.544CH_2O+ 0.794CH_3COCHO+0.794HO_2+ 0.206CH_3COOH+0.25CO	2.475×10^{-12}	13
k147	MACROOH+OH	→	MACRO2+H_2O	1.9×10^{-12}exp(190/T)	13
k148	MACROOH+OH	→	2CH_3CHO+OH+H_2O	3.9×10^{-17}exp(253/T)T^2	13
k149	MACROOH+OH	→	MCO3+H_2O	2.27×10^{-17}exp(696/T)T^2	13
k150	MACROOH+OH	→	0.6C_2H_5OOH+HO_2+ 0.4CH_3CHO+H_2O	5.16×10^{-17}exp(253/T)T^2	13
k151	MCO3+NO	→	CH_3CO_3+CH_2O+NO_2	5.3×10^{-12}exp(360/T)	13
k152	MCO3+NO_2+M	→	MPAN+M	$k_0=2.7\times10^{-28}(T/298)^{-7.1}$ $k_\infty=1.2\times10^{-11}(T/298)^{-0.9}$ F_c=0.3	13
k153	MPAN+M	→	MCO3+NO_2+M	$k_0=5.0\times10^{-2}$exp(-12875/T) $k_\infty=2.2\times10^{+16}$exp(-13435/T) F_c=0.27	13
k154	MCO3+NO_3	→	CH_3CO_3+CH_2O+NO_2+O_2	5.0×10^{-12}	13
k155	MCO3+HO_2	→	0.3O_3+0.3CH_3COOH+ 0.7O_2+0.7$CH_3C(O)OOH$	4.3×10^{-13}exp(1040/T)	13
k156	MCO3+CH_3O_2	→	1.655CH_2O+0.665HO_2+ 0.665CH_3CO_3+0.665CO_2	4.52×10^{-12}	13
k157	MCO3+CH_3CO_3	→	2CO_2+CH_3O_2+CH_2O+CH_3CO_3	4.6×10^{-12}exp(530/T)	13
k158	MCO3+MCO3	→	2CO_2+2CH_3O_2+ 2CH_2O+2CH_3CO_3	2.3×10^{-12}exp(530/T)	13
k159	CH_3COCHO+OH	→	CH_3CO_3+CO+H_2O	8.4×10^{-13}exp(830/T)	17
k160	CH_3COCHO+NO_3	→	CH_3CO_3+CO+HNO_3	1.4×10^{-12}exp(-1860/T)	13
k161	PCHO+OH	→	PCO3+H_2O	9.1×10^{-11}	13
k162	PCHO+NO_3	→	PCO3+HNO_3	5.4×10^{-14}	13
k163	PCO3+NO	→	PROPEO2+NO_2+CO_2+XO2	5.3×10^{-12}exp(360/T)	13
k164	PCO3+NO_2+M	→	PCO3PAN+M	$k_0=2.7\times10^{-28}(T/298)^{-7.1}$ $k_\infty=1.2\times10^{-11}(T/298)^{-0.9}$ F_c=0.3	13
k165	PCO3PAN+M	→	PCO3+NO_2+M	$k_0=5.0\times10^{-2}$exp(-12875/T) $k_\infty=2.2\times10^{+16}$exp(-13435/T) F_c=0.27	13
k166	PCO3+NO_3	→	PROPEO2+NO_2+CO_2+XO2	5.0×10^{-12}	13
k167	PCO3+HO_2	→	0.3O_3+0.3CH_3COOH+ 0.7O_2+0.7$CH_3C(O)OOH$	4.3×10^{-13}exp(1040/T)	13
k168	PCO3+CH_3O_2	→	0.665PROPEO2+CH_2O+ 0.665HO_2+0.665XO2	4.52×10^{-12}	13
k169	PCO3+CH_3CO_3	→	2CO_2+PROPEO2+XO2+CH_3O_2	4.6×10^{-12}exp(530/T)	13
k170	PCO3+PCO3	→	2CO_2+2PROPEO2+2XO2	2.3×10^{-12}exp(530/T)	13
k171	ONITU+OH	→	0.694ONITUO2+0.25HNO_3+ 0.25HO_2+0.3CH_3COCH_3+0.05NO_2	1.83×10^{-12}	13
k172	ONITUO2+NO	→	1.294NO_2+0.706ONITR+ 0.4HO_2+0.116CH_2O+ 0.386CH_3CHO+0.209MEK+ 0.395XO2	2.7×10^{-12}exp(360/T)	13
k173	ONITUO2+NO_3	→	1.294NO_2+0.706ONITR+ 0.4HO_2+0.116CH_2O+ 0.386CH_3CHO+0.209MEK+ 0.395XO2	2.4×10^{-12}	13
k174	ONITUO2+HO_2	→	0.7ONITR+0.3ONITUO2	1.9×10^{-13}exp(1300/T)	13
k175	ONITR+OH	→	MCO3+0.75HNO_3+0.25NO_2+0.25HO_2	1.5×10^{-11}	13

Table 4. Continued.

#	reaction			rate coefficient	refs.
k176	ONITR+NO_3	→	MCO3+0.4HNO_3+0.8NO_2+0.8NO	1.4×10^{-12}exp(-1860/T)	13
k177	MEK+OH	→	MEKO2	3.24×10^{-18}exp(414/T)T^2	13
k178	MEKO2+NO	→	NO_2+1.329CH_3CHO+ 0.6CH_3CO_3+0.07CH_2O+ 0.4HO_2+0.197MEK	2.7×10^{-12}exp(360/T)	13
k179	MEKO2+NO_3	→	NO_2+1.329CH_3CHO+ 0.6CH_3CO_3+0.07CH_2O+ 0.4HO_2+0.197MEK	2.4×10^{-12}	13
k180	MEKO2+HO_2	→	MEKOOH	1.9×10^{-13}exp(1300/T)	13
k181	MEKO2+CH_3O_2	→	0.305CH_3OH+0.699HO_2+ 0.75CH_2O+0.08CH_3CO_3+ 0.295MEK+0.654CH_3CHO+ 0.042CH_3COCHO	9.764×10^{-13}	13
k182	MEKOOH+OH	→	MEKO2+H_2O	1.9×10^{-12}exp(190/T)	13
k183	MEKOOH+OH	→	MEK+ OH+H_2O	1.17×10^{-17}exp(696/T)T^2	13
k184	MEKOOH+OH	→	CH_3CHO+0.5MEK+OH+H_2O	9.75×10^{-17}exp(253/T)T^2	13
k185	MEKOOH+OH	→	CH_3COCHO+OH+H_2O	3.28×10^{-18}exp(253/T)T^2	13
k186	ALKEN+OH	→	ALKENO2	9.19×10^{-12}exp(-522.22/T)	13
k187	ALKEN+O_3	→	0.9CH_3CHO+0.23ALKENO2+ 0.09CH_3COCH_3+0.34CH_3O_2+ 0.08CH_4+0.02C_2H_6+0.3CO+ 0.01CH_3OH+0.42OH	4.95×10^{-15}exp(-1054.84/T)	13
k188	ALKEN+NO_3	→	ALKENO2+NO_2	3.95×10^{-12}exp(-327.93/T)	13
k189	ALKENO2+NO	→	0.034ONITU+0.406CH_2O+ 1.666CH_3CHO+0.966NO_2+ 0.38CH_3COCH_3+0.966HO_2	2.7×10^{-12}exp(360/T)	13
k190	ALKENO2+NO_3	→	0.393CH_3COCH_3+NO_2+HO_2+ 0.724CH_3CHO+0.42CH_2O	2.4×10^{-12}	13
k191	ALKENO2+HO_2	→	ALKENOOH	1.9×10^{-13}exp(1300/T)	13
k192	ALKENO2+CH_3O_2	→	0.305CH_3OH+0.265CH_3CHO+ 0.695CH_2O+0.06CH_3COCH_3+ 0.305CH_3COCHO+0.78HO_2	1.22×10^{-13}	13
k193	ALKENOOH+OH	→	ALKENO2+H_2O	1.9×10^{-12}exp(190/T)	13
k194	ALKENOOH+OH	→	CH_3COCHO+OH+H_2O	9.46×10^{-17}exp(253/T)T^2	13
k195	ALKAN+OH	→	ALKANO2	1.63×10^{-17}exp(385.22/T)T^2	13
k196	ALKANO2+NO	→	0.007CH_2O+0.362CH_3CHO+ 0.289CH_3COCH_3+0.799NO_2+ 0.412MEK+0.082CH_3O_2+ 0.2ONITU+0.268XO2+ 0.449HO_2	2.7×10^{-12}exp(260/T)	13
k197	ALKANO2+NO_3	→	NO_2+0.562HO_2+0.336XO2+ 0.101CH_3O_2+0.517MEK+ 0.001CH_2O+0.454CH_3CHO	2.4×10^{-12}	13
k198	ALKANO2+HO_2	→	ALKANOOH	1.9×10^{-13}exp(1300/T)	13
k199	ALKANO2+CH_3O_2	→	0.045CH_3COCH_3+0.626HO_2+ 0.305CH_3OH+0.696CH_2O+ 0.315MEK+0.012CH_3O_2+ 0.442CH_3CHO+0.14XO2	3.7652×10^{-13}	13
k200	ALKANOOH+OH	→	ALKANO2+H_2O	1.9×10^{-12}exp(190/T)	13
k201	ALKANOOH+OH	→	CH_3CHO+OH+H_2O	1.07×10^{-17}exp(253/T)T^2	13
k202	ALKANOOH+OH	→	MEK+OH+H_2O	3.82×10^{-17}exp(696/T)T^2	13
k203	AROM+OH	→	0.77AROMO2+0.212HO_2	1.01×10^{-11}exp(58.45/T)	13
k204	AROMO2+NO	→	0.423CH_3COCHO+NO_2+ 0.658CH_3CO_3+0.658CO+1.658HO_2	2.7×10^{-12}exp(360/T)	13
k205	AROMO2+NO_3	→	0.423CH_3COCHO+NO_2+ 0.658CH_3CO_3+0.658CO+1.658HO_2	2.4×10^{-12}	13
k206	AROMO2+HO_2	→	AROMOOH	1.9×10^{-13}*exp(1300/T)	13
k207	AROMO2+CH_3O_2	→	0.087*CH_3COCHO + 0.135*CO+ 0.135*CH_3CO_3 + 0.305*CH_3OH+ 0.695*CH_2O + 0.915*HO_2	2.31×10^{-13}	13
k208	AROMOOH+OH	→	AROMO2 + H_2O	1.9×10^{-12}*exp(190/T)	13

Table 4. Continued.

#	reaction			rate coefficient	refs.
k209	AROMOOH+OH	→	OH+H_2O	$4.61\times10^{-18}\exp(253/T)T^2$	13
k210	AROMOOH+OH	→	CH_3CO_3+CO+OH+ HO_2+H_2O	$4.19\times10^{-17}\exp(696/T)T^2$	13
k211	XO2+NO	→	NO_2+HO_2	$2.7\times10^{-12}\exp(360/T)$	13
k212	XO2+NO_3	→	NO_2+HO_2	2.4×10^{-12}	13
k213	XO2+HO_2	→	XOOH	$1.9\times10^{-13}\exp(1300/T)$	13
k214	XO2+CH_3O_2	→	0.305CH_3O_2+0.695CH_2O+0.39HO_2	1.22×10^{-13}	13
k215	XO2+CH_3CO_3	→	0.275CH_3COOH+0.725CO_2+ 0.725CH_3O_2	7.37×10^{-13}	13
k216	XOOH+OH	→	XO2+H_2O	$1.9\times10^{-12}\exp(190/T)$	13
k217	XOOH+OH	→	OH+H_2O	$7.69\times10^{-17}\exp(253/T)T^2$	13

T=temperature (K); M=air density (molecules cm^{-3})
Rate coefficients are in cm^3 $molecules^{-1}$ s^{-1} for bimolecular reactions
and in cm^6 $molecules^{-2}$ s^{-1} for termolecular reactions.
In the latter case, the rate coefficient is defined by

$$k(T,M) = \left[\frac{k_0(T)\cdot[M]}{1+\frac{k_0(T)\cdot[M]}{k_\infty(T)}}\right]\cdot F_c^{\left\{1+\left[\log_{10}\left(\frac{k_0(T)\cdot[M]}{k_\infty(T)}\right)\right]^2\right\}^{-1}}$$

References:
1, Atkinson et al. (1997); 2, DeMore et al. (1997); 3, Jenkin and Cox (1987); 4, Matzkies and Manthe (1998)
5, Yu and Varandas (1997); 6, Hall et al. (1988); 7, Matsumi et al. (1993); 8, Greenberg and Heicklen (1972)
9, Bradley et al. (1971); 10, Kukui et al. (1995); 11, Tyndall et al. (1998); 12, Baulch et al. (1992)
13, Brocheton (1999); 14, Brasseur et al. (1998); 15, Hauglustaine et al. (1998); 16, McCabe et al. (2001)
17, Tyndall et al. (1995)

The LMDz version used in this study (referred to as 3.3) has a horizontal resolution of 3.8 degrees in longitude and 2.5 degrees in latitude (96×72 grid cells). The model is composed of 19 vertical levels on σ-p coordinates extending from the surface to 3 hPa. Also higher-resolution versions of LMDz have been developed and applied recently (e.g. Bauer et al., 2004).

The primitive equations in the GCM are solved with a 3 min time-step, large-scale transport of tracers is carried out every 15 min, and physical processes are calculated at a 30 min time interval. For a more detailed description and an extended evaluation of the GCM we refer to the work of, e.g., Le Treut et al. (1994) and Harzallah and Sadourny (1995). Recently, Hauglustaine et al. (2004) have coupled LMDz to the tropospheric chemistry model INCA, during which the GCM has been reevaluated.

2.2 The INCA-NMHC chemistry and aerosol model

INteraction with **C**hemistry and **A**erosols (INCA) is coupled on-line to the LMDz general circulation model. INCA prepares the surface and in situ emissions, calculates dry deposition and wet scavenging rates, and integrates in time the concentration of atmospheric species with a time step of 30 min. INCA uses a sequential operator approach, a method generally applied in chemistry-transport-models (Muller and Brasseur, 1995; Brasseur et al., 1998; Wang et al., 1998a; Poisson et al., 2000). The INCA-NMHC version applied in this study is based on an earlier version which was developed to represent the background chemistry of the troposphere (Hauglustaine et al., 2004). Results from this version of the model related to the impact of chemistry on the budget of CO_2 have been published by Folberth et al. (2005).

2.2.1 Chemistry

The version of INCA used in this study includes a comprehensive photochemical scheme originally intended to represent the photochemistry of the troposphere in regional scale chemistry-transport models. In addition to the CH_4–NO_x–CO–O_3 photochemistry representative of the tropospheric background, INCA, in its NMHC-implementation, also takes into account the photochemical oxidation pathways of non-methane hydrocarbons (NMHC) and non-methane volatile organic compounds (NMVOC) from natural and anthropogenic sources as well as their photochemical oxidation products. The model can be applied to calculate the distribution of tropospheric ozone and its precursors, but due to the comprehensive chemistry scheme the model is also suited to be used in studies of biosphere-atmosphere interrelation and the impact of a changing biosphere on the global climate. The species included in this more extensive version of LMDz-INCA are summarized in Tab. 1. We consider only one photochemical family (O_x=$O_3 + O(^1D) + O(^3P)$), and for species with very short photochemical lifetimes transport is not taken into account.

Tables 1, 2, 3, and 4 summarize the chemical scheme in LMDz-INCA. The scheme includes a total of 83 species, 58 of which are subject to transport. In INCA-NMHC short-chained NMVOC are treated explicitly whereas a lumping approach is applied in the case of higher NMVOC as proposed by Brocheton (1999). Alkanes up to three carbon atoms (C_3) per molecule are treated explicitly including methane, ethane, and propane. All C_4- and higher alkanes are lumped into one artificial species (C_4^+-alkanes). Likewise, the model distinguishes ethene, propene, and C_4^+-alkenes. The isoprene oxidation pathway has been represented with some complexity, comparable to the one proposed by Pöschl et al. (2000) including explicitly the major oxidation products methyl vinyl ketone and methacrolein; all higher isoprenoid species are lumped into one group to which we refer to as "terpenes". INCA-NMHC includes two alcohols (methanol and C_2^+-alcohols, eleven hydroperoxides, one group representing organic acids, three aldehyde species (formaldehyde, acetaldehyde including higher monocarboxy aldehydes, and a group representing higher aldehydes produced by terpene oxidation), three ketones (acetone, methyl ethyl ketone, and methyl vinyl ketone), four species representing peroxy acetyl nitrate (PAN) and analogues, two general organic nitrate groups (organic nitrates with low or high reactivity toward OH), as well as the corresponding organic radicals arising in the oxidation of the above species (cf. Tables 1 and 4). Lumping in all cases follows the generally applied method of grouping individual compounds by their reactivity toward the OH-radical while also taking into account compound groups, molecular weights, and atmospheric abundances (for a general description of these methods see, e.g., Stockwell et al., 1997).

43 photolytic reactions (Table 2), 217 thermochemical reactions (Table 4), and 4 heterogeneous reactions (Table 3) are taken into account by the model. The set of reactions and reaction rates is based on the scheme of Brocheton (1999). All reaction rates have been reviewed and updated with respect to the compilations of Atkinson et al. (1997) and DeMore et al. (1997) as well as subsequent updates (Sander et al., 2000, 2002). The reaction rates are calculated by the model at each time interval on the basis of temperature, pressure, and water vapour distribution provided by the GCM.

Pretabulated clear-sky photolysis frequencies j are used to determine the values at each time step and model grid cell by means of a multivariate log-linear interpolation through a Taylor series expansion (Burden and Faires, 1985). This look-up table is prepared with the Troposphere-Ultraviolet-Visible (TUV) model (version 4.1) from Madronich and Flocke (1998) using a pseudo-spherical 16 stream discrete-ordinate method. The effect of cloudiness is taken into account according to Chang et al. (1987) as described by Brasseur et al. (1998). Further details can be found in

Hauglustaine et al. (2004). Where no spectral data is available for a specific species to be used with TUV we assume the photolysis frequencies to be linearly dependent on chemically similar compounds (cf. Table 2). The LMDz-INCA chemical scheme includes four heterogeneous reactions (Table 3) following the recommendations of Jacob (2000) and using the monthly averaged sulfate aerosol fields from Boucher et al. (2002) to determine the aerosol distribution as discussed by Hauglustaine et al. (2004). The NMHC-version of LMDz-INCA uses the identical parameterization for the representation of these processes.

The mechanism implicitly accounts for a carbon loss through formation of secondary organic aerosols (SOA). This tropospheric carbon sink is taken into account in the scheme as a carbon imbalance for specific reactions in the terpene oxidation pathway. The estimate of the global carbon sink as derived with LMDz-INCA amounts to approximately 39% ($\sim$37 Tg C yr^{-1}) of the total annual carbon surface flux emitted as terpenes. Our estimate seems in satisfactory agreement with the calculated variation of the global annual SOA production of 2.5 to 44 Tg C yr^{-1} for the biogenically produced SOA (Tsigaridis and Kanakidou, 2003). Note that explicit secondary organic aerosol formation is not calculated in the current implementation of LMDz-INCA and SOA are not included in the INCA species inventory.

Interactive calculation of chemistry and transport of species extends up to the upper model level. However, in the current version of INCA no chlorine or bromine chemistry is taken into account and heterogeneous reactions on polar stratospheric clouds (PCS) is not yet considered. Therefore, ozone concentrations are relaxed toward observations at the uppermost model levels at each time step applying a relaxation time constant of ten days above the 380K potential temperature surface. The ozone observations are taken from the monthly mean 3-D climatologies of Li and Shine (1995). Further details and an evaluation of the stratospheric boundary conditions in INCA can be found in Hauglustaine et al. (2004); the NMHC version of INCA applies the same approach.

Forward integration in time of the chemical equations is conducted on the basis of five possible numerical algorithms with a time step of 30 minutes as described by Hauglustaine et al. (2004). In the current configuration of LMDz-INCA we apply the explicit Euler forward algorithm (Brasseur et al., 1999) for the integration of long-lived species (marked "l" in Table 1) and the implicit Euler backward with Newton-Raphson iteration scheme for all other species (marked "s" in Table 1). A species to be long-lived in the above sense and suitable for the less resourceful numerical algorithm requires the mean atmospheric lifetime of this species to be at least a few weeks.

2.2.2 Emissions

Surface emission inventories have been compiled for this version of LMDz-INCA using the same methods of data preparation as described in Hauglustaine et al. (2004). These inventories are based on various compilations, with the exception of the biogenic surface source. Biogenic surface emissions were prepared using a global vegetation model which includes a biogenic emission module. Table 5 summarizes the emission magnitude for the individual species that are considered in the version of LMDz-INCA and used in the current study.

LMDz-INCA uses anthropogenic emissions (industry, fossil fuel, and industrial biofuel) based on the EDGAR v3.2 and EDGAR v2.0 emission databases. Anthropogenic sources for nitrogen oxides (NO_x), carbon monoxide (CO), and methane (CH_4) are introduced on the basis of the estimates provided in EDGAR v3.2 (Olivier and Berdowski, 2001) representative of the year 1995. The CO global emissions are rescaled to the values given by Prather et al. (2001). In addition, the LMDz-INCA emission inventory also includes NO_x emissions from oceangoing ships based on Corbett et al. (1999) and NO_x aircraft emissions based on the ANCAT/EC2 inventory (Gardner et al., 1998).

At the time of creation of the current LMDz-INCA emission inventory the more recent version EDGAR v3.2 did not yet include NMVOC emissions on a per-compound basis. Therefore, it was decided to use anthropogenic NMVOC emission estimates as given by the EDGAR v2.0 database (Olivier et al., 1996) which includes estimates for individual compounds. NMVOC emissions based on EDGAR v2.0 are representative of the year 1990 and include alkanes (C_2H_6, C_3H_8, C_4^+-alkanes), alkenes and alkynes (C_2H_4, C_3H_6, C_4^+-alkenes, C_2H_2), aromatics, aldehydes (CH_2O, CH_3CHO plus higher aldehydes) as well as ketones (CH_3COCH_3 and higher ketones, methylethyl ketone, methylvinyl ketone). Species explicitly included in EDGAR v2.0 that are not explicit in LMDz-INCA were aggregated into the specific compound group based on their individual molecular weights, their reactivity towards the hydroxyl radical, and their relative atmospheric abundances.

Biomass burning emissions are introduced according to the satellite based inventory developed by Van der Werf et al. (2003), averaged over the period 1997–2001. This data set is used to provide the geographical distribution and seasonal variation for each compound. Domestic biofuel use and agricultural waste burning emissions are also included in the biomass burning category and are based on the EDGAR database. Emission factors compiled by Andreae and Merlet (2001) are then used to derive the emission magnitude of the biomass burning surface flux for the individual compounds.

NO soil emissions are introduced on the basis of Yienger and Levy II (1995), emissions of CH_4 from rice paddies, wetlands, termites, wild animal and ruminants, and the ocean are taken from Fung et al. (1991), and emissions of N_2O

Table 5. Global Surface Emissions of Trace Gases in LMDz-INCA.

Species	Emission
NO_x (TgN yr^{-1})	
Fossil Fuel + Industry + Indst. Biofuel	22.87
Biomass Burning	9.20
Soils	5.48
Lightning	5.00
International Shipping	3.08
Aircraft	0.70
Total	*46.33*
N_2O (TgN yr^{-1})	
Soils	7.20
Ocean	3.50
Execra	1.02
Biomass Burning	0.83
Fossil Fuel + Industry + Indst. Biofuel	0.73
Deforestation	0.36
Total	*13.64*
CO (Tg yr^{-1})	
Biomass Burning	994.56
Fossil Fuel + Industry + Indst. Biofuel	488.46
Ocean	50.00
Total	*1533.03*
CH_4 (Tg yr^{-1})	
Wetlands, Swamps, and Bogs	177.78
Fossil Fuel + Industry + Indst. Biofuel	94.72
Ruminants	93.21
Rice Cultivation	79.56
Biomass Burning	36.36
Landfills	35.70
Termites	20.00
Tundra	3.24
Total	*540.57*
Isoprene (Tg C yr^{-1})	
Vegetation	410.67
Ocean	0.88
Total	*411.55*
Terpenes (Tg C yr^{-1})	
Vegetation	96.06
Total	*96.06*
Methanol (Tg C yr^{-1})	
Vegetation	86.94
Plant Decay	13.00
Biomass Burning	4.30
Total	*104.24*
Ethane (Tg C yr^{-1})	
Biomass Burning	4.61
Fossil Fuel + Industry + Indst. Biofuel	3.18
Vegetation	0.80
Total	*8.59*
Propane (Tg C yr^{-1})	
Fossil Fuel + Industry + Indst. Biofuel	6.95
Vegetation	1.60
Biomass Burning	1.26
Total	*9.81*
C_4- and higher alkanes (Tg C yr^{-1})	
Fossil Fuel + Industry + Indst. Biofuel	19.99
Biomass Burning	1.97
Total	*21.96*
Aromatics (Tg C yr^{-1})	
Fossil Fuel + Industry + Indst. Biofuel	7.82
Biomass Burning	4.69
Total	*12.51*
Ethene (Tg C yr^{-1})	
Biomass Burning	8.63
Fossil Fuel + Industry + Indst. Biofuel	4.45
Vegetation	4.30
Ocean	0.67
Total	*18.05*
Propene (Tg C yr^{-1})	
Biomass Burning	3.14
Fossil Fuel + Industry + Indst. Biofuel	1.68
Vegetation	0.80
Ocean	0.34
Total	*5.96*
C_4- and higher alkenes (Tg C yr^{-1})	
Biomass Burning	6.00
Fossil Fuel + Industry + Indst. Biofuel	2.40
Vegetation	1.70
Ocean	0.28
Total	*10.38*
Ethyne (Tg C yr^{-1})	
Biomass Burning	2.67
Fossil Fuel + Industry + Indst. Biofuel	1.02
Vegetation	0.80
Ocean	0.20
Total	*4.69*
Acetone (Tg C yr^{-1})	
Vegetation	34.72
Ocean	12.41
Biomass Burning	2.00
Fossil Fuel + Industry + Indst. Biofuel	0.63
Total	*49.76*
Formaldehyde (Tg C yr^{-1})	
Biomass Burning	2.39
Fossil Fuel + Industry + Indst. Biofuel	0.25
Total	*2.64*
C_3- and higher aldehyde (Tg C yr^{-1})	
Biomass Burning	3.40
Fossil Fuel + Industry + Indst. Biofuel	0.35
Total	*3.75*
Ketones other than acetone (Tg C yr^{-1})	
Fossil Fuel + Industry + Indst. Biofuel	0.95
Total	*0.95*
Hydrogen (Tg yr^{-1})	
Fossil Fuel + Industry + Indst. Biofuel	16.00
Biomass Burning	13.00
Ocean and Soils (50% each)	10.00
Total	*39.0*

are based on Bouwman and Taylor (1996) and Kroeze et al. (1999) for continental emissions and on Nevison and Weiss (1995) for the oceanic N_2O surface flux. NO emissions from lightning are calculated interactively in LMDz-INCA on the basis of the occurrence of convection and cloud top heights. The parameterization of NO from lightning sources as it is used in LMDz-INCA is discussed in more detail by Jourdain and Hauglustaine (2001) and Hauglustaine et al. (2004).

Biogenic emissions of isoprene, terpenes, methanol, and acetone have been prepared with the dynamical global vegetation model ORCHIDEE (**O**rganizing **C**arbon and **H**ydrology in **D**ynamic **E**cosyst**E**ms) (Krinner et al., 2005). ORCHIDEE essentially includes three different components, namely the surface-vegetation-atmosphere transfer scheme SECHIBA (Ducoudré-De Noblet et al., 1993; de Rosnay and Polcher, 1998), the dynamic global vegetation model LPJ (Sitch et al., 2003), and STOMATE (**S**aclay-**T**oulouse-**O**rsay **M**odel for the **A**nalysis of **T**errestrial **E**cosystems), a newly developed model simulating plant phenology and carbon dynamics. For a detailed description and extended evaluation of ORCHIDEE and the new carbon dynamics model STOMATE we refer to the paper by Krinner et al. (2005).

In order to calculate NMVOC surface fluxes from the terrestrial biosphere, a biogenic emission module has recently been integrated into ORCHIDEE. The calculation is based on the emission model by Guenther et al. (1995) and uses input from ORCHIDEE for the key parameters (leaf area index, PFT distribution, specific leaf weight, etc.). This model takes into account changes in the flux strength due to leaf temperature, photosynthetically active radiation (direct and diffuse), and leaf ageing. A detailed description and evaluation of the terrestrial NMVOC emission model is given by Lathière et al..

Warneke et al. (1999) first suggested a significant source of methanol from decaying plant matter and recent estimates of its magnitude range between 4 and 17 $\mathrm{Tg\,C\,yr^{-1}}$ (Singh et al., 2000; Heikes et al., 2002; Galbally and Kirstine, 2002). The LMDZ-INCA emission inventory includes biogenic methanol emissions deriving from plant decay with a global source strength of 13 $\mathrm{Tg\,C\,yr^{-1}}$. It is assumed that this methanol source collocates with methanol emissions from the terrestrial vegetation.

LMDz-INCA takes into account oceanic emissions of CO and several NMVOC (cf. Tab. 5 for compounds that possess oceanic sources). The spatial distribution and variation in time of oceanic CO emissions is based on Erickson and Taylor (1992) and scaled to a global mean of 50 $\mathrm{Tg\,C\,yr^{-1}}$ (Prather et al., 2001). It was furthermore assumed that the global geographic distribution of oceanic NMVOC emissions equals the global oceanic CO source distribution. The oceanic NMVOC emission magnitude is based on Jacob et al. (2002) in case of acetone and on the work of Bonsang et al. (1992) and Bonsang and Boissard (1999) for all other NMVOC that posses non-zero oceanic sources in the LMDz-INCA emission inventory.

2.3 Dry deposition and wet removal

Dry deposition in LMDz-INCA is based on the resistance-in-series approach (Wesely, 1989; Walmsley and Wesely, 1996; Wesely and Hicks, 2000). Deposition velocities (v_d) are calculated at each time step according to:

$$v_d = \frac{1}{R_a + R_b + R_c}, \tag{1}$$

where R_a, R_b, and R_c (s/m) are the aerodynamic, quasi-laminar, and surface resistance, respectively. R_a and R_b are determined on the basis of Walcek et al. (1986). The surface resistance calculation for all species included in LMDz-INCA is based on their temperature dependent Henry's Law Equilibrium Constant and reactivity factor for the oxidation of biological substances. Henry's Law Coefficients tabulated for standard conditions have been taken from Sander (1999) and reactivity factors are taken from Wesely (1989) and Walmsley and Wesely (1996). The vegetation map classification of De Fries and Townshend (1994), interpolated to the model grid and redistributed into the classification of Wesely (1989), is used to parameterize land use dependencies of the surface resistance R_c. A complete list of species that are subject to dry deposition is given in Table 1. During the transition from LMDz-INCA-CH_4 to LMDz-INCA-NMHC the parameterization of dry deposition in the model has undergone some revision taking into account recent work (see cf., e.g., Ganzeveld et al., 1998; Wesely and Hicks, 2000).

Wet scavenging in INCA is parameterized as a first-order loss process as proposed by Giorgi and Chameides (1985):

$$\frac{d}{dt}C_g = -\beta C_g, \tag{2}$$

where C_g is the gas-phase concentration of the considered species and β is the scavenging coefficient (1/s). Wet scavenging associated with large scale stratiform precipitation is calculated adopting the falling raindrop approach (Seinfeld and Pandis, 1998) and wet removal of soluble species by convective precipitation is calculated as part of the upward convective mass flux on the basis of a modified version of the scheme proposed by Balkanski et al. (1993). INCA calculates wet scavenging of soluble species for convective and stratiform precipitation separately. Nitric acid is used as a reference and the scavenging rate of any other species subject to wet removal is scaled to the scavenging rate of HNO_3 according to the temperature dependent Henry's Law Equilibrium Constant on the basis of Seinfeld and Pandis (1998) using standard condition Henry's Law Coefficients from the literature (Sander, 1999). Table 1 provides a list of all species subject to wet removal in this version of LMDz-INCA. For a more detailed description and evaluation of both the dry deposition and wet scavenging parameterization in LMDz-INCA we refer to the paper of Hauglustaine et al. (2004). In the version of LMDz-INCA used in this study the same schemes have been applied.

3 Model evaluation

We present here a general evaluation of the LMDz-INCA model in its NMHC version using a simulation which is representative of the 1990s. During development the model has been run almost consecutively for more than 20 model years before a spin-up run for this study was initialized. A six months spin-up was then conducted from July to December using the restart files of the last development run. After this spin-up period the model has been run for another 24 consecutive months, the last 12 months have been used in the analysis. This approach was chosen to ensure that even long-lived species such as methane have reached equilibrium.

The large amount of species considered in this model and the still rather sparse observational data available from measurement campaigns only allow us to discuss the major aspects of global tropospheric chemistry in this evaluation of the model performance. Although the spatial distribution and time evolution of more than 80 species are calculated by LMDz-INCA, the discussion shall be focused on the key species and selected NMVOC. CO concentrations are evaluated by comparison with surface climatologies from Novelli et al. (2003), other species simulated by LMDz-INCA including hydrocarbons, acetone, NO_x, PAN, and HNO_3 are compared to observations from various aircraft missions based on the data compilation by Emmons et al. (2000) and references therein. Finally, calculated ozone concentrations are evaluated by comparison with climatological ozonesonde observations (Logan, 1999).

3.1 Carbon monoxide

Direct surface emission deriving from fossil fuel combustion as well as biomass burning are the most important CO sources in the atmosphere. In addition, carbon monoxide is produced in situ by oxidation of methane and non-methane hydrocarbons in the entire troposphere.

Figure 1 shows the monthly mean carbon monoxide surface mixing ratio for January and July. CO is most abundant near the surface sources of the tropics and the northern midlatitudes as well as during the northern hemispheric winter when its photochemical lifetime is increased owing to a decrease in the OH abundance and weak vertical mixing. Predicted mixing ratios reach 300 ppb over these regions. During the summer months CO concentrations decrease significantly in the photochemically more active atmosphere, mostly due to a strong increase in OH.

In the tropics the seasonal cycle of CO is controlled to a large extent by the seasonality of biomass burning, which account for half of the direct CO emissions. Biomass burning is most intense during the dry season (December–April in the northern tropics, July – October in the southern tropics). Over these areas with intense biomass burning (tropical regions of Africa and South America) the model calculates maximum mixing ratios in the range of 200 to 300 ppb. In the marine boundary layer of the southern hemisphere, background CO concentrations as predicted by LMDz-INCA are generally lower than 70 ppb.

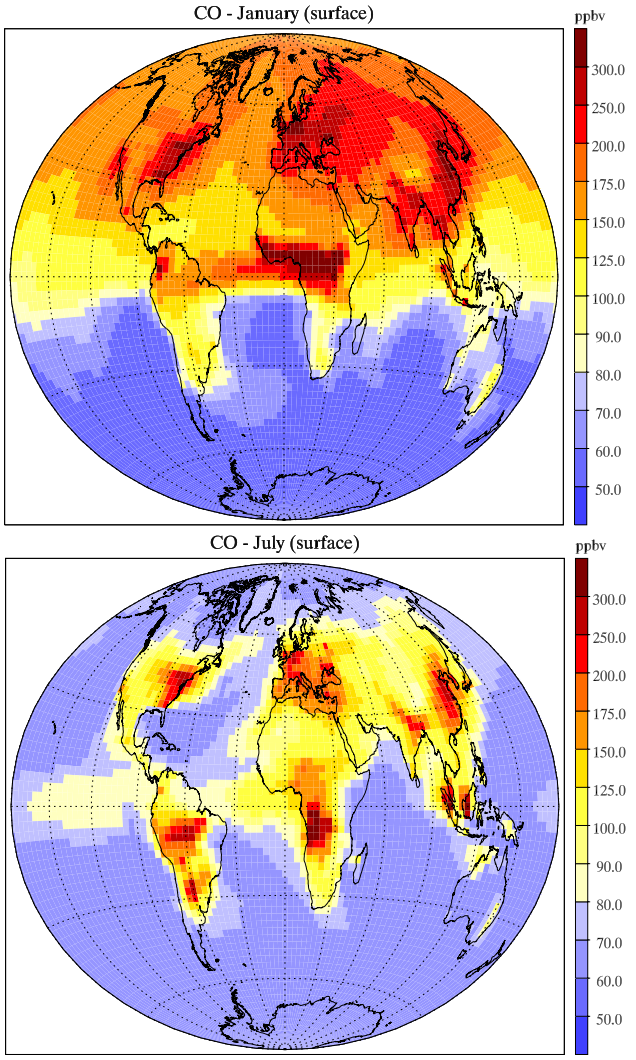

Fig. 1. Carbon monoxide surface mixing ratio for January and July (ppbv).

Simulated monthly mean carbon monoxide concentrations near the surface are compared with climatologies from observations for 18 selected stations from the CMDL network (Novelli et al., 2003) in Fig. 2. Measurements are depicted as monthly means including their standard deviation over the period of record (5 to 10 years, depending on the station).

The model captures well both the absolute values and the seasonal variation of CO mixing ratios in most cases, except for a tendency to overestimate CO by up to 20 ppb at southern mid and high latitudes (cf. Cape Grim, South Pole). The generally higher CO concentrations in the northern hemispheric mid- and high latitudes (e.g., Alert, Baltic Sea, Mace Head, Bermuda) are well captured by the model at virtually all sites,

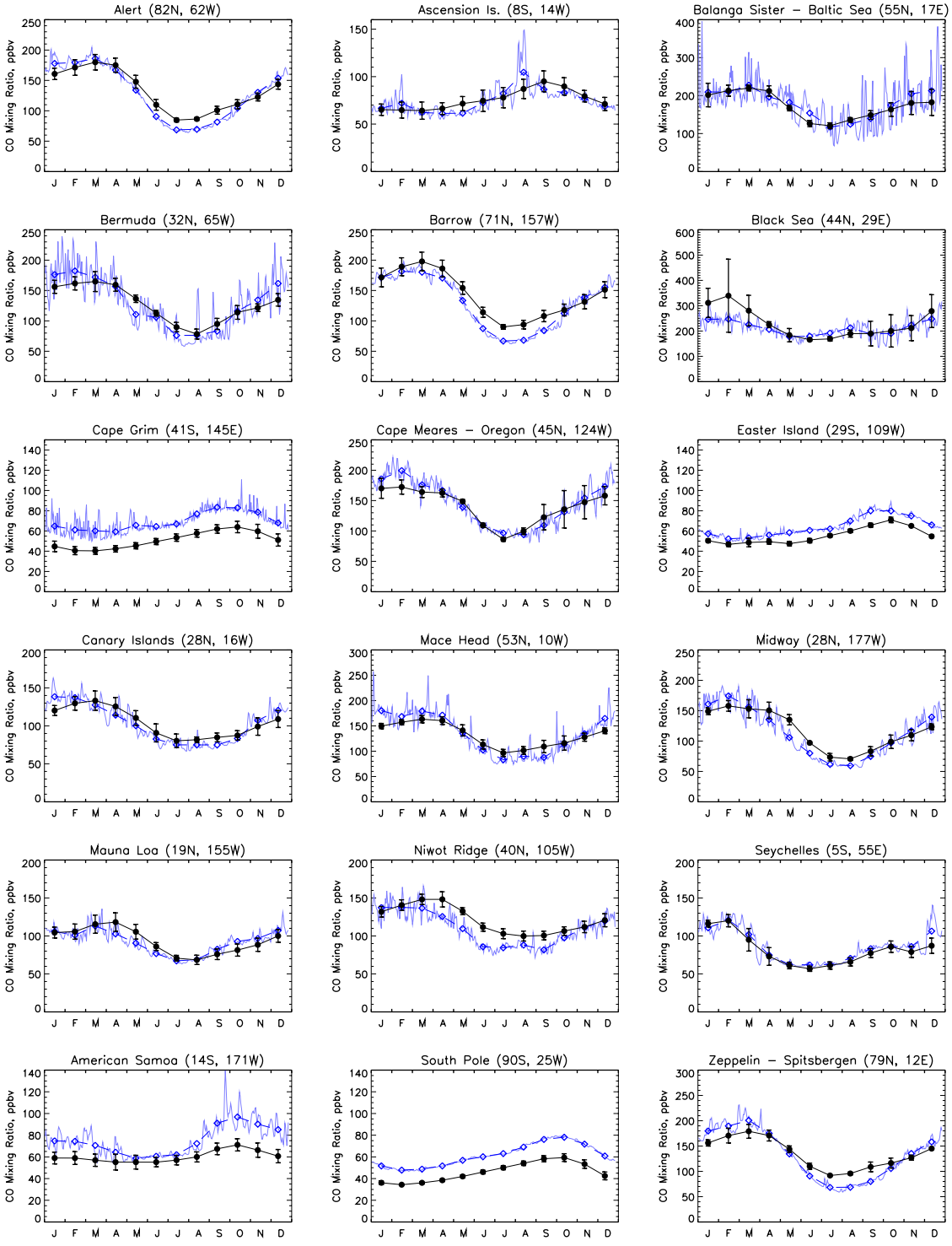

Fig. 2. Comparison of observed and calculated monthly mean CO mixing ratios at the surface. Black circles and solid lines denote observed values from Novelli et al. (2003) averaged over 5 to 10 years depending on the sites; vertical bars are standard deviations. Blue open diamonds and heavy dashed lines represent monthly mean CO concentrations calculated by the model. Solid thin blue lines depict the daily variation in the model data.

both in terms of seasonality and magnitude. The model also shows a good agreement with tropical sites in the northern hemisphere (e.g., Easter Islands, Canary Islands, Midway). The model reproduces the seasonal cycle and spring maximum in the southern tropics (Ascension Island and American Samoa) fairly well, which is governed by the seasonal biomass burning emissions (July to October in the southern hemisphere). However, the peak in CO is one month early at Ascension and overestimated but in phase at the Samoa site.

The comparison suggests that the model is capable of reproducing CO concentration well at locations where well constrained anthropogenic CO sources contribute a significant portion of the emissions (practically all of the northern hemisphere). In the southern hemisphere, where CO concentrations are generally lower and are dominated by biomass burning and, to some extent at southern high latitudes, even by the oceanic source, the model has a tendency of overestimating CO concentrations. This is most likely due to the CO biomass burning emission set, but could also be caused by an overestimate of the VOC emissions with subsequent in-situ formation of CO by photooxidation or an underestimate of the concentration of hydroxyl radicals near the surface at these locations. In general though, the tendency to underestimate CO concentrations, persistent in many current chemistry models both taking and not taking into account VOC photochemistry (cf., e.g., Hauglustaine et al., 1998; Poisson et al., 2000; Bey et al., 2001; Hauglustaine et al., 2004), is not discernible in the NMHC version of LMDz-INCA, which we tentatively attribute to the spatial and time variability of the OH abundance well reproduced by the model (cf. Sect. 3.2).

3.2 Hydroxyl radical and methane concentration

OH is most abundant in the tropical lower and mid troposphere reflecting high levels of ultraviolet radiation and water vapour. OH concentrations can reach 20 to 30×10^5 molecules cm^{-3} in this atmospheric domain and decrease with altitude due to a decline in water vapour abundance.

The global mean OH concentration as calculated by the model can be evaluated by using the methylchloroform (CH_3CCl_3) lifetime as a proxy (Spivakovsky et al., 1990; Prinn et al., 1995). Spivakovsky et al. (2000) calculated a global mean atmospheric lifetime of 4.6 years for methylchloroform, in close agreement with Prinn et al. (1995). Assessing stratospheric and oceanic sinks for CH_3CCl_3 with corresponding lifetimes of 43 and 80 years respectively, Spivakovsky et al. (2000) established a tropospheric methyl chloroform lifetime against OH reaction of 5.5 years. Houweling et al. (1998), Wang et al. (1998a), Mickley et al. (1999), and Bey et al. (2001) obtained corresponding lifetimes of 5.3, 6.2, 7.3, and 5.1 years from their model calculations, respectively. LMDz-INCA calculates a tropospheric CH_3CCl_3 lifetime with respect to oxidation by OH of 5.5 years in excellent agreement with the estimates of

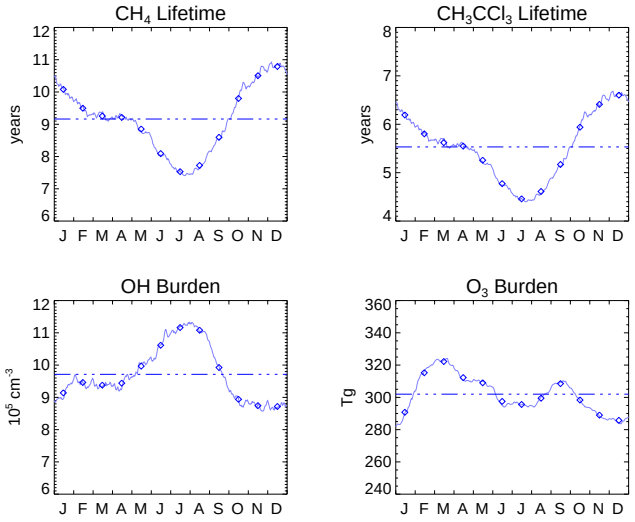

Fig. 3. Seasonal cycle of the globally averaged CH_4 and CH_3CCl_3 tropospheric lifetimes, OH abundance, and O_3 burden for the entire troposphere. Also shown are annual mean values of the above quantities (dashed-dotted lines).

Spivakovsky et al. (2000) and Prinn (2001) and well within the range of previously mentioned model studies.

A similar relation persisting between atmospheric methane lifetimes and hydroxyl radical concentrations, OH being the most important atmospheric CH_4 sink, can be used to further evaluate model performance in terms of photochemical activity. The annual mean tropospheric CH_4 lifetime due to reaction with OH as calculated by the model amounts to 9.2 years. In the 2001 IPCC report (Prather et al., 2001) an estimate for this quantity has been given suggesting a an annual mean tropospheric methane lifetime of 9.6 years. LMDz-INCA is in quite close agreement with this IPCC assessment. Fig. 3 summarizes the seasonal cycle of the globally averaged chemical lifetimes of methane and methylchloroform, the hydroxyl radical abundance, and the tropospheric ozone burden. The model calculates global annual mean tropospheric values of 9.6×10^5 molecules cm^{-3} and 303 Tg for the OH abundance and ozone burden, respectively.

As already mentioned, the OH abundance to a large extent defines the oxidizing capacity of the atmosphere (cf. Levy, 1971). Using OH concentrations calculated by LMDz-INCA, we give an assessment of the photochemical activity of the troposphere broken down into nine different subdomains based on recommendations by Lawrence et al. (2001). The subdomains are defined as follows: horizontal subdomains are the northern extratropics (NET, 90°–30° N), tropics (TRO, 30° N–30° S), and southern extratropics (SET, 30°–90° S). Vertical subdomains are defined as the planetary boundary layer (PBL, below 750 hPa), free troposphere (FT, 750–500 hPa), and upper troposphere and tropopause region (UT, 500–250 hPa), respectively. The results are summarized in Table 6.

Table 6. Break-down of annual average hydroxyl radical concentrations classified by tropospheric subdomains (10^5 molecules cm^{-3}). Horizontal domains: northern extratropics (NET, 90°–30° N), tropics (TRO, 30°N–30° S), southern extratropics (SET, 30°–90° S); vertical domains: planetary boundary layer (PBL, below 750 hPa), free troposphere (FT, 750–500 hPa), upper troposphere and tropopause region (UT, 500–250 hPa), respectively. The rows and columns denoted by *TOT* and **TOT**, respectively, refer to the mean calculated over the specific horizontal layer or altitude range.

subdomain	PBL	FT	UT	*TOT*
NET	9.0	6.4	5.6	*7.8*
TRO	16.6	10.7	7.7	*12.5*
SET	5.3	4.4	4.5	*5.4*
TOT	**11.9**	**8.1**	**6.4**	***9.6***

From Table 6 it can be seen that the tropical planetary boundary layer has the highest oxidative capacity of all tropospheric subdomains with an annual mean OH abundance of 16.6×10^5 molecules cm^{-3}. The oxidative capacity calculated by the model decreases with increasing altitude, consistent with the current knowledge. Viewed over the entire altitude range, the tropical troposphere shows the highest oxidative capacity, in the southern extratropical troposphere OH concentrations are on average significantly lower.

Methane itself is a prognostic tracer in LMDz-INCA. The model takes into account various primary sources of CH_4 (cf. Table 5), transport and mixing, tropospheric-stratospheric exchange, and atmospheric oxidation. A global sink of approximately 30 Tg yr^{-1} due to consumption of CH_4 by methanotropic bacteria in soil has been identified (cf., e.g., Prather et al., 2001). The uncertainties around this processes are still quite high and are expressed in terms of an uncertainty factor of 2. This process, though, is not accounted for in our model at the present. The sink would account for approximately 5% of the global primary source of methane. Non-neglible but small on the global scale, this sink could potentially be of importance on the regional scale, since it is concentrated over the continental areas and varies with soil conditions.

The methane concentration at the surface as depicted in Fig. 4 exhibits a pronounced seasonal cycle in both the CMDL measurements and the model with a minimum during the local summer months when photochemical depletion via reaction with OH is most active. The observed magnitude and phase of the seasonal variation in methane is fairly well reproduced by the model. Differences between model and observations are most pronounced at northern midlatitude continental stations. The agreement between model and observations increases at stations in the tropics and the southern hemisphere representative of tropospheric background conditions. At these stations the model shows less diurnal variation which we contribute to a decreased influence of the rapid photochemistry of NMVOC which also produces significant amounts of CH_4. This absence of photochemistry on short time-scales of hours or days could affect the comparison between climatological observations and the calculated methane concentration.

3.3 Nitrogen compounds

The importance of nitrogen compounds is a consequence of their role in the budget of other key tropospheric species, such as ozone and the hydroxyl radical. Odd nitrogen is mainly released in the form of NO, predominantly as a result of combustion processes (fossil fuel combustion, biomass burning) and soil microbial activity. Global lightning activity also represents a significant atmospheric source of NO. Once emitted, NO is rapidly converted by photochemical processes into other states of oxidation (NO_2, NO_3, N_2O_5) as well as HNO_3 and organic nitrates, including peroxyacetyl nitrate (PAN).

A comparison of observed and calculated profiles of NO_x and PAN are shown in Figs. 5 and 6. The calculated NO_x mixing ratio is generally in good agreement with observations, given the large spatial and time variability in this short-lived species. The typically "C-shaped" profiles with higher mixing ratios in the PBL and the upper troposphere as well as decreased mixing ratios in the free troposphere are also well captured. The model, however, overestimates NO_x over Ireland during SONEX below 8 km which could be due to an overestimate of the anthropogenic NO_x source in EDGAR v3.2 or the export of NO_x from the continent being too strong in our model over this region. The model underestimates NO_x concentrations in the upper troposphere during SUCCESS.

Organic nitrates in general, and in particular peroxyacetyl nitrate (PAN), are chemically more stable compounds than NO_x. PAN is the most abundant organic nitrate that has been detected in the atmosphere resulting from a variety of organic precursors, such as isoprene, acetaldehyde, and alkanes (e.g. Roberts, 1990; Altshuller, 1993). Predominantly produced in the PBL by reaction of peroxyacetyl radicals with NO_2, PAN subsequently becomes subject to long-distance transport to remote environments and to the free troposphere, where it acts as a reservoir of NO_x. Eventually, NO_x is released following thermal decomposition and photolysis (Crutzen, 1979; Kasibhatla, 1993; Moxim et al., 1996). PAN lifetimes vary from a few hours in the lower troposphere, where thermal decomposition effectively limits its residence time, to several months in the free and upper troposphere. LMDz-INCA also considers PAN analogs that derive from higher NMHC as well as other bulk organic nitrate species (cf. Table 1). They generally have shorter atmospheric lifetimes and, hence, significant concentrations are found only in the PBL.

Calculated profiles of the PAN mixing ratio are mostly within one standard deviation of the observations, but show

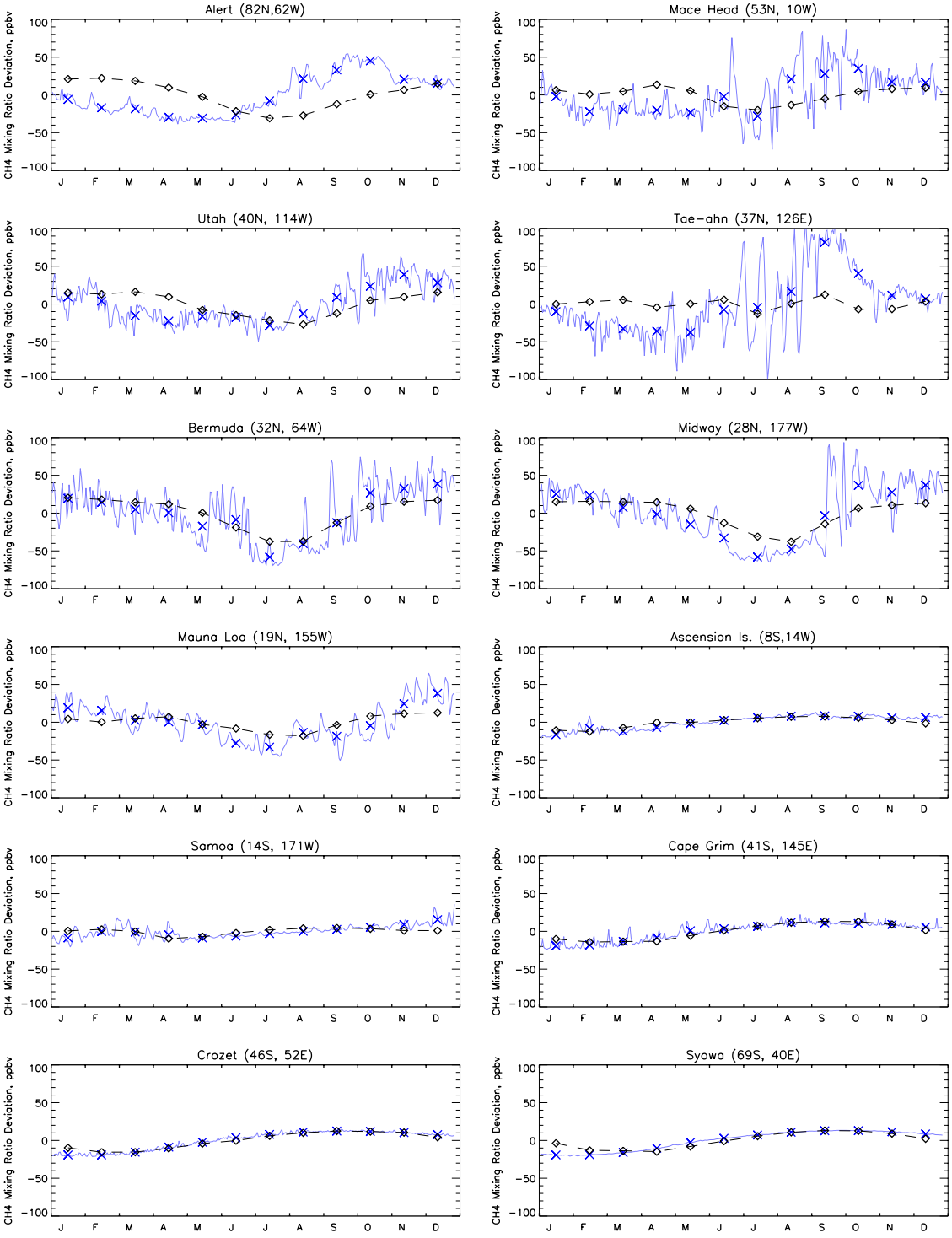

Fig. 4. Calculated (solid line is day-to-day variation and diamonds denote monthly means) and measured (by Dlugokencky et al. (1998) (black diamonds) at CMDL network stations) CH_4 mixing ratio deviation from the annual mean (ppbv) at selected surface sites.

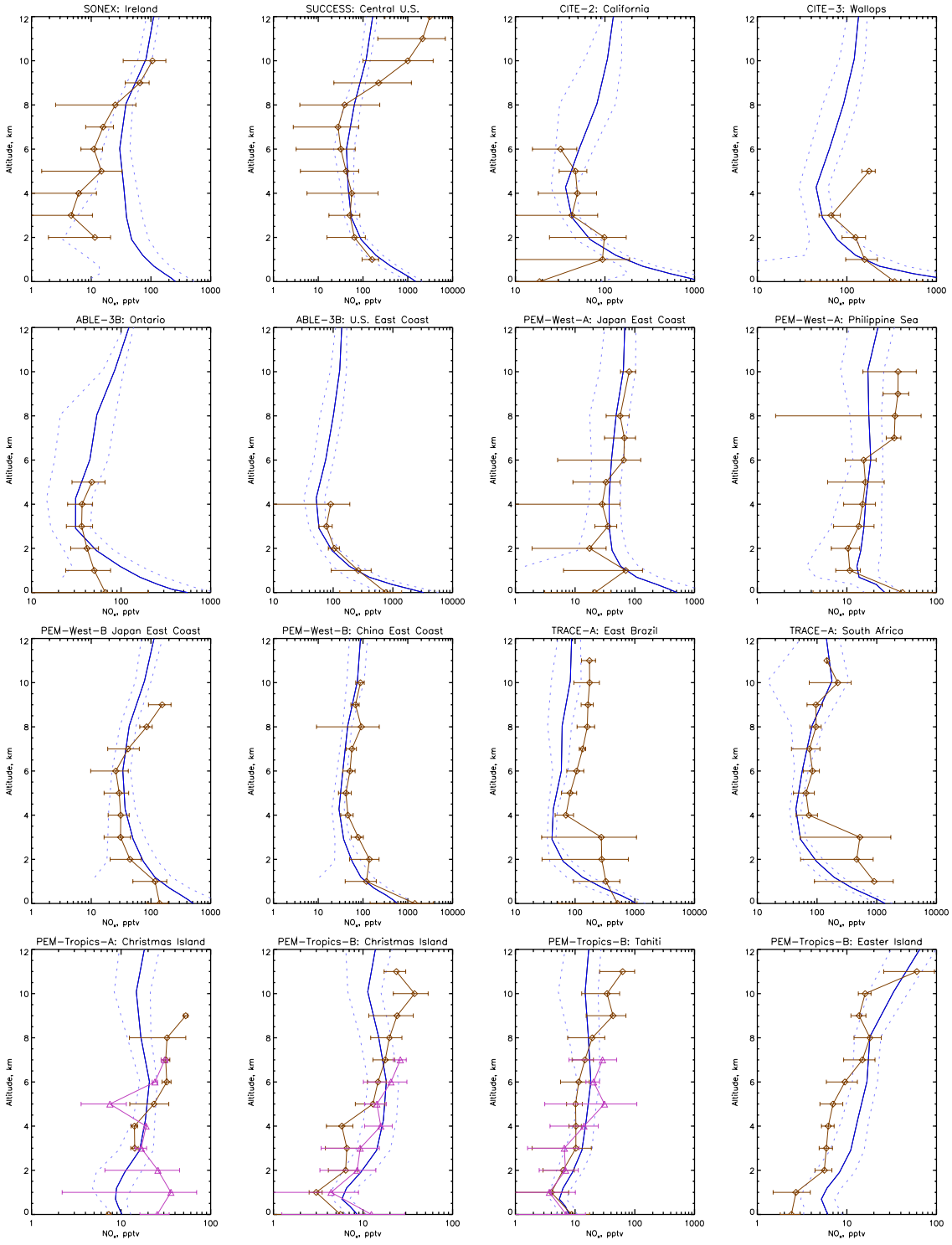

Fig. 5. Comparison of calculated and observed (Emmons et al., 2000) vertical profiles of the NO_x mixing ratio (pptv). Model results are shown as solid blue lines with dotted blue lines marking one standard deviation. Open diamonds represent mean observed values (with horizontal bars denoting the standard deviation). In case an additional data set is available deriving from a second aircraft used during a specific campaign, these data have been included and are denoted by open triangles. Simulated values have been sampled from the model output over the same region and month as the observational data.

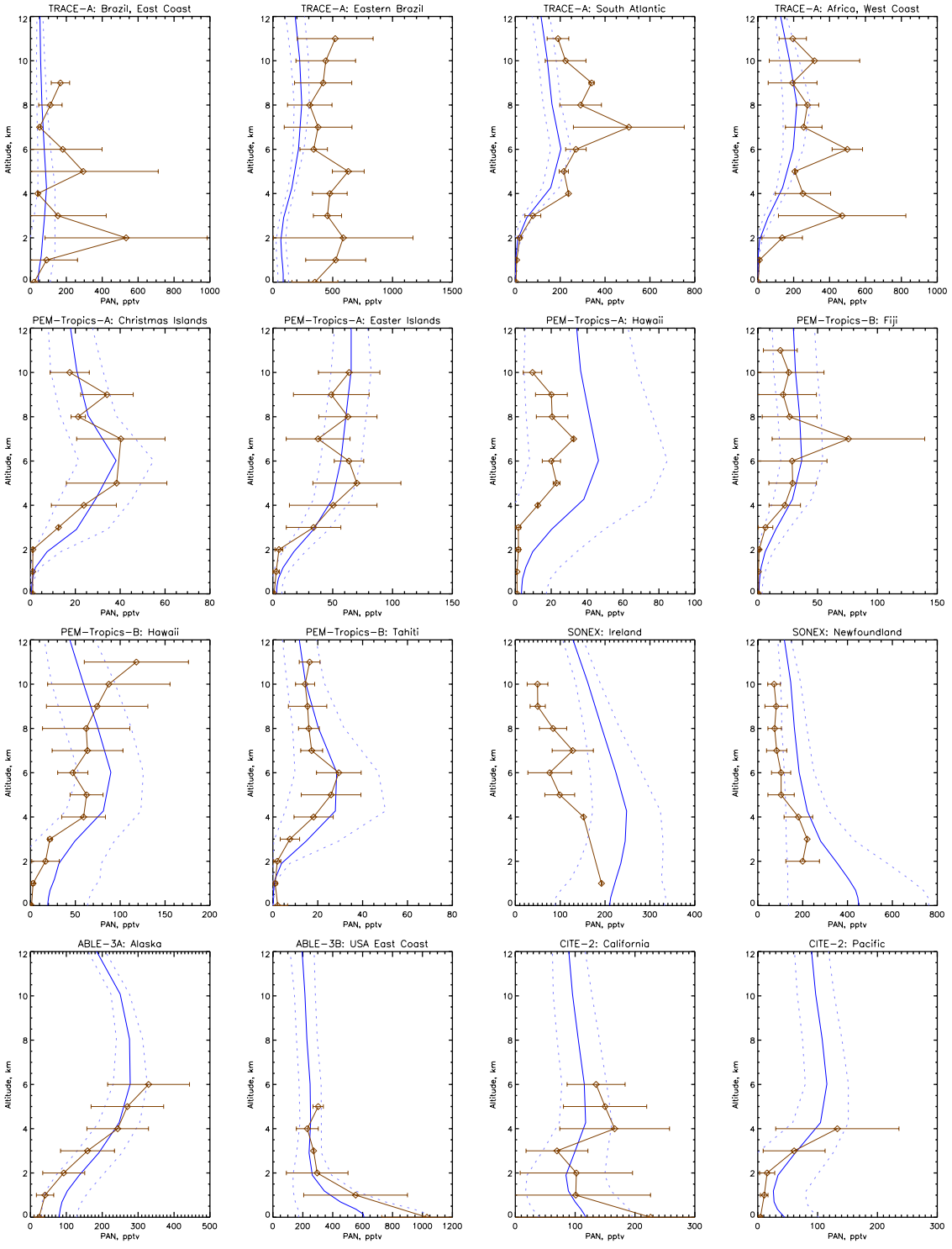

Fig. 6. Same as Fig. 5, but for PAN.

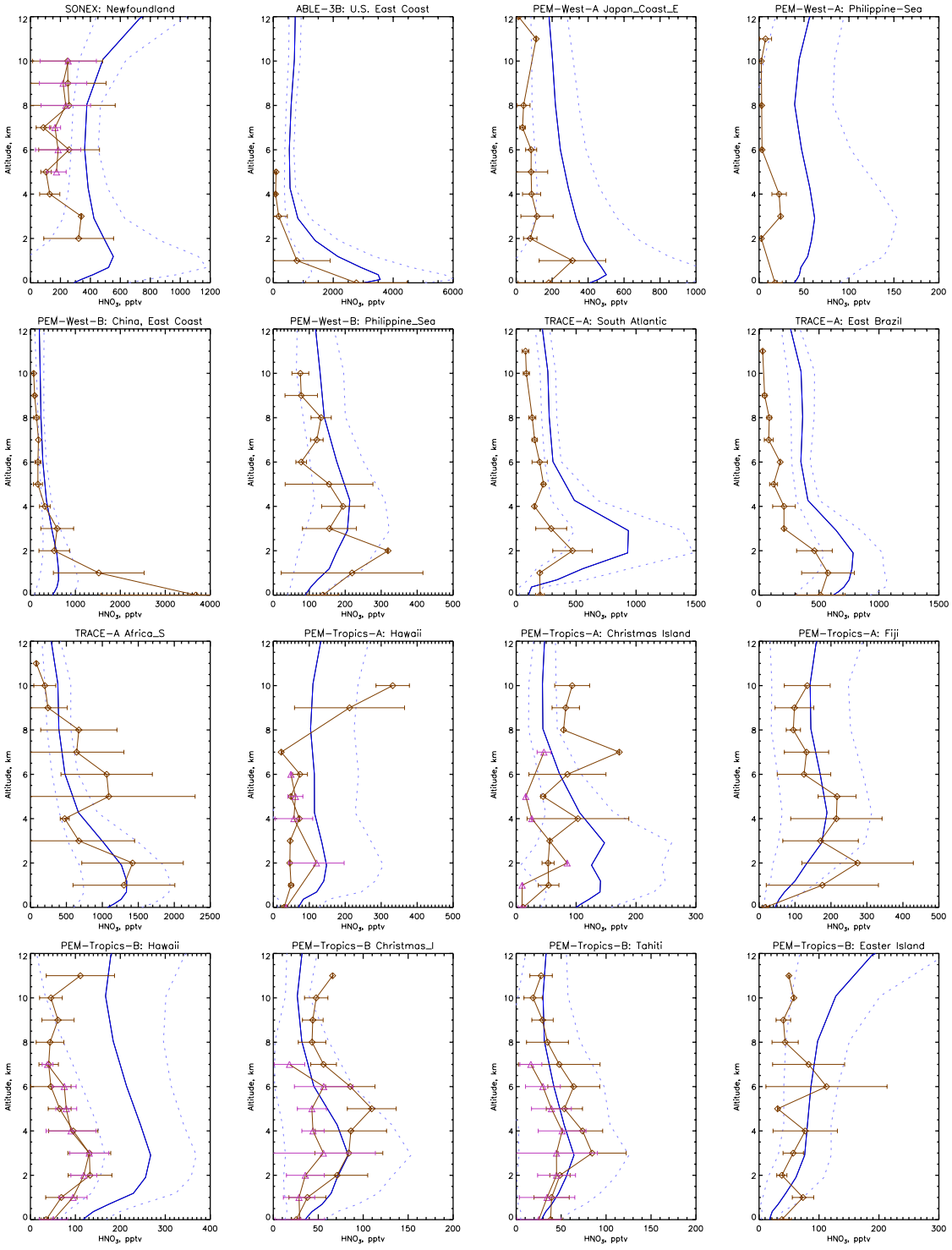

Fig. 7. Same as Fig. 5, but for HNO_3.

a tendency to underestimate PAN in regions affected by biomass burning as during TRACE-A. A tendency to overestimate PAN over polluted areas as during SONEX is also discernible. The model seems to better reproduce PAN profiles over unpolluted remote regions (PEM-West, PEM-Tropics, TRACE-A) than over regions with a strong continental influence (SONEX, ABLE). Observed PAN concentrations show a maximum between approximately 4 and 8 km depending on the individual location. This mid-tropospheric maximum is a consequence of an increasing lifetime against thermal decomposition with increasing altitude and a decreasing lifetime against photolysis with increasing altitude. The model qualitatively and quantitatively captures this feature reasonably well.

Nitric acid (HNO_3) in the atmosphere is produced by reaction of NO_2 with OH and by hydrolysis of N_2O_5; major sinks are dry and wet deposition. Comparison of simulated vertical profiles of HNO_3 with observations as shown in Fig. 7 reveals a pronounced tendency of LMDz-INCA to overestimate HNO_3 concentrations, typically by a factor of two. The largest deviations are found in the upper troposphere between 9 and 12 km. This problem is common to most current global 3-D models of tropospheric chemistry (Hauglustaine et al., 1998; Lawrence et al., 1999; Poisson et al., 2000; Bey et al., 2001; Hauglustaine et al., 2004). However, in the NMHC implementation of LMDz-INCA this tendency to overestimate HNO_3 concentrations seems to be less pronounced. Bey et al. (2001) have suggested partitioning of nitric acid into aerosols as a possible explanation for this common model deficiency, since most current tropospheric chemistry model do not differentiate between gaseous and aerosol nitrate as is also the case for LMDz-INCA. Studies by Bauer et al. (2004) with a version of LMDz-INCA including such fractionation processes but without NMVOC photochemistry seem to support this argument. A better agreement between calculated HNO_3 concentrations and observations is obtained over remote regions, in particular during the PEM-Tropics campaigns, indicating that HNO_3 overestimation in the model is most pronounced over areas with high NO_x emissions.

3.4 Methanol, acetone, and other VOC

The seasonal mean methanol mixing ratio at the surface is depicted in Fig. 8 for the winter and summer seasons. The principal global CH_3OH source is plant growth. Methanol surface mixing ratios as calculated by the model follow the global seasonal vegetation cycle with low values at mid- and high latitudes in the winter hemisphere, elevated levels in the same latitudinal range in the summer hemisphere, and year-round relatively high mixing ratios over continental areas in the tropics. The methanol mixing ratio ranges between 10 and 25 ppbv over tropical South America and Africa during the winter season and reach 30 to 40 ppbv over Southeast Asia and the Eastern United States during the summer season.

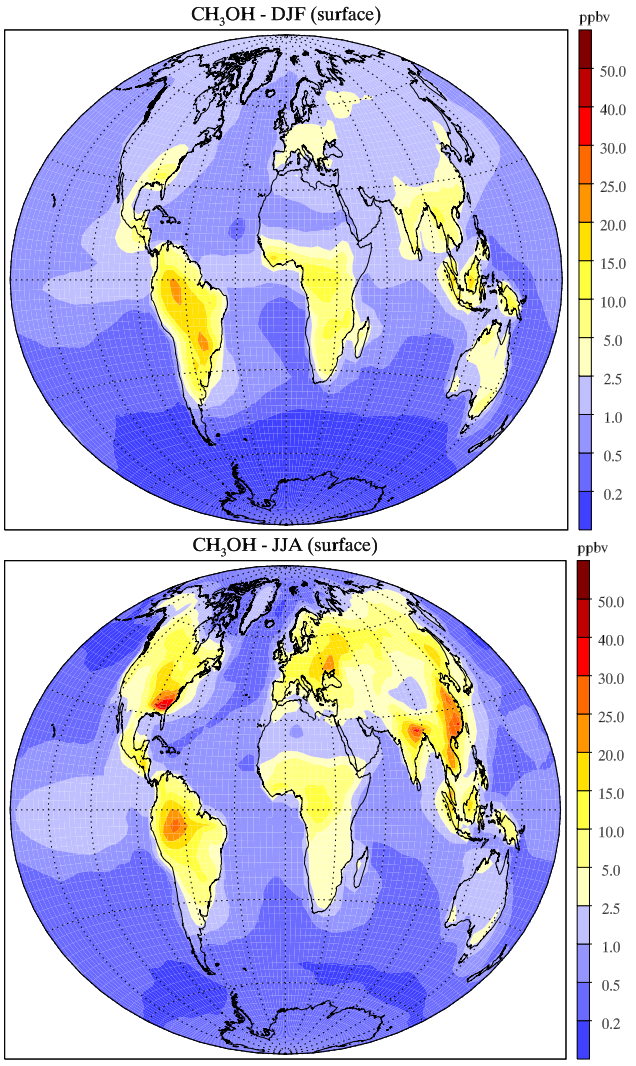

Fig. 8. Methanol surface mixing ratio for winter and summer season (ppbv).

Calculated vertical CH_3OH profiles are compared to observations in Fig. 9. The model shows a tendency to underestimate the methanol mixing ratio over remote areas (observations from PEM-Tropics B) where measured values can be higher by up to a factor of 2.5 in the lower troposphere. Generally, the agreement is better at higher altitudes. On the other hand, the model seems to overestimate CH_3OH significantly at northern hemispheric midlatitudes as compared to measurements from the SONEX campaign.

Formaldehyde (CH_2O) in the atmosphere originates from various sources. These include fossil fuel combustion (minor), biomass burning and biogenic surface emissions as well as substantial secondary in-situ sources. This secondary photochemical source derives from photooxidation of methane and non-methane hydrocarbons, the most important of which

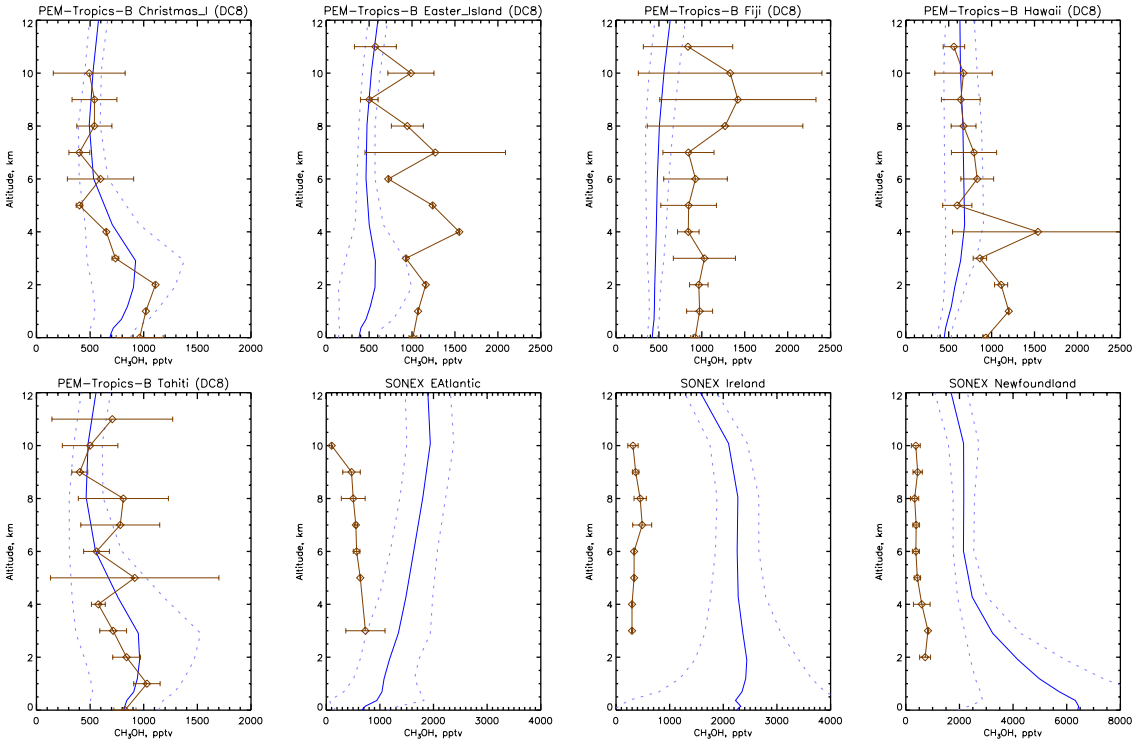

Fig. 9. Same as Fig. 5, but for methanol.

is isoprene. Figure 10 shows a comparison of the seasonal variation in CH_2O mixing ratios as calculated by the model with observations near the surface. Observational data has been collected in the framework of the CMDL network. Most of the available data has been collected at northern hemispheric midlatitudinal stations, except Zeppelin which is located at polar latitudes. The model shows a fair agreement with the observations at several stations but considerably underestimates formaldehyde concentrations at Ispra, Mace Head, and Zeppelin.

Figure 11 compares simulated formaldehyde profiles to aircraft measurements for various campaigns. Profiles calculated by LMDz-INCA are in good agreement with observations collected during SONEX which are representative of near continental regions under the influence of both primary and secondary CH_2O sources. The model shows a fairly good agreement close to the surface with observations obtained during TRACE-A near Brazil. This campaign was conducted during September and October of 1992 and covered a period of the year which is characterized by high net primary production of the vegetation in the southern hemisphere. The fairly good agreement would indicate that the isoprene emissions calculated with ORCHIDEE for the Amazon region are reasonable in magnitude, at least for this period of the year. Furthermore, fairly good agreement is achieved with data gathered during the PEM-Tropics B campaign. The region covered by this campaign can be considered typical for remote regions of the troposphere dominated by background conditions, a diminished continental influence that, if apparent, stems from long-range transport, and only weak local primary sources. The most pronounced deviation between model and measurements occurs for the TRACE-A campaign at the South Atlantic location, where LMDz-INCA seems to overestimate observed formaldehyde concentrations in the lower and middle troposphere by up to a factor of three. This disagreement could be related to sources of formaldehyde or its precursors from biomass burning or biogenic formation being too high in our emission inventory near this region (South American continental sources).

Vertical profiles of acetone from the model and observations are compared in Fig. 12. Over most regions (including those sampled during PEM-West B and PEM-Tropics B) the model estimates of the acetone mixing ratio agree fairly well with the observations. The higher levels observed during the TRACE-A campaign over Brazil and Africa, also well simulated by the model, are related to acetone emissions from biomass burning. The model captures the vertical gradients in most cases. It generally also reproduces the acetone mixing ratios observed in the Asian outflow during PEM-WEST B, but significantly overestimates acetone at the near continental sites measured during the SONEX campaign. However, acetone profiles calculated by LMDz-INCA do agree quite well with observations obtained during the ABLE-3B (Singh et al., 1994a) experiments.

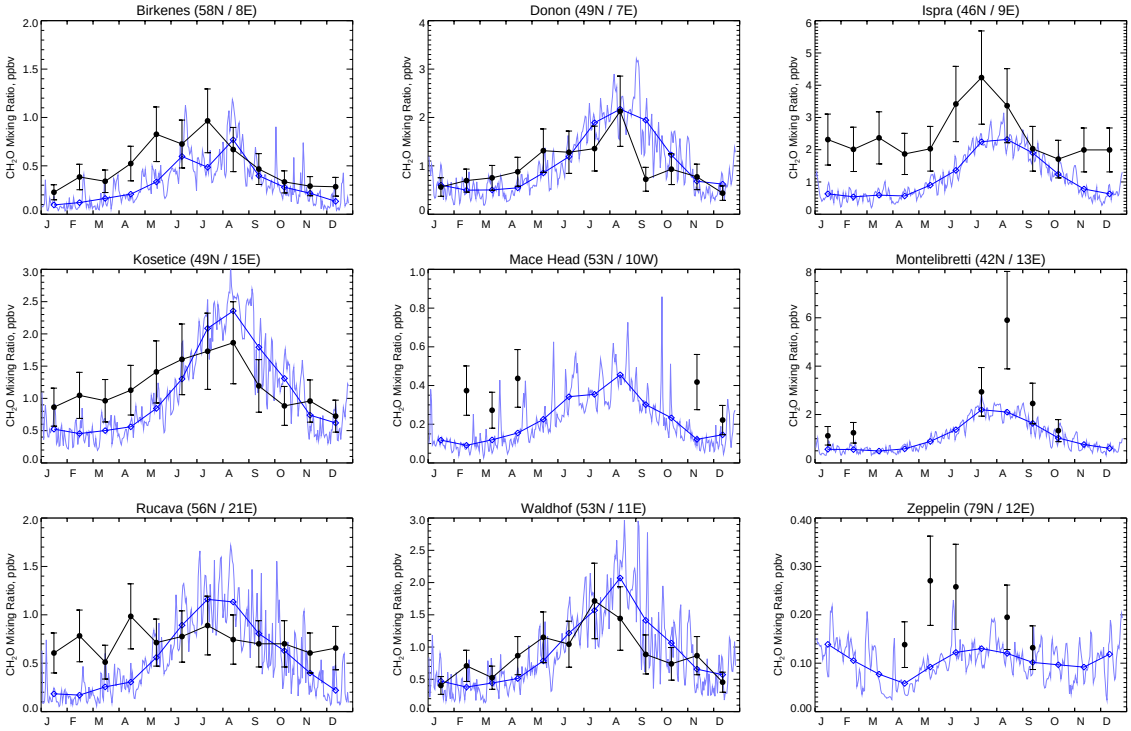

Fig. 10. Same as Fig. 2, but for CH_2O.

The observations gathered during PEM-Tropics B indicate surprisingly large abundances of acetone over the tropical Pacific (Singh et al., 2001), a region where most models previously predicted quite low concentrations (cf., e.g. Hauglustaine et al., 1998; Bey et al., 2001; Horowitz et al., 2003). These observations suggest the presence of a large natural, distributed source of oxygenated organic species as has been discussed by Horowitz et al. (2003). The current version of LMDz-INCA does not seem to show the same disagreement, possibly owing to the inclusion of an oceanic source for acetone based on the Jacob et al. (2002) recommendations.

3.5 Ozone

Figure 13 shows seasonal mean ozone mixing ratios calculated near the surface for the winter and summer seasons. Maximum mixing ratios reaching 50 to 70 ppbv are calculated over industrialized regions of the northern hemisphere during summertime, where strong biogenic NMVOC sources combine with pronounced NO_x concentrations (Eastern United States, Europe, Southeast Asia). Elevated ozone levels of up to 50 ppbv are also visible over ares with intense biomass burning emissions in the tropical continental domain. In general, the ozone distribution as calculated by LMDz-INCA is in good agreement with previous studies (cf. e.g. Hauglustaine et al., 1998; Wang et al., 1998b; Poisson et al., 2000; Bey et al., 2001; Horowitz et al., 2003).

Over the oceans the ozone background mixing ratio is generally less than 25 ppb in both hemispheres except over the North Pacific and the North Atlantic during wintertime, where export of O_3 from the continental boundary layer is clearly visible. In regions remote from any pollution sources, such as the Central Pacific Ocean, the Indian Ocean, or the Southern Ocean, ozone mixing ratios can drop to less than 15 ppb. A summertime minimum with less than 15 ppbv of ozone is calculated over the North Pacific, where NO_x concentrations are very low while ozone destruction by photolysis is significant.

Figure 14 provides an evaluation of the surface ozone mixing ratio as derived by the model by comparison with measurements at 15 selected stations. Observational data have been taken from the CMDL network (cf. Komhyr et al., 1989; Oltmans et al., 1989; Oltmans and Levy II, 1992, 1994) and represent monthly means, averaged over the total observational record at each station, which cover between 5 and 10 years. In general, calculated monthly mean ozone mixing ratios as well as the simulated seasonal cycle are in good agreement with the observed values at most sites. The simulated ozone mixing ratios reproduce generally well the observed values in subtropical regions and at midlatitudes in the Northern Hemisphere (Mace Head, Payerne, Hohenpeissenberg, Sable Island, Zugspitze, Mauna Loa). The model fails to capture the arctic springtime ozone minimum at Barrow, which has been attributed to bromine catalysed ozone depletion events (Barrie et al., 1988; Tang and McConnell,

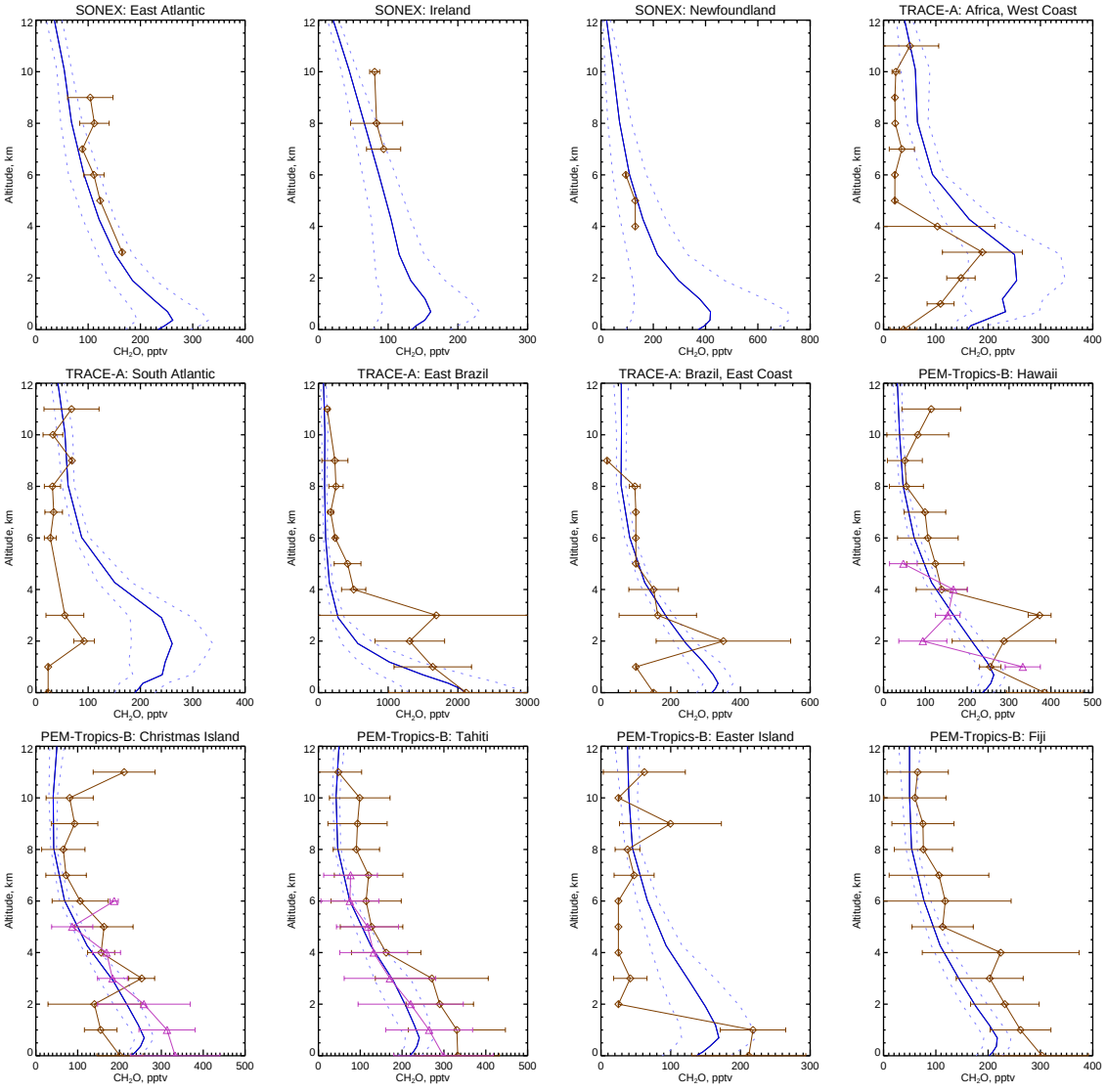

Fig. 11. Same as Fig. 5, but for formaldehyde.

1996; Martinez et al., 1999; Wennberg, 1999). In the Southern Hemisphere, the seasonal cycle and magnitude of ozone is fairly well reproduced at subtropical- (American Samoa) and mid latitudes (Cape Grim), but both the seasonality and magnitude are considerably underestimated at South Pole during most of the year (April to November). As photochemistry is slow in the polar regions, a connection of this discrepancy with transport processes seems likely.

The vertical distribution of the ozone mixing ratio as calculated by LMDz-INCA is evaluated against ozone soundings in Fig. 15. The observations are taken from the climatology described by Logan (1999). The comparison confirms the general good agreement with the observations at most stations. With only a few exceptions, model results are within 10 to 15 ppb of the observed values, they are well within their observed variability ($\pm 1\sigma$ standard variation), and show the correct seasonal phase.

At high northern latitudes (Alert station) the model captures the spring maximum in the lower troposphere and the maximum from May to August in the middle troposphere. The model underestimates, though, the monthly mean mixing ratios during spring and summer near the tropopause and also visibly underestimates the observed variability. The weakly developed variability in simulated upper tropospheric ozone as compared to the observations has been attributed to an overestimate of the tropopause height by the GCM (Hauglustaine et al., 2004) resulting in lower than observed O_3 mixing ratios in the above 300 hPa region.

Seasonal variations at northern mid-latitudes are fairly well reproduced (Hohenpeissenberg, Payerne). The timing of the ozone maximum in polluted regions (spring in the upper troposphere and a gradual shift toward the summer season with decreasing altitude) is also generally well reproduced by the model to within the constraints offered by

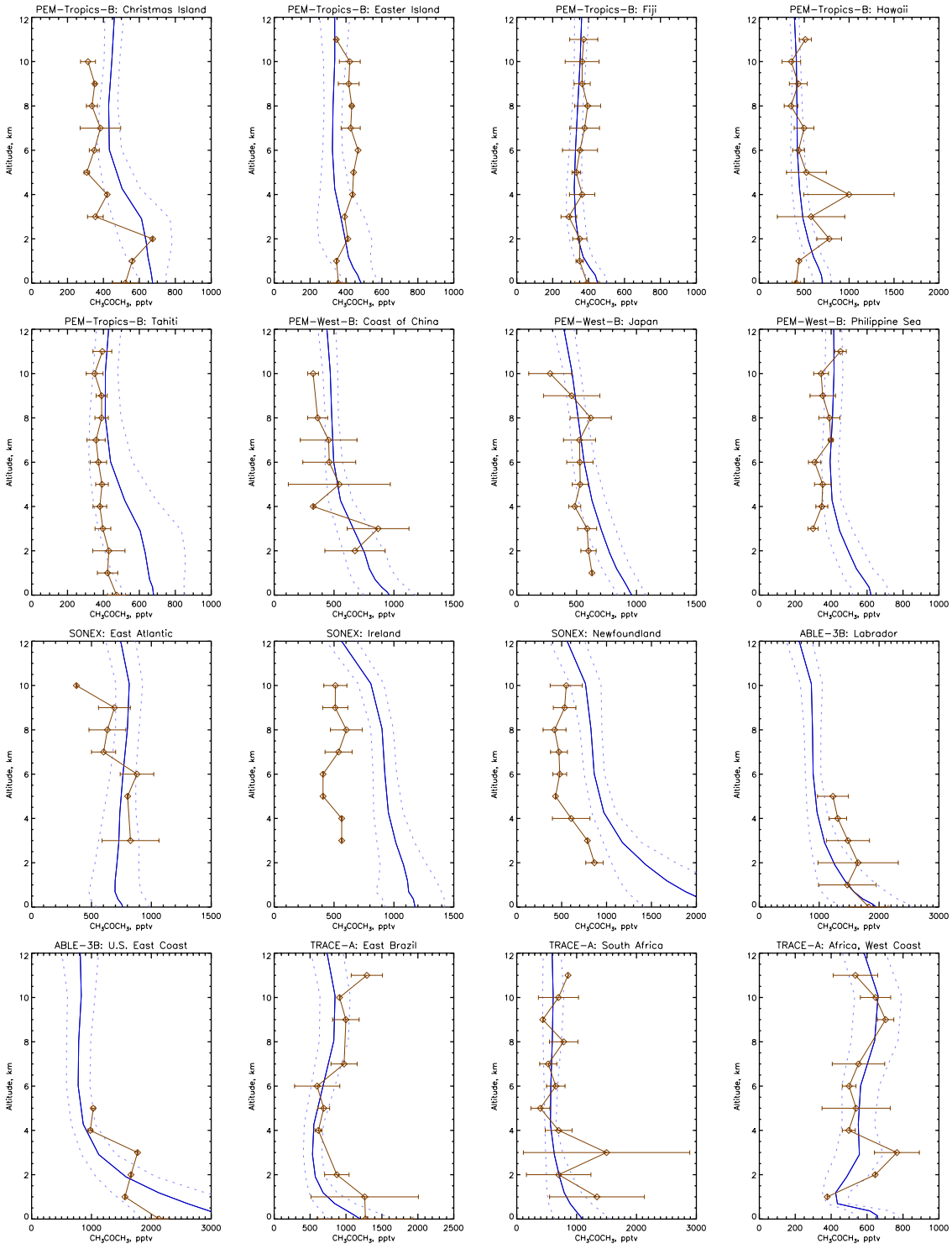

Fig. 12. Same as Fig. 5, but for acetone.

the observations at mid-latitude stations (Sapporo, Payerne, Boulder). A good model-to-measurement agreement over the entire troposphere is achieved at tropical (American Samoa) and at southern midlatitude (Asperton) stations.

Table 7 provides an estimate of the annual ozone budget in the troposphere (defined as the domain extending from the surface up to 200 hPa) as calculated with LMDz-INCA. The results indicate that sources and sinks in the troposphere

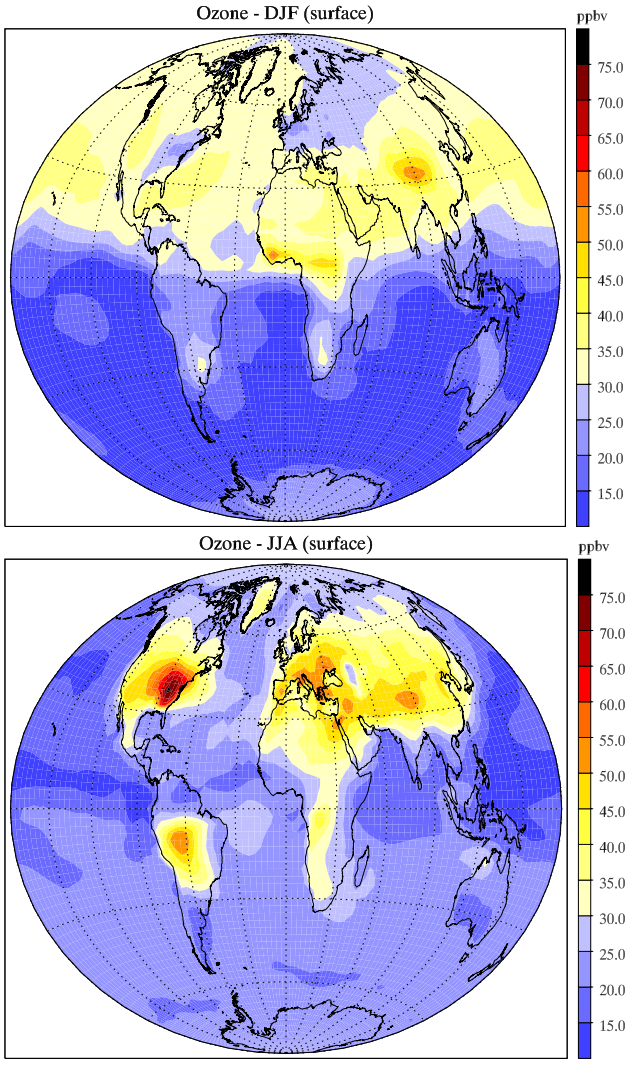

Fig. 13. Ozone surface mixing ratio for winter and summer season (ppbv).

Table 7. Global Tropospheric Ozone Budget in LMDz-INCA ($Tg\,O_3\,yr^{-1}$).

	Global	Northern Hemisphere	Southern Hemisphere
Photochemical production	4436	2773	1663
Stratospheric influx	715	366	349
Photochemical destruction	−3890	−2304	−1586
Dry deposition	−1261	−835	−426
Net photochemistry	546	469	77
Ozone Burden ($Tg\,O_3$)	303	178	125

are dominated by photochemistry. The global photochemical ozone production and destruction amount to 4436 and 3890 $Tg\,O_3\,yr^{-1}$, respectively. Clearly, gross photochemical production by far exceeds stratospheric influx, which contributes 715 $Tg\,O_3\,yr^{-1}$ to the total tropospheric budget. Net tropospheric photochemical production of ozone, calculated as the difference between gross production and destruction, totals 546 $Tg\,O_3\,yr^{-1}$.

According to the calculations with LMDz-INCA, 1261 $Tg\,O_3\,yr^{-1}$ are removed from the troposphere by dry deposition at the surface. Dry deposition of ozone is almost two times more effective in the Northern Hemisphere (835 $Tg\,O_3\,yr^{-1}$) than in the Southern Hemisphere (426 $Tg\,O_3\,yr^{-1}$). This can be explained by the fact that the northern hemispheric continental area substantially exceeds the southern hemispheric land mass and by the rather weak solubility of ozone in water which significantly limits ozone surface deposition rates over the oceans. The average photochemical ozone lifetime calculated on the basis of the tropospheric ozone burden of 303 Tg and the photochemical destruction is 28.4 days. Taking into account physical removal of ozone by dry deposition, the tropospheric O_3 lifetime is 21.5 days on global average.

Photochemical production of ozone is much more pronounced in the Northern Hemisphere (2773 $Tg\,O_3\,yr^{-1}$) than in the Southern Hemisphere (1663 $Tg\,O_3\,yr^{-1}$), likely due to the significant bias in NO_x sources toward the Northern Hemisphere related to a higher degree of industrialization as well as the overall stronger biogenic NMVOC surface flux from the terrestrial vegetation, the latter a consequence of the larger land mass in the Northern Hemisphere. More than 60% of the gross production occurs in the Northern Hemisphere and about than 85% of the net photochemical ozone production arises within the same hemisphere.

Previous studies with global 3-D models indicate photochemical production rates ranging from 3314 to 4550 $Tg\,O_3\,yr^{-1}$ and photochemical loss rates in the range between 2511 and 4065 $Tg\,O_3\,yr^{-1}$ (World Meteorological Organisation, 1998; Lelieveld and Dentener, 2000; Prather et al., 2001). Given these numbers, net photochemical production is estimated to amount between 485 and 803 $Tg\,yr^{-1}$. Stratospheric inputs in these models vary from 390 to 768 $Tg\,O_3\,yr^{-1}$ (World Meteorological Organisation, 1998). The estimates calculated by LMDz-INCA are well within the range given by previous models, even though they reside on the high end.

Global tropospheric photochemical production and loss of ozone are fairly similar to previous results obtained with the CH_4-only version of LMDz-INCA (Hauglustaine et al., 2004), but dry deposition (1261 $Tg\,O_3\,yr^{-1}$ as opposed to 1090 $Tg\,O_3\,yr^{-1}$ in LMDz-INCA-CH_4) and net stratospheric influx (715 $Tg\,O_3\,yr^{-1}$ versus 523 $Tg\,O_3\,yr^{-1}$, respectively) have changed significantly. It is difficult to attribute these changes to one specific process because several portions of the model have evolved during the transition from LMDz-

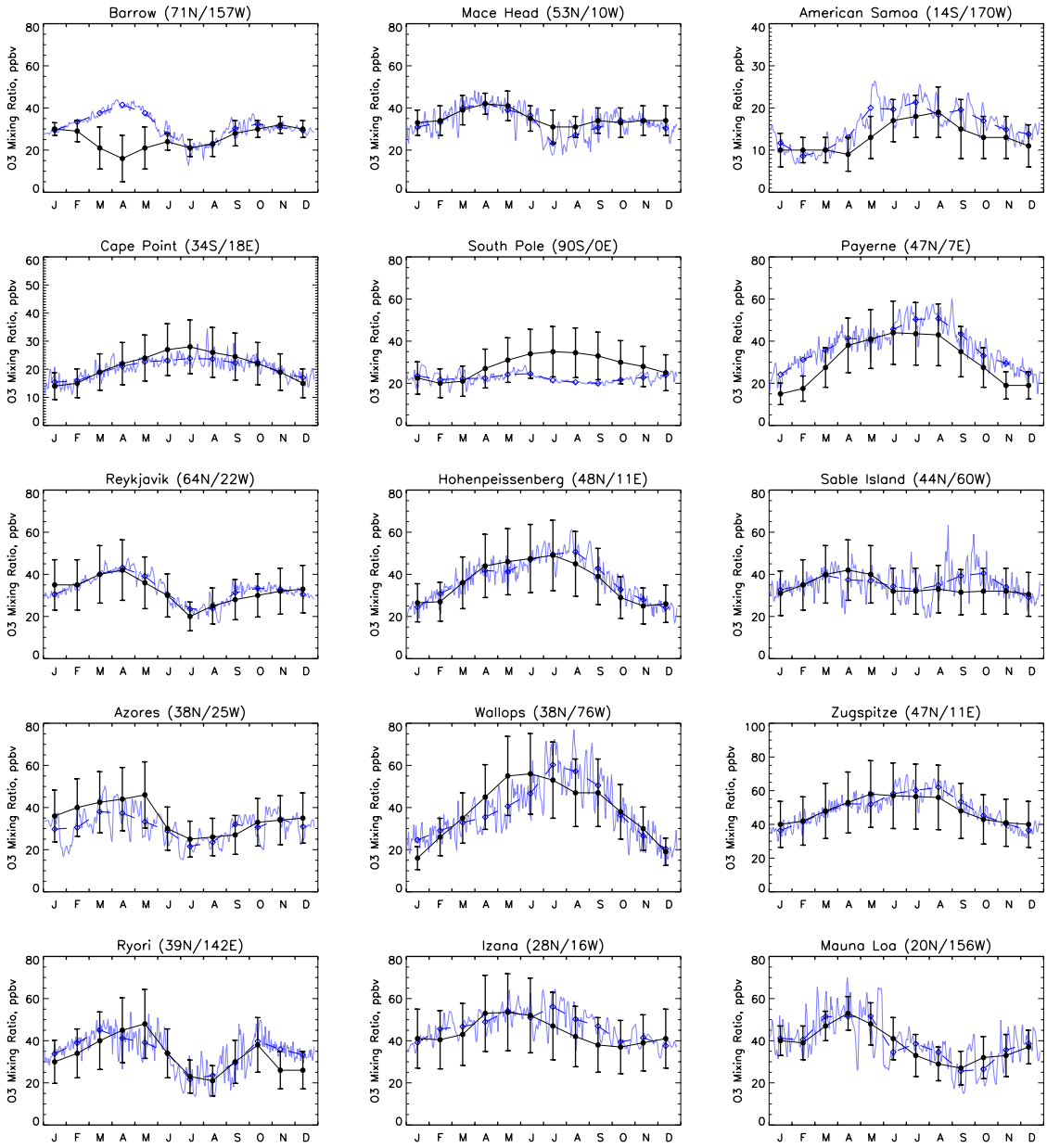

Fig. 14. Same as Fig. 2, but for O_3.

INCA-CH_4 to the NMHC version including the model dynamics as well as the dry deposition scheme. The tropospheric ozone budget is sensitive to all those changes. This fact needs to be borne in mind when comparing the ozone budgets for both model versions. Apparently, substantial uncertainties still persist around the calculation of net stratospheric ozone influx that have to be addressed in future work.

The NMHC-version of the model also shows a substantially more pronounced imbalance in the net photochemical production of ozone between the two hemispheres (469 and 77 Tg O_3 yr^{-1} for the northern and southern hemisphere, respectively, as compared to 451 and 116 Tg O_3 yr^{-1} in the LMDz-INCA-CH_4 version) which we attribute to the impact of NMHC. The model calculates a global mean O_3 burden of 303 Tg O_3 which divides into a hemispheric burden of 178 Tg O_3 (59%) and 25 Tg O_3 (41%) for the northern and-southern hemisphere, respectively.

4 Results and discussion

The results presented in this section are based on a control run which is identical to the run used in the model evaluation. As mentioned above, this control run has been taken over 30

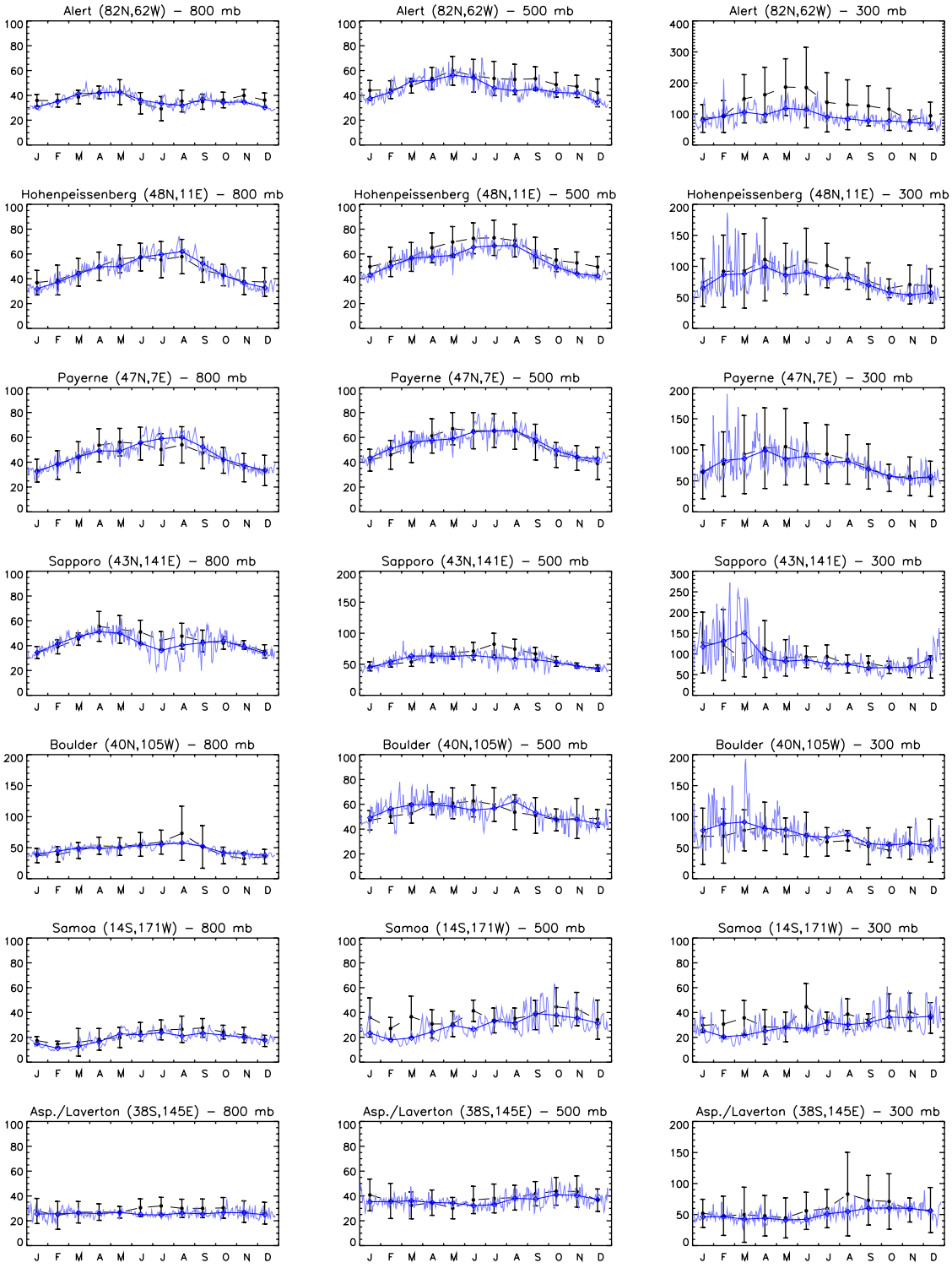

Fig. 15. Measured (solid circles) and calculated (solid light blues lines indicate day-to-day variations, open diamonds denote monthly mean values) seasonal cycle of O_3 mixing ratios (ppbv) at 7 stations and at the 800, 500, and 300 hPa levels. Observations were compiled by Logan (1999).

model months including a six months spin-up. The last 12 months have been used in the analysis. In addition, we conducted several model experiments to study various aspects of the impact of NMVOC on tropospheric chemical composition and photochemistry. These experiments are focused on the impact of biogenic NMVOC which have their predominant or unique source in the terrestrial biosphere, such as for instance isoprene or methanol.

To quantify the impact of these compounds, four experiments have been carried out assessing the impact of isoprene, biogenic methanol and acetone, as well as terpenes. In these experiments the respective emissions were turned off separately and changes in key tropospheric species, such as ozone, OH, NO_x and PAN, and HO_x have been analyzed. We note that non-linearities in photochemistry can somewhat bias the results of these sensitivity experiments affecting the oxidation capacity of the atmosphere, likely towards an increase in the reactivity (measured by the OH concentration) when turning off the emissions, because the highly reactive biogenic VOC are a strong OH sink. To quantify the uncertainties associated with the above mentioned non-linearities, we have performed an additional experiment with isoprene emissions reduced to 90% of their standard magnitude and compared the results to the "standard" experiment with zero isoprene emissions. All experiments were initialized with the July restart files of the first year of the control run and then continued over 18 model months. The last 12 months were used for comparison.

4.1 Impact of Isoprene

The major impact of isoprene on tropospheric photochemistry and chemical composition lies in its role as an ozone precursor and in the formation of organic nitrates in the course of isoprene photooxidation. Poisson et al. (2000) have shown that organic nitrate formation in the course of NMVOC oxidation is responsible only for a minor decrease of a few percent in NO_x concentrations over polluted regions. The impact of NMVOC oxidation via the formation of PAN and analogues significantly increases NO_x concentrations in remote environments with only feeble NO_x emissions, such as the marine PBL. Thermal decomposition of PAN can increase NO_x concentrations by almost a factor of 2, which is enough to significantly impact ozone and OH formation in these remote areas.

During the northern hemispheric winter isoprene emissions are located predominantly at southern hemispheric tropical latitudes. Emission rates reach maximum values of 60 to 70×10^{-11} kg m^{-2} s^{-1} over the Amazon and Kongo rain forest areas. At the same time, the NO_x emissions occur primarily at northern continental midlatitudes, where emission fluxes can reach up to 18×10^{-11} kg m^{-2} s^{-1} over the Eastern United States and Europe. A significant NO_x source of approximately 6×10^{-11} kg m^{-2} s^{-1} appears over equatorial Africa which derives from a pronounced soil source during the wet season in this region. In July the tropical isoprene sources have shifted toward the northern hemisphere. In addition, a large new sources appears over the entire northern hemispheric continental midlatitudes. Here emission rates are as high as 60×10^{-11} kg m^{-2} s^{-1} over the Eastern United States and Europe. On the other hand, the global distribution and magnitude of NO_x surface sources has not changed much with the only exception of the NO-soil source over equatorial Africa that is no longer present at this time of the year.

As a consequence, the global isoprene and NO_x surface sources appear to be separated in January during the northern hemispheric winter months. Half a year later, in July, these two sources coincide in many regions at northern hemispheric continental midlatitudes. This seasonally driven switch between separation and coincidence of NO_x and isoprene sources has important consequences for the chemistry of the lower troposphere. In January, isoprene oxidation largely proceeds under NO_x-limited conditions at southern low- and midlatitudes with only a weak, biogenically driven ozone formation potential in the PBL. For these regions and time of year the isoprene model experiment shows an increase in the ozone concentration at the surface of less than 8 ppbv as depicted in the upper left map in Fig. 16. Moreover, the most pronounced increase occurs close to the NO soil source over equatorial Africa. By contrast, the coinciding NO_x and isoprene surface sources in July clearly hold a strong ozone formation potential. This is reflected in the results of the isoprene experiment by a strong increase of ozone directly over the source regions of up to 30 ppbv over the Eastern United States and up to 20 ppbv over Europe as shown in the upper right map in Fig. 16. This positive and highly effective feedback between primarily anthropogenic NO_x and entirely biogenic isoprene surface sources during summertime frequently leads to high-ozone episodes with related air quality problems.

Furthermore, the changes in the ozone burden of the troposphere due to this coincidence-effect in particular and the biogenic isoprene source in general potentially could affect the radiative budget and, hence, contribute to climate change. To quantify the magnitude of the ozone net radiative forcing as a result of increased ozone levels we performed an offline radiative transfer calculation using the ozone fields provided by the control run and the isoprene experiment. This calculation predicts a global mean net radiative forcing of ozone due to isoprene emissions of 0.09 W m^{-2}. The ozone net radiative forcing is most pronounced at tropical latitudes ranging between 0.07 and 0.15 W m^{-2}. Maximum values of up to 0.17 W m^{-2} are found over the desert regions of northern Africa and the Arabic Peninsula. At mid- and high latitudes of both hemispheres the O_3 net radiative forcing ranges between 0.02 and 0.09 W m^{-2}.

Isoprene photooxidation is a significant source of carbon monoxide. As shown in the lower two panels of Fig. 16, isoprene oxidation near the surface results in an increase of carbon monoxide mixing ratios ranging from 25 to 60 ppbv

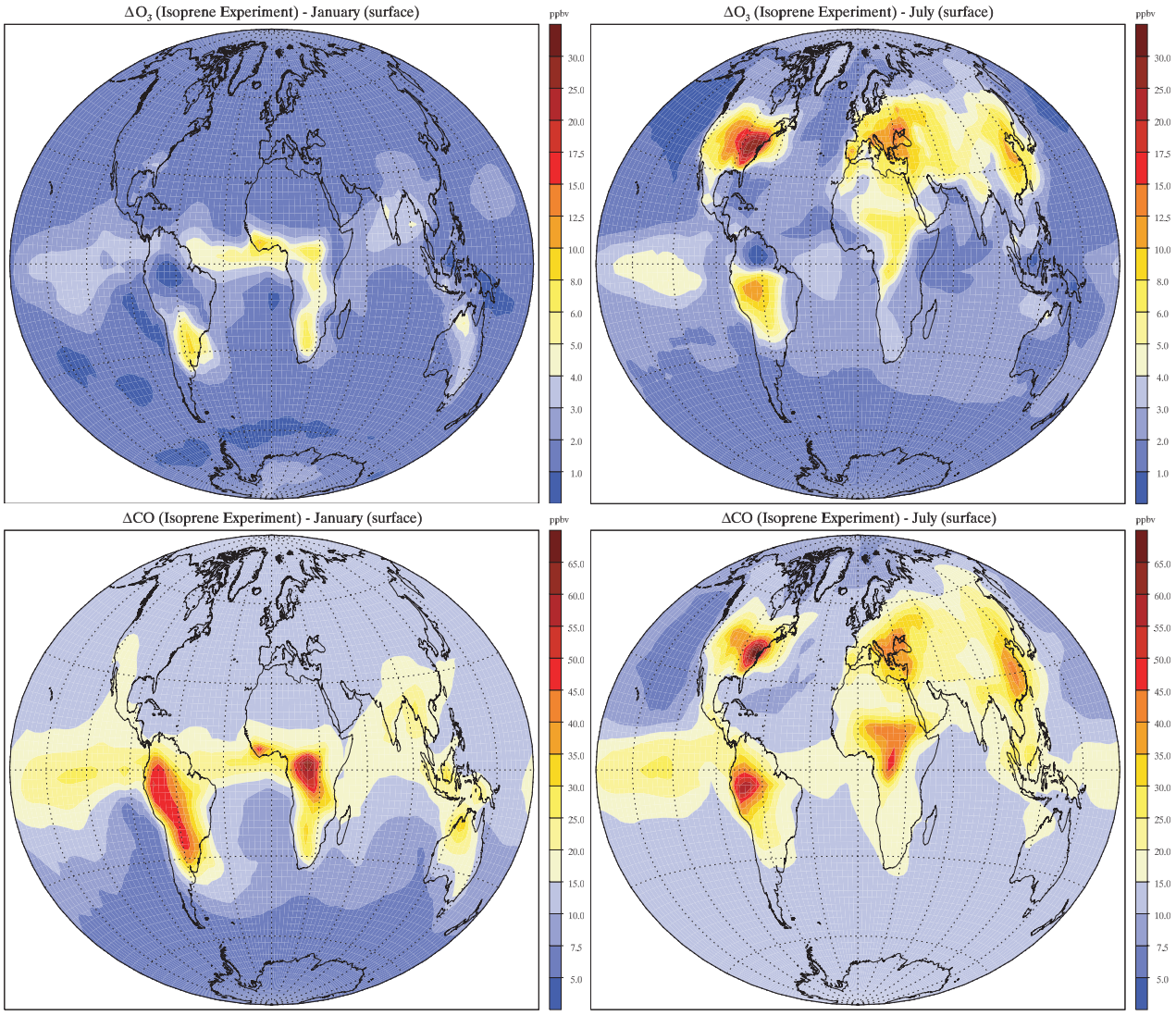

Fig. 16. Change in ozone (ΔO_3) and CO (ΔCO) surface mixing ratios (ppbv) due to isoprene for January and July.

over the major isoprene source areas, of the Eastern United States, equatorial Africa, tropical South America, and, to a lesser extend, Southeast Asia, for both, January and July. Atmospheric transport of CO away from these source areas has a significant impact on the equatorial regions of the marine planetary boundary layer. A substantial CO entrainment to remote and relatively unpolluted regions by the trade winds can be seen over the equatorial Atlantic and Pacific ocean enhancing CO levels in the marine PBL between 15 and 35 ppbv. A marked increase in CO mixing ratios ranging from 30 to 65 ppbv is calculated by the model for the Eastern US and Europe during summer.

The changes in surface NO_x mixing ratios due to the presence of isoprene are depicted in the upper two panels of Fig. 18 for January and July. The impact of isoprene emissions is apparent on the global scale. In both cases, the effect of isoprene-NO_x-separation in January and isoprene-NO_x-coincidence in July is clearly visible. Calculations with LMDz-INCA show a strong decrease in NO_x mixing ratios over regions with generally high levels of NO_x (Eastern United States and Europe) for both January and July, but the effect is more pronounced in the summer. A decrease in NO_x mixing ratios between 50 and 250 pptv in January is discernible over these regions. In July NO_x levels can even be reduced by up to 1000 pptv over the same regions due to the strong isoprene sources during the summer months.

Once NO_x has been converted into PAN and analogue compounds which posses much longer lifetimes than nitrogen oxides themselves, NO_x is redistributed globally. Figure 18 shows an increase in the NO_x mixing ratio of up to

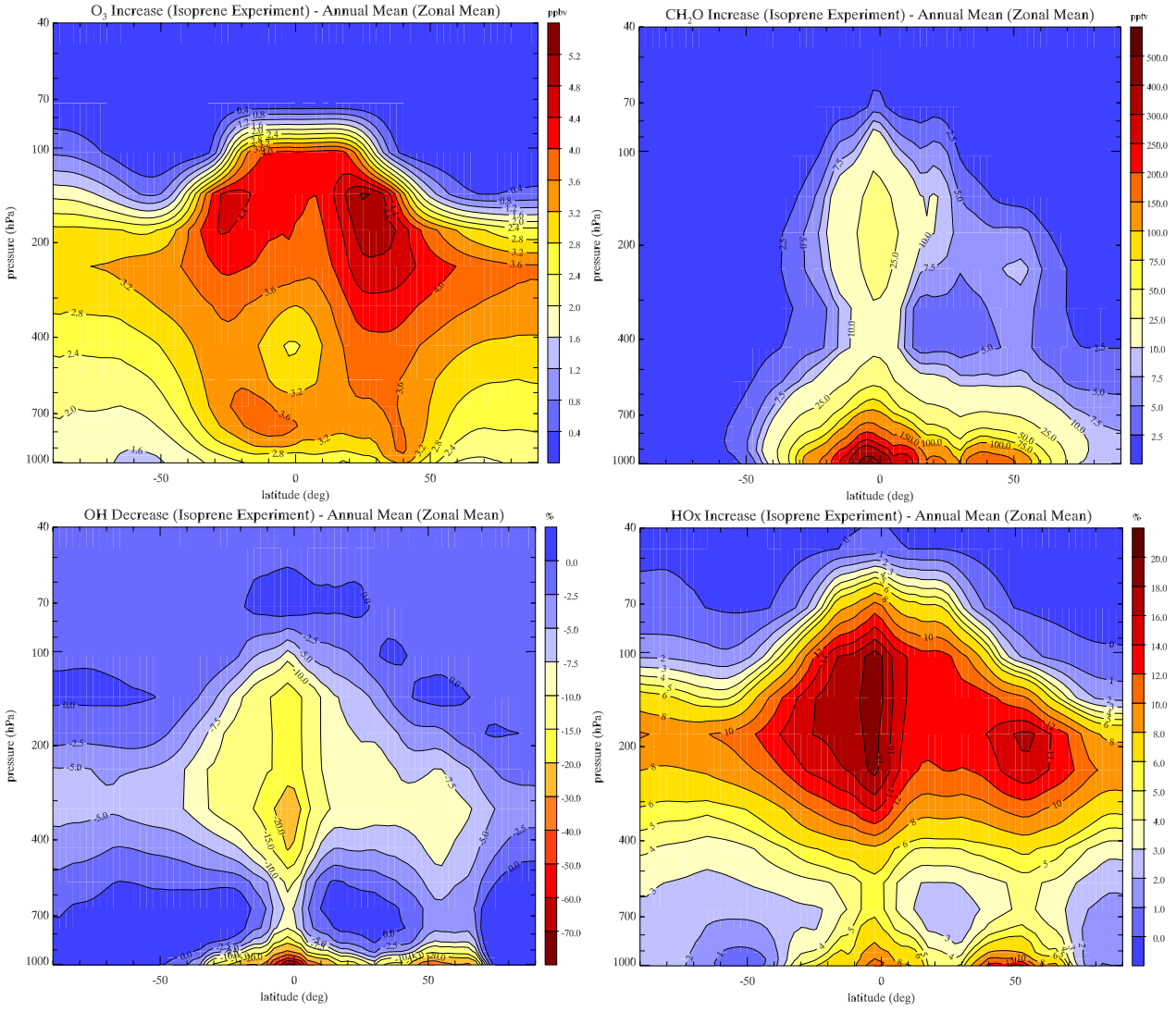

Fig. 17. Calculated annually and zonally averaged changes in O_3 (ppbv), CH_2O (ppbv), OH (%), and HO_x (%) due to isoprene biogenic surface emissions (412 Tg C yr^{-1}).

50 pptv in January over the tropical oceans in the vicinity of the western continental regions. In July LMDz-INCA calculations seem to indicate that NO_x is preferably released closer to the regions with high levels of nitrogen oxides, in particular over the northern hemispheric continental areas. This seems to be a consequence of the the shorter PAN lifetimes during the northern hemispheric summer months.

The lower two panels in Fig. 18 show the increase in PAN mixing ratios at the surface for the isoprene experiment for January and July. During the northern hemispheric winter a homogeneous increase in PAN over the entire extratropical northern hemisphere ranging from 10 to 50 pptv is calculated by LMDz-INCA. This ubiquitous enhancement is a consequence of the longer PAN lifetimes during the winter when thermal decomposition is less effective. The increase in PAN in January is particularly strong close to the primary isoprene sources of equatorial Africa, tropical South America, and Southeast Asia. Over these regions the presence of isoprene enhances PAN mixing ratios by up to 250 pptv.

In July the region of strong enhancements in the PAN surface mixing ratios is shifted to the northern hemispheric mid-latitudes. An increase in PAN between 75 and 750 pptv is discernible over most of the United States, Europe, and extratropical Southeast Asia as a consequence of the isoprene-NO_x-coincidence. This pronounced increase in PAN mixing ratios is even more remarkable since PAN lifetimes are significantly shorter during the northern hemispheric summer months. A homogeneous enhancement in PAN mixing ratios, albeit somewhat less pronounced, is apparent over southern hemispheric mid- to high latitudes in July, similar to the PAN

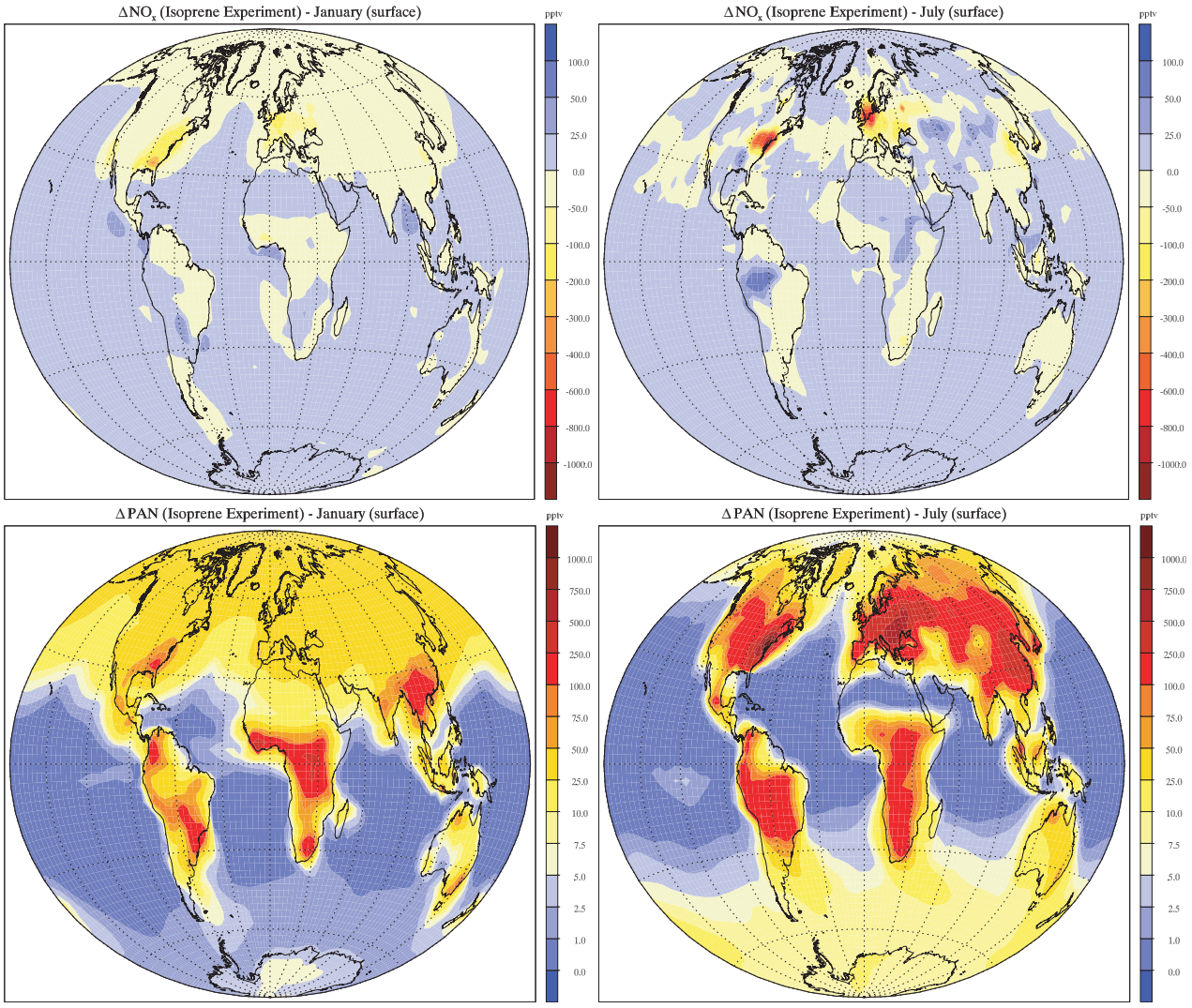

Fig. 18. Change in NO_X (ΔNO_X) and PAN (ΔPAN) surface mixing ratios (pptv) due to isoprene for January and July.

increase during northern hemispheric winter months. The development of this extratropical "PAN plume" during the southern hemispheric winter owes its existence to the same extension in PAN lifetimes but it is less distinctive due to significantly lower NO_x sources in the Southern Hemisphere. The increase in PAN mixing ratios in the tropics is less pronounced in July as well reaching a surplus of up to 100 pptv over the tropical regions of South America and Africa.

The major sink of non-methane VOC in the troposphere is the reaction with hydroxyl radicals. As a result it is expected that NMVOC have a significant impact on the global distribution of OH and, hence, the tropospheric oxidizing capacity. Isoprene, and all other NMVOC that are emitted in significant amounts, will compete for the OH radical.

Figure 17 shows the impact of global biogenic isoprene emissions on the ozone, formaldehyde, OH, and HO_x distribution and magnitude. LMDz-INCA calculates a reduction in the OH concentration reaching 50% near the surface over the tropics and northern hemispheric mid-latitudes where isoprene emissions are strongest. A decrease in OH ranging between 5% and 25% is also apparent in the free troposphere over the tropical and northern hemispheric mid- and high latitudes. In addition, the model calculates an isoprene induced reduction of the global mean tropospheric OH concentration by approximately 0.7×10^5 molecules cm^{-3} or roughly 8%. This reduction in OH is most likely caused by isoprene photooxidation products such as methacrolein and formaldehyde which posses a substantially longer photochemical lifetime than isoprene.

On the other hand, Formaldehyde and methacrolein lifetimes are too short for those species to be homogeneously mixed in the troposphere. These two products of isoprene ox-

idation are displaced predominantly to the upper troposphere by deep convection in the tropics where they contribute significantly to the HO_x budget of the UTLS region. Figure 17 shows that whereas the isoprene source reduces OH in most of the troposphere its photochemical decomposition significantly adds to the HO_x concentration. This contribution is most pronounced in the tropical UTLS region where the model calculates an increase in HO_x between 10% and 20%. The additional HO_x source is provided by photolysis of oxidation products such as for instance formaldehyde. Figure 17 depicts a corresponding increase of CH_2O in the tropics on account of isoprene oxidation. Furthermore, it can be seen from Fig. 17 that isoprene oxidation yields an increase in HO_x by more than 2.5% over the entire free and upper tropospher which translates into and increase of ozone concentrations between 2 and 5 ppbv.

Another important consequence of a reduced oxidative capacity of the troposphere is the change in the lifetime of methane. The CH_4 tropospheric lifetime is predominantly determined by its most important sink, the reaction with hydroxyl radicals. Calculations with LMDz-INCA indicate an increase in the global annual mean methane lifetime averaged over the entire tropospheric domain by approximately 7 months or 6.5% as a consequence of global biogenic isoprene emissions.

The major products of isoprene photooxidation are methyl vinyl ketone (MVK), methacrolein (MACR), and formaldehyde (cf., e.g., Sprengnether et al., 2002, and references therein). As discussed in detail by Apel et al. (2002) the reaction of isoprene with OH favours the production of MVK over MACR (MVK/MACR≈1.4) whereas the reaction with ozone produces MACR more abundantly than MVK (MVK/MACR≈0.4). In our mechanism these ratios are somewhat different (for a detailed discussion of differences in current condensed isoprene oxidation mechanisms and their impact on global 3-D chemistry modelling see, e.g., von Kuhlmann et al. (2004)): Under NO_x-rich conditions the production ratio of MVK to MACR following the reaction of isoprene with OH is 0.9. This can become as low as 0.6 under NO_x-depleted conditions. In these NO_x limited environments the predominant products of the isoprene-OH reaction pathway are organic peroxides (Miyoshi et al., 1994) with increased methacrolein yields due to peroxide recycling. The reaction of isoprene with ozone produces a MVK/MACR ratio even more biased toward production of MACR with ratios reduced to approximately 0.4 in our model. On the other hand, methyl vinyl ketone has a significantly longer photochemical lifetime than methacrolein. Hence, close to the isoprene sources at the surface the 0.9 contour of the [MVK]/[MACR] ratio would indicate the transition from NO_x-rich to NO_x-depleted areas.

Furthermore, due to the short photochemical lifetime of isoprene of only a few hours the [MVK]/[MACR] ratio reflects the aging of the isoprene-MVK-MACR mixture yielding potentially higher MVK/MACR ratios away from the isoprene sources. At considerable distance from the initial location of production the difference in lifetime takes precedence over the production ratio and the [MVK]/[MACR] concentration ratio will shift toward a value equal or greater than one. It is on account of this aspect that the ratio of the oxidation products MVK and MACR holds information about the history of the isoprene oxidation process.

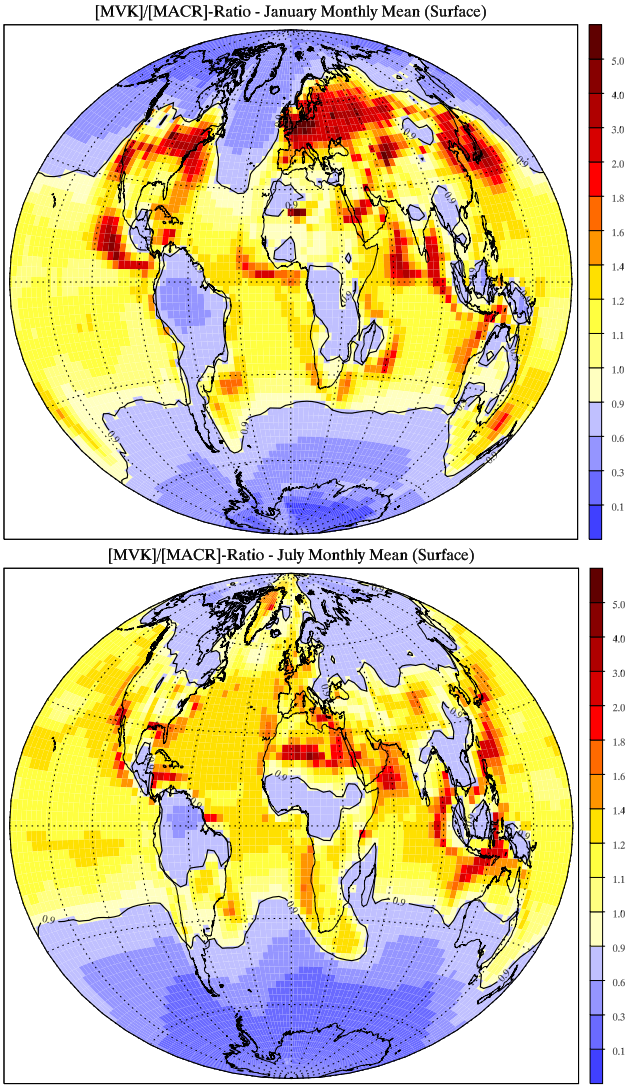

Fig. 19. Ratio of the monthly mean methyl vinyl ketone and methacrolein surface mixing ratios, [MVK]/[MACR], for Jannuary and July.

Figure 19 depicts the monthly mean [MVK]/[MACR] concentration ratio at the surface for January and July as calculated by LMDz-INCA. The major isoprene source areas of tropical South America, Africa, and South-East Asia are clearly marked by a [MVK]/[MACR] ratio of less than 0.9 for both January and July indicating areas of isoprene oxidation in low-NO_x environments and possibly non-negligible

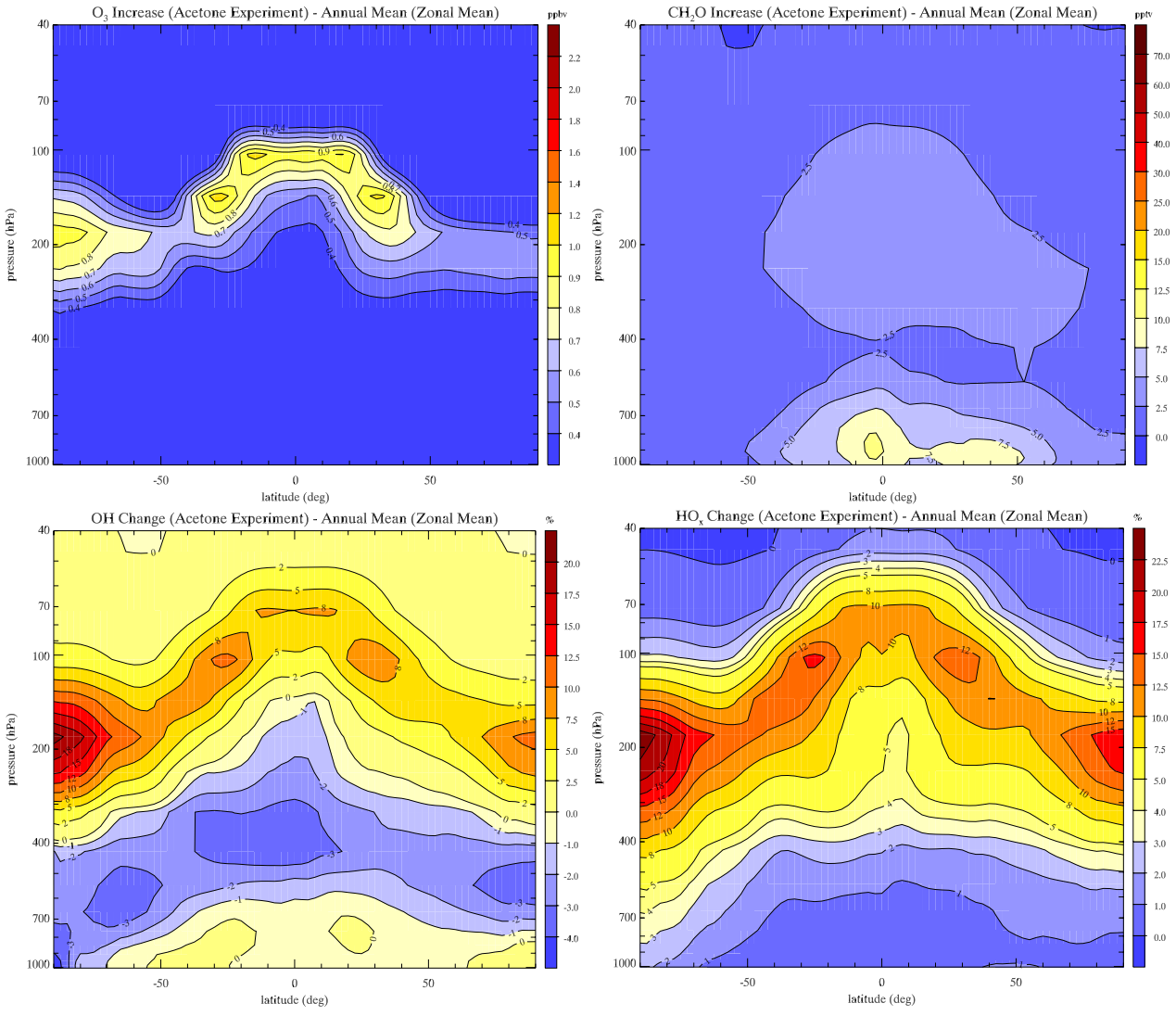

Fig. 20. Calculated annually and zonally averaged changes in O_3 (ppbv), CH_2O (ppbv), OH (%), and HO_x (%) due to acetone biogenic surface emissions (47 Tg C yr^{-1}).

contributions to isoprene oxidation by ozone. On the other hand, most of the isoprene emissions in the Eastern United States during the summer months coincide with an abundance of NO_x. This is reflected in the lower panel of Fig. 19 by [MVK]/[MACR] concentration ratios of 1.0 to 1.4 directly over this region.

Large portions of the globe are characterized by [MVK]/[MACR] ratios between 1.1 and 1.2 which seem to indicate typical background conditions in regions that are still under a direct influence of continental biogenic NMVOC emissions. Outside these regions, at high northern latitudes (northward of about 60° N) and in southern mid- and high latitudes the concept of [MVK]/[MACR] concentration ratios as an indicator for the chemical history of air seems to break down on account of the vanishing concentration of both methylvinyl ketone and methacrolein. We refrain from further speculating about these regions.

It is important, though, to emphasize that large uncertainties exists around the photochemistry of isoprene, and the photochemistry of most organic compounds of biogenic origin in general, as well as their representation in global 3-D models of atmospheric chemistry. These uncertainties are related not only to uncertainties in the global isoprene source distribution and magnitude but also to the lack of detailed knowledge of all the chemical processes involved in the photochemical decomposition of isoprene. Recently, efforts have been undertaken to quantify some of these uncertainties and their impact on modelling the chemical composition of the atmosphere (e.g. Pöschl et al., 2000; von Kuhlmann et al., 2004). Uncertainties with the most pronounced impact

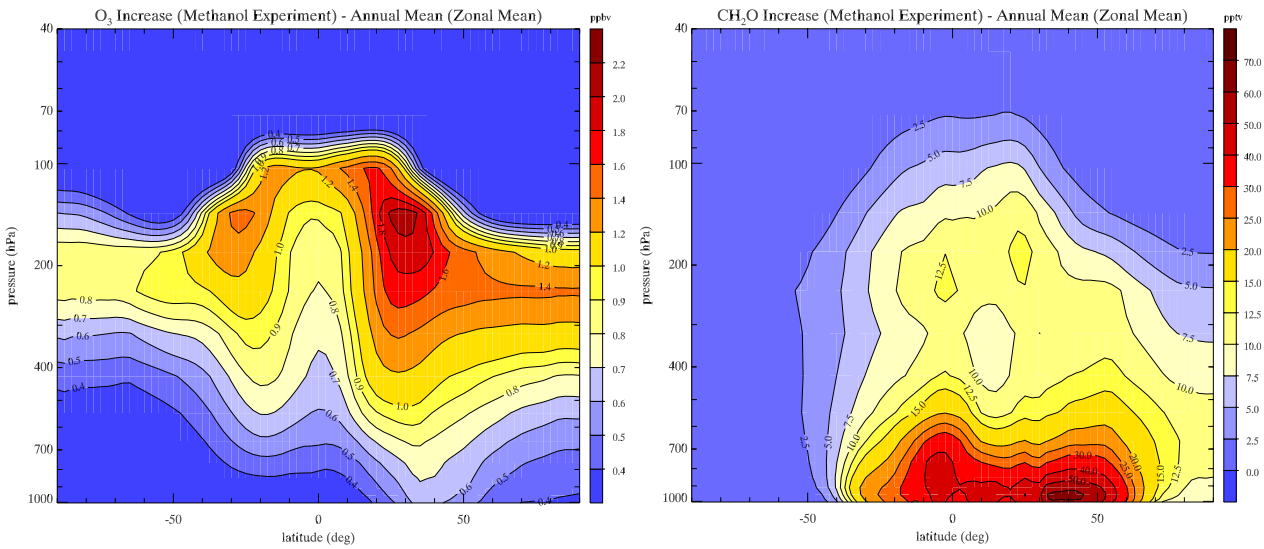

Fig. 21. Calculated annually and zonally averaged changes in O_3 (ppbv), CH_2O (ppbv), OH (%), and HO_x (%) due to methanol biogenic surface emissions (100 Tg C yr^{-1}).

seem to exist around the formulation of the condensed isoprene mechanism in general and the representation of nitrates formed in the oxidation of isoprene (and possibly other biogenic NMVOC) in particular. For instance, variations of up to 30% in the global ozone burden as a consequence of applying different state-of-the-art chemical mechanisms have been found in those studies (von Kuhlmann et al., 2004). These uncertainties must be addressed in future measurement and modelling efforts.

4.2 Impact of acetone

Acetone is photochemically produced by propane oxidation. Further important precursors are iso-alkanes, iso-alkenes, and terpenes. Moreover, acetone has surface emissions from anthropogenic sources, biomass burning, and the terrestrial vegetation (Warneke et al., 1999). Jacob et al. (2002) have presented a global acetone budget claiming the ocean as an additional important primary source. Acetone is destroyed by reaction with OH and photolysis. Lifetimes range from about 10 days to a few months varying with location and season (Singh et al., 1994b). Photolysis of acetone has been reported a significant source of HO_x radicals in the upper troposphere (Jaeglé et al., 2001).

Figure 20 shows the impact of global acetone surface emissions from natural sources (terrestrial vegetation and the ocean, 47 Tg C yr^{-1}) on concentrations of O_3, CH_2O, OH, and HO_x (HO_x=OH+HO_2+$\sum RO_2$). Changes in the ozone concentration are limited to the upper troposphere/lower stratosphere (UT/LS) region and are generally small. LMDz-INCA calculates an increase of O_3 of generally less than 1 ppbv. On the other hand, acetone surface emissions seem to have a significant impact on the concentration of OH and HO_x in the UT/LS region. Fig. 20 shows an increase in OH of up to 10% in the tropical and midlatitudinal UT. Positive OH anomalies due to acetone exceed 20% in the Antarctic UT/LS. The changes in HO_x are even more distinct. An increase of up to 15% prevails in the entire UT/LS region exceeding 20% at polar latitudes. The acetone sensitivity experiment shows basically no impact on ozone, OH, or HO_x in the lower troposphere. Acetone surface emissions also seem to have an almost negligible impact on global formaldehyde concentrations. The model calculates changes in CH_2O concentrations of generally less than 10 pptv for the entire troposphere. The maximum impact is found for the lower troposphere.

4.3 Impact of methanol

Due to its relatively long lifetime, a large amount of methanol can be transported from the PBL into the free troposphere and has a potentially significant impact on the concentration of oxidants. We conducted a sensitivity experiment designed to study this impact of global methanol surface emissions from natural sources (terrestrial vegetation and plant decay, 100 Tg C yr^{-1}) on ozone levels, formaldehyde concentrations, and OH as well as HO_x mixing ratios. The results of this experiment are summarized in Fig. 21.

An increase in the ozone concentration is visible over the entire free troposphere, albeit relatively small, and shows two maxima at about 30 degrees latitude in both hemispheres. A maximum increase of 2 ppbv is calculated at the northern hemispheric subtropical tropopause. concentrations. The calculations with LMDz-INCA also show an increase in OH

on the order of one to two percent only. On the other hand, these calculations predict enhancements in the level of peroxy radicals, such as HO_2 and organic peroxy radicals, combined to HO_x, between 8 and 15% in the UT/LS region depending on latitude. The increased supply of peroxy radicals seems to drive the changes in ozone mixing ratios. The large increase in HO_x in the UT/LS region could also be a consequence of CH_2O photolysis. LMDz-INCA calculates a pronounced increase of formaldehyde in the lower troposphere between 50° S and 50°N up to about 700 hPa with maximum positive anomalies of 70 pptv in the PBL at about 40° N. At these altitudes formaldehyde photolysis is relatively weak and consequently CH_2O lifetimes will be longer. The impact of methanol emissions on formaldehyde levels decreases with increasing altitude. The highly efficient destruction of formaldehyde by photolysis seems to be the reason for the very small impact of methanol in the upper troposphere.

4.4 Global carbon monoxide budget for the troposphere

LMDz-INCA includes a set of tagged model tracers pertaining to the conversion of primary emitted VOC and intermediate products of tropospheric photooxidation to carbon monoxide and CO_2 (Folberth et al., 2005). Using these tagged tracers we present an updated estimate of the global CO budget and compare our results to the estimates given by Bergamaschi et al. (2000). Tab. 8 summarizes both studies. Note that our estimates are based on the assumption that global sources and sinks are in perfect equilibrium. In particular, this pertains to the tropospheric-stratospheric exchange of CO which has been derived as the residual of all other sources and sinks calculated directly with the model. It should be pointed out as well that we have not attempted to calculate uncertainty limits for our CO budget. Uncertainties in the global CO source are expected to be high and will depend primarily on the uncertainties in the global emission inventory. The uncertainties in the global sink are a consequence of the source uncertainties and are also expected to be substantial.

Whereas the range of CO sources and sinks for individual tropospheric processes in the study by Bergamaschi et al. (2000) represent a posteriori estimates obtained by an inverse modelling approach, the current CO budget has been derived with a forward model. Furthermore, the studies are based on fundamentally different emission inventories. Nevertheless, both modelling studies agree surprisingly well in their predictions of the total global CO sources and sinks. Note that in the LMDz-INCA standard emission inventory (cf. Table 5) CO emissions deriving from agricultural waste burning and domestic biofuel use have been attributed to the global biomass burning source. In the study of Bergamaschi et al. (2000) these sources are included in the technological source category. For the purpose of this comparison we limited the CO biomass burning source to savannah and forest fires only attributing carbon monoxide emissions from agricultural waste burning and domestic biofuel use to the technological sources. With these changes in categories, the carbon monoxide budget calculated by LMDz-INCA and summarized in Table 8 appears to be in very good agreement with the study of Bergamaschi et al. (2000).

Secondary CO sources in LMDz-INCA deriving from reactive carbon compound (RCC) photooxidation in the troposphere amount to 1489 Tg CO yr^{-1}. RCC include all carbon containing compounds that are chemically broken down in the troposphere, excluding only CO_2 which is chemically inert. Oxidation of methane, isoprene, methanol, terpenes, acetone, and other non-methane VOC (mostly of anthropogenic origin), respectively, contribute 854, 359, 110, 49, 28, and 89 Tg CO yr^{-1} to this secondary carbon monoxide source. In general, conversion efficiencies – defined as the ratio of the amount of carbon emitted in the form of individual species to the amount of carbon converted to CO expressed in percent – are less than 50% (20%–45%) for all species other than methane and CO. Therefore, it follows that these species must posses other highly efficient sinks. These sinks are found to be the physical removal of primary emitted VOC as well as their stable intermediate photochemical products (such as alcohols, aldehydes, ketones, and organic nitrates) through surface dry deposition and wet removal. The CH_4 conversion efficiency of 90% indicates that photochemical destruction is by far the most important atmospheric sink, CH_4 entrainment to the stratosphere being the only other significant removal process in our model. It has been shown, however, that dry deposition of methane at the surface due to soil-microbial activity amounts to approximately 30 TgCH_4 (cf. Prather et al. (2001)) and is roughly of equal importance as stratospheric destruction. For lack of a parameterization of this process suitable for global chemistry-climate models we decided to neglect methane dry deposition in LMDz-INCA at this stage.

Both studies agree closely on the global CO sink. Photochemical oxidation of carbon monoxide, which represents a significant secondary CO_2 source (Folberth et al., 2005), constitutes a slightly stronger sink in LMDz-INCA. Calculations with LMDz-INCA indicate a global CO-to-CO_2 conversion efficiency of 88%. On the other hand, dry deposition of CO at the surface seems to be significantly weaker in LMDz-INCA than in the study of Bergamaschi et al. (2000). The residual of all sources and sinks of carbon monoxide in our model is interpreted as a CO entrainment to the stratosphere. The estimate of this particular sink significantly exceeds the estimate of Bergamaschi et al. (2000) as a consequence of the substantially weaker CO surface deposition.

5 Summary and conclusions

In this paper we provide a first description and evaluation of a new version of the 3-D-chemistry-climate model LMDz-INCA. This new version is based on the recently devel-

oped CH_4-NO_x-CO-O_3 version of LMDz-INCA to which a comprehensive representation of the photochemistry of non-methane hydrocarbons (NMHC) and volatile organic compounds (VOC) has been added. The current version runs with a horizontal resolution of 3.8×2.5 degrees in longitude and latitude, respectively, and the vertical model domain extends over 19 levels from the surface up to 3 hPa. The model calculates the distribution of tropospheric ozone and its precursors as well as a substantial number of primary NMVOC and intermediate photochemical products, such as isoprene, acetone, methanol, PAN and analogues, or formaldehyde. Surface emissions are based on state-of-the-art emission inventories. Biogenic VOC emissions from the terrestrial vegetation are calculated with the dynamic vegetation and emission model ORCHIDEE and are provided off-line to LMDz-INCA. The model is run in climatological mode and the results are evaluated by thorough comparison with observations inasmuch as they are available.

The model captures well the distribution and seasonal cycle of carbon monoxide except for a tendency to overestimate CO by up to 20 ppb at southern mid and high latitudes. The tropospheric annual mean methane (9.2 years) and methylchloroform (5.5 years) chemical lifetimes are in excellent agreement with estimates obtained by observations indicating that LMDz-INCA simulates the global tropospheric OH distribution and magnitude (annual mean OH abundance of 9.6×10^5 molecules cm^{-3}) fairly well. A comparison with observed vertical profiles of NO_x, PAN, and HNO_3 indicate that LMDz-INCA is capable of well reproducing the distribution of nitrogen compounds, even though the problem of overestimated nitric acid concentrations, prevailing in many current chemistry models, also persists in LMDz-INCA, albeit to a somewhat reduced extent.

The model also satisfactorily simulates a variety of non-methane volatile organic compounds, such as acetone, methanol, and formaldehyde. The comparison with observations reveal a generally good agreement for these species. Locally, however, methanol can be underestimated by up to a factor of 2.5 at some remote locations. The comparison also indicates that the model overestimates measured formaldehyde concentrations in the lower and middle troposphere over the South Atlantic by up to a factor of three. This disagreement could be related to an overestimate of formaldehyde or its precursors from biomass burning being too high in our emission inventory near this region (South American continental sources). The comparison of acetone profiles with observations show a fairly well model-to-data agreement over the entire troposphere.

The model reproduces fairly well the magnitude and distribution of ozone in the entire troposphere. Annual mean tropospheric photochemical production (4436 Tg O_3 yr^{-1}), and destruction (3890 Tg O_3 yr^{-1}), dry deposition at the surface (1261 Tg O_3 yr^{-1}), and stratospheric influx (715 Tg O_3 yr^{-1}) are in good agreement with analogue estimates of current photochemical models. A net tropospheric ozone production rate of 546 Tg O_3 yr^{-1} is calculated by LMDz-INCA which is about 75% of the the stratospheric influx.

Table 8. Carbon monoxide budget for the global troposphere defined as the region extending from the surface up to the 250 hPa altitude level. LMDz-INCA results are compared to the a posteriori estimates obtained by an inverse modelling study of the global CO cycle as given by Bergamaschi et al. (2000). All numbers are written as Tg CO yr^{-1}. The average and range (in brackets) of estimates for the study of Bergamaschi et al. is denoted. Percent values in parentheses indicate VOC-to-CO conversion efficiencies calculated with the LMDz-INCA model.

	LMDz-INCA	Bergamaschi et al. (2000)
Global Source	**3019**	**2818 (2244–3392)**
Primary Source	*1533*	*1349 (1022–1675)*
Biomass Burning	811	674 (506–840)
Technological	672	656 (511–800)
Oceanic	50	19 (5–35)
RCC [a] Oxidation	*1489 (55%)*	*1468 (1220–1715)*
Methane[b]	854 (90%)	831
Isoprene	359 (37%)	348 (231–464)
Methanol	110 (45%)	—
Terpenes	49 (22%)	145 (98–191)
Acetone	28 (24%)	—
$\sum$ other VOC[c]	89 (38%)	145 (61–229)
Global Sink	**3019**	**2938 (2863–3010)**
Photochemical Destruction	2653	2471 (2415–2529)
Dry Deposition	135	301 (292–308)
Stratospheric Entrainment	231	166 (156–173)

[a] reactive carbon compounds (cf. text for definition)
[b] fixed in Bergamaschi et al. (2000); calculated in LMDz-INCA
[c] mostly anthropogenic

The new version of LMDz-INCA has been applied to study the impact of isoprene (411 Tg C yr^{-1}), acetone (50 Tg C yr^{-1}), and methanol (104 Tg C yr^{-1}) surface emissions on ozone and other tropospheric oxidants. Isoprene emissions are found to have a substantial impact on ozone and carbon monoxide concentrations. The isoprene experiment also shows a separation of NO_x and isoprene sources in January and an isoprene-NO_x-coincidence in July with a low and high ozone formation potential in January and July, respectively. The calculations with LMDz-INCA show a strong increase of up to 30 ppbv at the surface over the Eastern United States and Europe in the summer as a consequence of the coincidence of NO_x and isoprene surface sources. To assess the potential importance of these changes in the tropospheric ozone burden on the radiative budget of the atmosphere, an offline radiative calculation has been conducted. A global mean ozone net radiative forcing of 0.09 W m^{-2} is calculated with maximum values reaching

0.17 $W\,m^{-2}$ at tropical latitudes. The radiative effect of an increasing ozone burden in the troposphere as a result of biogenic isoprene surface emissions on the atmospheric radiative budget, therefore, appears to be non-negligible but rather small as compared to other seemingly more important effects. However, an increase in the source of tropospheric ozone precursors, such as NO_x and BVOC originating from a more active biosphere, as a consequence of a changing climate (c.f., e.g., Lathière et al., 2005a; Hauglustaine et al., 2005), could potentially represent a positive feedback process enhancing global warming. Clearly, a more detailed investigation is needed.

Compared with a non-isoprene run, carbon monoxide mixing ratios are found to increase between 25 and 60 ppbv over continental isoprene source regions and between 15 and 30 ppb in the remote marine boundary layer. An important role role of isoprene lies in its impact on the redistribution of nitrogen oxides in the entire troposphere due to the conversion of short-lived NO_x into organic nitrates with significantly longer lifetimes. Photooxidation of isoprene provides large amounts of organic nitrate precursors. An increase in PAN mixing ratios at the surface ranging from 10 to 250 pptv and 75 to 750 pptv during northern hemispheric winter and summer months, respectively, is calculated by LMDz-INCA. A decrease in the zonally averaged annual mean OH concentration ranging between 5% and 25% in the tropical and northern hemispheric free troposphere is calculated by our model as a consequence of the global biogenic isoprene source. An isoprene induced reduction of the tropospheric OH concentration by approximately 0.7×10^5 molecules cm^{-3} or roughly 8% is calculated on the global average. Ensuing this reduction in the oxidative capacity the model predicts an increase of the global mean tropospheric methane lifetime by approximately seven months. At the same time the model shows an increase of the HO_x concentration in the entire free and upper troposphere due to isoperene with a maximum value of 20% for the tropical UTLS region. Our simulations reveal [MVK]/[MACR] ratios of less than 0.9 over NO_x depleted isoprene source regions for both January and July whereas a [MVK]/[MACR] ratio of up to 1.4 is calculated over the Eastern United States in July where pronounced isoprene emissions coincide with a high NO_x burden. It has to be kept in mind, though, that the treatment of isoprene photochemistry in current global chemistry models is still associated with large uncertainties pertaining to its sources and representation of the chemistry. These uncertainties must be reduced in future measurement and modelling efforts because the photochemistry of isoprene and its oxidation products represents a key component in the understanding of tropospheric photochemistry.

Acetone and methanol play a significant role in controlling tropospheric oxidants in the upper troposphere/lower stratosphere region. The sensitivity experiments show a small impact of global acetone surface emissions on tropospheric ozone but indicate a strong impact on the OH and peroxy radical budget of the UT/LS region. An increase between 10% and 15% in the UT/LS in the OH and HO_x concentration is calculated by the model. Interestingly, acetone seems to have the most pronounced impact over the polar regions, at least when measured as percent changes. In case of the methanol sensitivity experiments, calculations show maximum positive anomalies of 2 ppbv for ozone, 2% for OH, and 8 to 15% for HO_x, respectively. Both species show relatively small impacts on tropospheric formaldehyde concentrations with maximum changes of 10 pptv and 70 pptv for acetone and methanol, respectively. Both these maxima occur in the lower troposphere or even in the PBL.

We also attempted an estimate of the CO budget for the global troposphere and compared the results to a recently published inverse modelling study. Even though our study and the study by Bergamaschi et al. (2000) have used fundamentally different approaches to derive their estimates of global tropospheric CO sources and sinks (a forward calculation in LMDz-INCA versus a posteriori estimates obtained by means of an inverse modelling approach in the study Bergamaschi et al.) both studies show a strikingly similar global picture. A global carbon monoxide source of 3019 $Tg\,CO\,yr^{-1}$, which divides into a primary CO source of 1533 $Tg\,CO\,yr^{-1}$ originating from biomass burning, technological, and oceanic sources and a secondary CO source of 1489 $Tg\,CO\,yr^{-1}$ due to methane and VOC photooxidation, is calculated by LMDz-INCA. Oxidation of methane, isoprene, methanol, terpenes, acetone, and other non-methane VOC, respectively, are found to contribute 854, 359, 110, 49, 28, and 89 $Tg\,CO\,yr^{-1}$ to this secondary CO source. The model calculates global VOC-to-CO conversion efficiencies ranging from 20 to 45%, a 90% conversion efficiency is prognosticated in case of methane. Oxidation of CO represents by far the most important tropospheric sink. According to our calculations, 2653 $Tg\,CO\,yr^{-1}$ are removed from the troposphere by this process indicating a global CO-to-CO_2 conversion efficiency of 88%. Surface deposition of CO (135 $Tg\,CO\,yr^{-1}$) and stratospheric CO entrainment (231 $Tg\,CO\,yr^{-1}$) are identified as the only significant tropospheric carbon monoxide sinks other than CO oxidation.

In summary, the NMHC version of LMDz-INCA provides an overall satisfactory representation of the complex photochemical processes of the tropospheric VOC composition as well as the budgets of key tropospheric species such as, e.g., O_3 and CO. The new version has been applied in several sensitivity studies addressing the interaction between the continental biosphere and atmospheric chemical composition. Current development efforts are focused on halogen photochemistry, an interactive climate-chemistry coupling, and integration of LMDz-INCA with the dynamic vegetation and emission model ORCHIDEE providing a comprehensive modelling tool to study more directly the numerous feedbacks between the biosphere, the atmosphere, climate, and photochemistry. Results from these new versions will be reported in forthcoming studies.

Acknowledgements. This work was partly funded by the European Commission under contract EVK2-CT-2002-00170. GF acknowledges support provided by the Canadian Centre for Climate Modelling and Analysis. We would like to thank William J. Collins and an anonymous reviewer for their adjuvant comments which helped to improve the manuscript significantly. Additional funding has been received from the GCC project and support by NSERC and CFCAS is gratefully acknowledged. Computer resources were provided by the Commissariat à l'Energie Atomique under project p24.

Edited by: A. B. Guenther

References

Altshuller, A. P.: PANs in the atmosphere, J. Air & Waste Manage. Assoc., 43, 1221–1230, 1993.

Andreae, M.: Climatic effects of changing atmospheric aerosol levels, in: Future Cliamtes of the World, edited by: Henderson-Sellers, A., Vol. 16 of World Survey of Climatology, pp. 341–392, Elsvier, Amsterdam, 1995.

Andreae, M. and Crutzen, P.: Atmospheric aerosols: biogeochemical sources and role in atmospheric chemistry, Science, 276, 1052–1058, 1997.

Andreae, M. O. and Merlet, P.: Emission of trace gases and aerosols from biomass burning, Global Biogeochem. Cycles, 15, 955–966, 2001.

Apel, E. C., Riemer, D. D., Hills, A., Baugh, W., Orlando, J., Faloona, I., Tan, D., Brune, W., Lamb, B., Westberg, H., Carroll, M. A., Thornberry, T., and Geron, C. D.: Measurement and interpretation of isoprene fluxes and isoprene, methacrolein, and methyl vinyl ketone mixing ratios at the prophet site during the 1998 intensive, J. Geophys. Res.-Atmos., 107(D3), 4034, doi:10.1029/2000JD000225, 2002.

Atkinson, R., Baulch, D., Cox, R., Hampson, R., Kerr, J., Rossi, M., and Troe, J.: Evaluated kinetic and photochemical data for atmospheric chemistry: Supplement v, J. Physi. Chem. Ref. Data, 26, 1125–1568, 1997.

Balkanski, Y., Jacob, D., Gardner, G., Graustein, W., and Turekian, K.: Transport and residence times of tropospheric aerosols inferred from a global three-dimensional simulation of ^{210}Pb, J. Geophys. Res., 98, 20 573–20 586, 1993.

Barrie, L. A., Bottenheim, J. W., Schnell, R. C., Crutzen, P. J., and Rasmussen, R. A.: Ozone destruction and photochemical-reactions at polar sunrise in the lower arctic atmosphere, Nature, 334, 138–141, 1988.

Bauer, S. E., Balkanski, Y., Schulz, M., Hauglustaine, D. A., and Dentener, F.: Global modeling of heterogeneous chemistry on mineral aerosol surfaces: Influence on tropospheric ozone chemistry and comparison to observations, J. Geophys. Res.-Atmos., 109, D02304, doi:10.1029/2003JD003868, 2004.

Baulch, D., Cobos, C., Cox, R. A., Esser, C., Frank, P., Just, T., Kerr, J., Pilling, M., Troe, J., Walker, R., and Warnatz, J.: Evaluated kinetic data for combustion modelling, J. Phys. Chem. Ref. Data, 21, 411–429, 1992.

Bergamaschi, P., Hein, R., Heimann, M., and Crutzen, P. J.: Inverse modeling of the global CO cycle 1. inversion of CO mixing ratios, J. Geophys. Res.-Atmos., 105, 1909–1927, 2000.

Bernard, S. M., Samet, J. M., Grambsch, A., Ebi, K. L., and Romieu, I.: The potential impacts of climate variability and change on air pollution-related health effects in the united states, Environ. Health Perspect., 109, 199–209, 2001.

Berntsen, T. K., Isaksen, I. S. A., Myhre, G., Fuglestvedt, J. S., Stordal, F., Larsen, T. A., Freckleton, R. S., and Shine, K. P.: Effects of anthropogenic emissions on tropospheric ozone and its radiative forcing, J. Geophys. Res.-Atmos., 102, 28 101–28 126, 1997.

Bey, I., Jacob, D. J., Yantosca, R. M., Logan, J. A., Field, B. D., Fiore, A. M., Li, Q. B., Liu, H. G. Y., Mickley, L. J., and Schultz, M. G.: Global modeling of tropospheric chemistry with assimilated meteorology: Model description and evaluation, J. Geophys. Res.-Atmos., 106, 23 073–23 095, 2001.

Bonsang, B. and Boissard, C.: Global distribution of reactive hydrocarbons in the atmosphere, in: Reactive Hydrocarbons in the Atmosphere, pp. 209–265, Academic Press, 1999.

Bonsang, B., Polle, C., and Lembert, G.: Evidence for marine production of isoprene, Geophys. Res. Lett., 19, 1129–1132, 1992.

Boucher, O., Pham, M., and Venkataraman, C.: Simulation of the atmospheric sulfur cycle in the laboratoire de météorologie dynamique general circulation model. Model description, model evaluation, and global and european budgets, Note scientifique de l'IPSL n. 23, 2002.

Bouwman, A. F. and Taylor, J. A.: Testing high-resolution nitrous oxide emission estimates against observations using an atmospheric transport model, Global Biogeochem. Cycles, 10, 307–318, 1996.

Bradley, J. N., Edwards, A. D., and Gilbert, J. R.: Gas-phase reactions of singlet oxygen atoms with methane, Journal of the Chemical Society a -Inorganic Physical Theoretical, p. 326pp., 1971.

Brasseur, G. and Chatfield, R.: The fate of biogenic trace gases in the atmosphere, in: Trace Gas Emissions from Plants, edited by: Sharkey, T., Holland, E., and Mooney, H., pp. 1–27, Academic Press, 1991.

Brasseur, G. and Solomon, S.: Aeronomy of the Middle Atmosphere: Chemistry and Physics of the Stratosphere and Mesosphere, Atmospheric Science Library, D. Reidel Pub. Co., 2nd edn., 1987.

Brasseur, G., Orlando, J., and Tyndall, G.: Atmospheric Chemistry and Global Change, Oxford Univ. Press, New York, 1999.

Brasseur, G. P., Hauglustaine, D. A., Walters, S., Rasch, P. J., Muller, J. F., Granier, C., and Tie, X. X.: Mozart, a global chemical transport model for ozone and related chemical tracers 1. model description, J. Geophys. Res.-Atmos., 103, 28 265–28 289, 1998.

Brocheton, F.: Représentation des émissions anthropogiques dans les models globaux de chimie-transport: sensibilité à la représentation spatiale des émissions et au degré de raffinement du schéma chimique, Ph.D., Université Paris 12 – Val de Marne, 1999.

Burden, R. and Faires, J.: Numerical Analysis, PWS, Boston, Mass., 1985.

Chang, J., Brost, R., Isaksen, I., Madronich, S., Middleton, P., Stockwell, W., and Walcek, C.: A three-dimensional Eulerian acid deposition model: Physical concepts and formulation, J. Geophys. Res., 92, 14 681–14 700, 1987.

Collins, W. J., Derwent, R. G., Johnson, C. E., and Stevenson, D. S.: The oxidation of organic compounds in the troposphere and their global warming potentials, Climatic Change, 52, 453–479, 2002.

Constable, J. V. H., Guenther, A. B., Schimel, D. S., and Monson, R. K.: Modelling changes in voc emission in response to climate

change in the continental united states, Global Change Biology, 5, 791–806, 1999.

Corbett, J. J., Fischbeck, P. S., and Pandis, S. N., Global nitrogen and sulfur inventories for oceangoing ships, J. Geophys. Res.-Atmos., 104, 3457–3470, 1999.

Crutzen, P.: The role of NO and NO_2 in the chemistry of the troposphere and stratosphere, Ann. Rev. Earth Planet. Sci., 7, 443–472, 1979.

Crutzen, P.: Ozone in the troposphere, in: Composition, Chemistry, and Climate of the Atmosphere, edited by: Singh, H., pp. 349–393, Van Nostrand Reinold, New York, 1995.

Crutzen, P. and Zimmermann, P.: The changing photochemistry of the troposphere, Tellus, 43, 136–151, 1991.

De Fries, R. and Townshend, J.: NDVI-derived land classification at global scales, Int. J. Remote Sens., 15, 3567–3586, 1994.

de Rosnay, P. and Polcher, J.: Modelling root water uptake in acomplex land surface scheme coupled to a gcm, Hydrol. Earth Syst. Sci., 2, 239–256, 1998.

DeMore, W., Sander, S., Golden, D., Hampson, R., Kurylo, M., Howard, C., Ravishankara, A., Kolb, C., and Molina, M.: Chemical kinetics and photochemical data for use in stratospheric modeling, evaluation number 12, 1997.

Dlugokencky, E. J., Masarie, K. A., Lang, P. M., and Tans, P. P.: Continuing decline in the growth rate of the atmospheric methane burden, Nature, 393, 447–450, 1998.

Doskey, P. and Gao, W.: Vertical mixing and chemistry of isoprene in the atmospheric boundary layer: Aircraft-based measurements and numerical modeling, J. Geophys. Res., 104, 21 263–21 274, 1999.

Ducoudré-De Noblet, N., Laval, K., and Perrier, A.: Sechiba, a new set of parametrizations of the hydrologic exchanges at the land/atmosphere interface within the lmd atmospheric general circulation model, J. Climate, 2, 248–273, 1993.

Dufresne, J. L., Friedlingstein, P., Berthelot, M., Bopp, L., Ciais, P., Fairhead, L., Le Treut, H., and Monfray, P.: On the magnitude of positive feedback between future climate change and the carbon cycle, Geophys. Res. Lett., 29, 10, 1405, doi:10.1029/2001GL013777, 2002.

Emmons, L. K., Hauglustaine, D. A., Muller, J. F., Carroll, M. A., Brasseur, G. P., Brunner, D., Staehelin, J., Thouret, V., and Marenco, A.: Data composites of airborne observations of tropospheric ozone and its precursors, J. Geophys. Res.-Atmos., 105, 20 497–20 538, 2000.

Erickson, D. J. and Taylor, J. A.: 3-d tropospheric co modeling – the possible influence of the ocean, Geophys. Res. Lett., 19, 1955–1958, 1992.

Fehsenfeld, F., Calvert, J., Fall, R., Goldan, P., Guenther, A., Hewitt, C., Lamb, B., Liu, S., Trainer, M., Westberg, H., and Zimmerman, P.: Emissions of volatile organic compounds from vegetation and the implications for atmospheric chemistry, Global Biogeochem. Cycles, 6, 389–430, 1992.

Finlaysonpitts, B. J. and Pitts, J. N.: Atmospheric chemistry of tropospheric ozone formation - scientific and regulatory implications, J. Air & Waste Manage. Assoc., 43, 1091–1100, 1993.

Fishman, J.: The global consequences of increasing tropospheric ozone concentrations, Chemosphere, 22, 685–695, 1991.

Folberth, G., Hauglustaine, D. A., Ciais, P., and Lathiere, J.: On the role of atmospheric chemistry in the global CO_2 budget, Geophys. Res. Lett., 32, L08801, doi:10.1029/2004GL021812, 2005.

Friedlingstein, P., Bopp, L., Ciais, P., Dufresne, J. L., Fairhead, L., Le Treut, H., Monfray, P., and Orr, J.: Positive feedback between future climate change and the carbon cycle, Geophys. Res. Lett., 28, 1543–1546, 2001.

Fung, I., John, J., Lerner, J., Matthews, E., Prather, M., Steele, L., and Fraser, P., Three-dimensional model synthesis of the global methane cycle, J. Geophys. Res.-Atmos., 96, 13 033–13 066, 1991.

Galbally, I. E. and Kirstine, W.: The production of methanol by flowering plants and the global cycle of methanol, J. Atmos. Chem., 43, 195–229, 2002.

Ganzeveld, L. and Lelieveld, J.: Dry Deposition Parameterization in a Chemistry General-Circulation Model and Its Influence On the Distribution of Reactive Trace Gases, J. Geophys. Res.-Atmos., 100(D10), 20 999–21 012, 1995.

Ganzeveld, L. and Lelieveld, J., and Roelofs, G. J.: A dry deposition parameterization for sulfur oxides in a chemistry and general circulation model, J. Geophys. Res.-Atmos. , 103(D5) , 5679–5694, 1998.

Gardner, R. et al., ANCAT/EC2 global aircraft emission inventories for 1991/92 and 2015: Report by the ECAC/ANCAT and EC Working Group, Tech. rep., Def. Eval. and Res. Agency, Farnborough, UK, 1998.

Giorgi, F. and Chameides, W.: The rainout parameterization in a photochemical model, J. Geophys. Res., 90, 7872–7880, 1985.

Graedel, T.: Terpenoids in the atmosphere, Rev. Geophys. Space Phys., 17, 937–947, 1979.

Granier, C., Petron, G., Muller, J., and Brasseur, G.: The impact of natural and anthropogenic hydrocarbons on the tropospheric budget of carbon monoxide, Atmos. Environ., 34, 5255–5270, 2000.

Greenberg, R. and Heicklen, J.: The reaction of $O(^1D)$ with CH_4, Int. J. Chem. Kinet., 4, 471, 1972.

Guenther, A., Hewitt, C., Erickson, D., Fall, R., Geron, C., Graedel, T., Harley, P., Klinger, L., Lerdau, M., McKay, W., Pierce, T., Scholes, B., Steinbrecher, R., Tallamraju, R., Taylor, J., and Zimmerman, P.: A global model of natural volatile organic compound emissions, J. Geophys. Res., 100, 8873–8892, 1995.

Guenther, A., Archer, S., Greenberg, J., Harley, P., Helmig, D., Klinger, L., Vierling, L., Wildermuth, M., Zimmerman, P., and Zitzer, S.: Biogenic hydrocarbon emissions and landcover/climate change in a subtropical savanna, Phys. Chem. Earth Part B-Hydrol. Oceans Atmos., 24, 659–667, 1999.

Guenther, A., Geron, C., Pierce, T., Lamb, B., Harley, P., and Fall, R.: Natural emissions of non-methane volatile organic compounds; carbon monoxide, and oxides of nitrogen from north america, Atmos. Environ., 34, 2205–2230, 2000.

Hall, I., Wayne, R. P., Cox, R. A., Jenkin, M., and Hayman, G.: Kinetics of the reaction of NO_3 with HO_2, J. Phys. Chem., 92(17), 5049–5054, 1988.

Hao, W. and Liu, M.: Spatial and temporal distribution of tropical biomass burning, Global Biogeochem. Cycles, 8, 495–503, 1994.

Harzallah, A. and Sadourny, R.: Internal versus sst-forced atmospheric variability as simulated by an atmospheric general-circulation model, J. Climate, 8, 474–495, 1995.

Hauglustaine, D. A. and Brasseur, G. P.: Evolution of tropospheric ozone under anthropogenic activities and associated radiative forcing of climate, J. Geophys. Res.-Atmos., 106, 32 337–32 360, 2001.

Hauglustaine, D. A., Granier, C., Brasseur, G. P., and Megie, G.: The importance of atmospheric chemistry in the calculation of radiative forcing on the climate system, J. Geophys. Res.-Atmos., 99, 1173–1186, 1994.

Hauglustaine, D. A., Brasseur, G. P., Walters, S., Rasch, P. J., Muller, J. F., Emmons, L. K., and Carroll, C. A.: Mozart, a global chemical transport model for ozone and related chemical tracers 2. model results and evaluation, J. Geophys. Res.-Atmos., 103, 28 291–28 335, 1998.

Hauglustaine, D. A., Hourdin, F., Jourdain, L., Filiberti, M. A., Walters, S., Lamarque, J. F., and Holland, E. A.: Interactive chemistry in the laboratoire de meteorologie dynamique general circulation model: Description and background tropospheric chemistry evaluation, J. Geophys. Res.-Atmos., 109, D04314, doi:10.1029/2003JD003 957, 2004.

Hauglustaine, D. A., Lathière, J., Szopa, S., and Folberth, G. A.: Future tropospheric ozone simulated with a climate-chemistry-biosphere model, Geophys. Res. Lett., 32, L24807, doi:10.1029/2005GL024031, 2005.

Heikes, B. G., Chang, W. N., Pilson, M. E. Q., Swift, E., Singh, H. B., Guenther, A., Jacob, D. J., Field, B. D., Fall, R., Riemer, D., and Brand, L.: Atmospheric methanol budget and ocean implication, Global Biogeochem. Cycles, 16(4), 1133, doi:10.1029/2002GB001895, 2002.

Highwood, E. J., Shine, K. P., Hurley, M. D., and Wallington, T. J.: Estimation of direct radiative forcing due to non-methane hydrocarbons, Atmos. Environ., 33, 759–767, 1999.

Horowitz, L. W., Walters, S., Mauzerall, D. L., Emmons, L. K., Rasch, P. J., Granier, C., Tie, X. X., Lamarque, J. F., Schultz, M. G., Tyndall, G. S., Orlando, J. J., and Brasseur, G. P.: A global simulation of tropospheric ozone and related tracers: Description and evaluation of MOZART, version 2, J. Geophys. Res.-Atmos., 108(D24), 4784, doi:10.1029/2002JD002853, 2003.

Hourdin, F. and Armengaud, A.: The use of finite-volume methods for atmospheric advection of trace species-1. test of various formulations in a general circulation model, Mon. Wea. Rev., 127(5), 822–837, 1999.

Houweling, S., Dentener, F., and Lelieveld, J.: The impact of non-methane hydrocarbon compounds on tropospheric photochemistry, J. Geophys. Res., 103, 10 673–10 696, 1998.

Jacob, D. J.: Heterogeneous chemistry and tropospheric ozone, Atmos. Environ., 34, 2131–2159, 2000.

Jacob, D. J., Field, B. D., Jin, E. M., Bey, I., Li, Q. B., Logan, J. A., Yantosca, R. M., and Singh, H. B.: Atmospheric budget of acetone, J. Geophys. Res.-Atmos., 107(D10), 4100, doi:10.1029/2001JD000694, 2002.

Jaeglé, L., Jacob, D. J., Brune, W. H., and Wennberg, P. O.: Chemistry of hox radicals in the upper troposphere, Atmos. Environ., 35, 469–489, 2001.

Jenkin, M. and Cox, R. A.: Kinetics of the gas-phase reaction of oh with nitrous acid, Chem. Phys. Lett., 137(6), 548–552, 1987.

Jourdain, L. and Hauglustaine, D.: The global distribution of lightning nox simulated on-line in a general circulation model, Phys. Chem. Earth Part B-Hydrol. Oceans Atmos., 26, 585–591, 2001.

Kanakidou, M., Tsigaridis, K., Dentener, F., and Crutzen, P.: Human-activity-enhanced formation of organic aerosols by biogenic hydrocarbon oxidation, J. Geophys. Res., 105, 9243–9254, 2000.

Kasibhatla, P.: NO_y from sub-sonic aircraft emissions: A global, three-dimensional model study, Geophys. Res. Lett., 20, 1707–1710, 1993.

Kellomaki, S., Rouvinen, I., Peltola, H., Strandman, H., and Steinbrecher, R.: Impact of global warming on the tree species composition of boreal forests in finland and effects on emissions of isoprenoids, Global Change Biology, 7, 531–544, 2001.

Kirstine, W., Galbally, I., Ye, Y. R., and Hooper, M.: Emissions of volatile organic compounds (primarily oxygenated species) from pasture, J. Geophys. Res.-Atmos., 103, 10 605–10 619, 1998.

Komhyr, W., Oltmans, S., Franchois, P., Evans, W., and Matthews, W., The latitudinal distribution of ozone to 35km altitude from ecc ozonesonde observations, 1985-1987, in: Ozone in the atmosphere, edited by: Bojkov, R. and Fabian, P., A. Deepak, Hampton, VA, 1989.

Krinner, G., Viovy, N., De Noblet-Ducoudr, N., Ogee, J., Polcher, J., Friedlingstein, P., Ciais, P., Sitch, A., and Prentice, I., A dynamical global vegetation model for studies of the coupled atmosphere-biosphere system, Global Biogeochem. Cycles, 19, GB1015, 2005.

Kroeze, C., Mosier, A., and Bouwman, L.: Closing the global n2o budget: a retrospective analysis 1500–1994, Global Biogeochem. Cycles, 13, 1–8, 1999.

Kukui, A., Jungkamp, T., and Schindler, R., Aldehyde formation in the reaction of methoxy radicals with NO_3, Ber. Bunsenges. Phys. Chem., 99, 1565–1567, 1995.

Lacis, A. A., Wuebbles, D. J., and Logan, J. A.: Radiative forcing of climate by changes in the vertical-distribution of ozone, J. Geophys. Res.-Atmos., 95, 9971–9981, 1990.

Lathière, J., Hauglustaine, D. A., Friend, A., De Noblet-Ducoudré, N., Viovy, N., and Folberth, G.: Impact of climate variability and land use changes on global biogenic volatile organic compound emissions, Atmos. Chem. Phys. Discuss., 5, 10 613–10 656, 2005.

Lathière, J., Hauglustaine, D. A., De Noblet-Ducoudré, N., Krinner, N., and Folberth, G. A.: Past and future changes in biogenic volatile organic compound emissions simulated with a global dynamic vegetation model, Geophys. Res. Lett., 32, doi:10.1029/2005GL024164, 2005a.

Lawrence, M., Crutzen, P., Rasch, P., Eaton, B., and Mahowald, N.: A model for studies of tropospheric photochemistry: Description, global distributions, and evaluation, J. Geophys. Res., 104, 26 245–26 277, 1999.

Lawrence, M. G., Jockel, P., and von Kuhlmann, R.: What does the global mean oh concentration tell us?, Atmos. Chemi. Phys., 1, 37–49, 2001.

Le Treut, H., Li, Z. X., and Forichon, M.: Sensitivity of the lmd general-circulation model to greenhouse forcing associated with 2 different cloud-water parameterizations, J. Climate, 7, 1827–1841, 1994.

Lelieveld, J. and Dentener, F.: What controls tropospheric ozone, J. Geophys. Res., 105, 3531–3551, 2000.

Levy, H.: Normal atmosphere: Large radical and formaldehyde concentrations predicted, Science, 173, 141–143, 1971.

Levy II, H., Kasibhatla, P., Moxim, W., Klonecki, A., Hirsch, A., Oltmans, S., and Chameides, W.: The global impact of human activity on tropospheric ozone, Geophys. Res. Lett., 24, 791–794, 1997.

Li, D. and Shine, K.: A 4-dimensional ozone climatology for UGAMP models, UGAMP internal report, U.K. Univ. Global

Atmos. Model. Program, Swindon, 1995.

Logan, A.: An analysis of ozonesonde data for the troposphere: recommendations for testing 3-D-models and development of a gridded climatology for tropospheric ozone, J. Geophys. Res., 104, 16 115–16 149, 1999.

MacDonald, R. and Fall, R.: Detection of substantial emissions of methanol from plants to the atmosphere, Atmos. Environ., 27, 1709–1713, 1993.

Madronich, S. and Flocke, S.: The role of solar radiation in atmospheric chemistry, in: Handbook of Environmental Chemistry, Springer-Verlag, Heidelberg, pp. 1–26, 1998.

Martinez, M., Arnold, T., and Perner, D.: The role of bromine and chlorine chemistry for arctic ozone depletion events in ny-alesund and comparison with model calculations, Annales Geophysicae-Atmospheres Hydrospheres and Space Sciences, 17, 941–956, 1999.

Matsumi, Y., Tonokura, K., Inagaki, Y., and Kawasaki, M.: Isotopic branching ratios and translational energy release of H and D atoms in reactions of $O(^1D)$ atoms with alkanes and alkyl chlorides, J. Phys. Chem., 97, 6816–6821, 1993.

Matzkies, F. and Manthe, U.: Accurate quantum calculations of thermal rate constants employing MCTDH: H_2 + OH=H + H_2O and D_2 + OH=D + DOH, J. Phys. Chem.-A, 108, 4828–4836, 1998.

McCabe, D. C., Gierczak, T., Talukdar, R. K., and Ravishankara, A. R.: Kinetics of the reaction OH plus CO under atmospheric conditions, Geophys. Res. Lett., 28, 3135–3138, 2001.

Mickley, L., Murti, P., Jacob, D., Logan, J., Rind, D., and Koch, D.: Radiative forcing from tropospheric ozone calculated with a unified chemistry-climate model, J. Geophys. Res., 104, 30 153–30 172, 1999.

Miyoshi, A., Hatakeyama, S., and Washida, N., Oh radical-initiated photooxidation of isoprene – an estimate of global co production, J. Geophys. Res.-Atmos., 99, 18 779–18 787, 1994.

Moxim, W. J., Levy, H., and Kasibhatla, P. S.: Simulated global tropospheric pan: Its transport and impact on nox, J. Geophys. Res.-Atmos., 101, 12 621–12 638, 1996.

Muller, J. F. and Brasseur, G.: Images – a 3-dimensional chemical-transport model of the global troposphere, J. Geophys. Res.-Atmos., 100, 16 445–16 490, 1995.

Nevison, C. and Weiss, R.: Global oceanic emissions of nitrous oxide, J.Geophys. Res., 100, 15 809–15 820, 1995.

Novelli, P. C., Masarie, K. A., Lang, P. M., Hall, B. D., Myers, R. C., and Elkins, J. W.: Reanalysis of tropospheric co trends: Effects of the 1997–1998 wildfires, J. Geophys. Res.-Atmos., 108(D15), 4464, doi:10.1029/2002JD003031, 2003.

Olivier, J. and Berdowski, J.: Global emission sources and sinks, in: The Climate System, edited by: Berdowski, J., Guicherit, R., and Heij, B., A. A. Balkema Publishers/Swets & Zeitlinger Publishers, Lisse, pp. 33–78, 2001.

Olivier, J., Bouwman, A., van der Maas, C., Berdowski, J., Veldt, C., Bloos, J., Visschedijk, A., Zandveld, P., and Haverlag, J.: Description of edgar version 2.0: A set of global emission inventories of greenhouse gases and ozone-depleting substances for all anthropogenic and most natural sources on a per country basis and on a 1x1 degree grid, RIVM report 771060 002/TNO-MEP report R96/119, National Institute of Public Health and the Environment, 1996.

Olivier, J., Berdowski, J., Peters, J., Bakker, J., Visschedijk, A., and Bloos, J.: Applications of edgar. including a description of edgar 3.0: reference database with trend data for 1970–1995, RIVM report 773301 001, RIVM, 2001.

Oltmans, S. and Levy II, H.: Seasonal cycle of surface ozone over the western north atlantic, Nature, 358, 392–394, 1992.

Oltmans, S. and Levy II, H.: Surface ozone measurements from a global network, Atmos. Environ., 28, 9–24, 1994.

Oltmans, S., Komhyr, W., Franchois, P., and Matthews, W.: Tropospheric ozone: Variations from surface and ecc ozonesonde observations, in: Ozone in the atmosphere, edited by: Bojkov, R. and Fabian, P., A. Deepak, Hampton, VA, 1989.

Poisson, N., Kanakidou, M., and Crutzen, P. J.: Impact of non-methane hydrocarbons on tropospheric chemistry and the oxidizing power of the global troposphere: 3- dimensional modelling results, J. Atmos. Chem., 36, 157–230, 2000.

Pöschl, U., von Kuhlmann, R., Poisson, N., and Crutzen, P. J.: Development and intercomparison of condensed isoprene oxidation mechanisms for global atmospheric modeling, J. Atmos. Chem., 37, 29–52, 2000.

Prather, M., Ehhalt, D., Dentener, F., Derwent, R., Dlugokencky, E., E., H., Isaksen, I., Katima, J., V., K., Matson, P., Midgley, P., and Wang, M.: Atmospheric chemistry and greenhouse gases, in: Climate Change 2001: The Scientific Basis. Contribution of Working Group 1 to the Third Assesment Report of the Intergovernmental Panel on Climate Change, edited by: Houghton, J., Ding, Y., Griggs, D., Noguer, M., van der Linden, P., Dai, X., Maskell, K., and Johnson, C., 801pp., Cambridge University Press, Cambrige, UK and New York, USA, 2001.

Prinn, R.: Evidence for substential variations of atmospheric hydroxyl radicals in the past two decades, Science, 292, 1882–1888, 2001.

Prinn, R., Weiss, R., Miller, B., Huang, J., Alyea, F., Cunnold, D., Fraser, P., Hartley, D., and Simmonds, P.: Atmospheric trends and lifetime of ch3ccl3 and global oh concentrations, Science, 269, 187–192, 1995.

Roberts, J.: The atmospheric chemistry of organic nitrates, Atmos. Environ., 24A, 243, 1990.

Sadourny, R. and Laval, K.: January and july performance of the lmd general circulation model, in: New Perspectives in Climate Modeling, edited by: Berger, A. and Nicolis, C., pp. 173–197, Elsevier, 1984.

Sander, R.: Compilation of henry's law constants for inorganic and organic species of potential importance in environmental chemistry (version 3), http://www.mpch-mainz.mpg.de/~sander/res/henry.html, 1999.

Sander, S., Golden, D., Hampson, R., Kurylo, M., Howard, C., Ravishankara, A., Kolb, C., and Molina, M.: Chemical kinetics and photochemical data for use in stratospheric modeling. supplement to evaluation 12: Update of key reactions, JPL Publ., 00-3, 2000.

Sander, S., Golden, D., Hampson, R., Kurylo, M., Howard, C., Ravishankara, A., Kolb, C., and Molina, M.: Chemical kinetics and photochemical data for use in stratospheric modeling, evaluation number 14, JPL Publ., 02-25, 2002.

Sanderson, M. G. and Jones, C. D. and Collins, W. J., Johnson, C. E., and Derwent, R. G.: Effect of climate change on isoprene emissions and surface ozone levels, Geophys. Res. Lett., 30(18), 1936, doi:10.1029/2003GL017642, 2003.

Seinfeld, J. and Pandis, S.: Atmospheric Chemistry and Physics,

John Wiley & Sons, Inc., New York, 1998.

Shallcross, D. and Monks, P.: New directions: a role for isoprene in biosphere-climate-chemistry feedbacks, Atmos. Environ., 34, 1659–1660, 2000.

Sharkey, T. and Singsaas, E.: Why plants emit isoprene, Nature, 374(6525), 769–769, 1995.

Singh, H., Chen, Y., Tabazadeh, A., Fukui, Y., Bey, I., Yantosca, R., Jacob, D., Arnold, F., Wohlfrom, K., Atlas, E., Flocke, F., Blake, D., Blake, N., Heikes, B., Snow, J., Talbot, R., Gregory, G., Sachse, G., Vay, S., and Kondo, Y.: Distribution and fate of selected oxygenated organic species in the troposphere and lower stratosphere over the atlantic, J. Geophys. Res.-Atmos., 105, 3795–3805, 2000.

Singh, H., Chen, Y., Staudt, A., Jacob, D., Blake, D., Heikes, B., and Snow, J.: Evidence from the pacific troposphere for large global sources of oxygenated organic compounds, Nature, 410, 1078–1081, 2001.

Singh, H. B., Herlth, D., Ohara, D., Zahnle, K., Bradshaw, J. D., Sandholm, S. T., Talbot, R., Gregory, G. L., Sachse, G. W., Blake, D. R., and Wofsy, S. C.: Summertime distribution of pan and other reactive nitrogen species in the northern high-latitude atmosphere of eastern canada, J. Geophys. Res.-Atmos., 99, 1821–1835, 1994a.

Singh, H. B., Ohara, D., Herlth, D., Sachse, W., Blake, D. R., Bradshaw, J. D., Kanakidou, M., and Crutzen, P. J.: Acetone in the atmosphere – distribution, sources, and sinks, J. Geophys. Res.-Atmos., 99, 1805–1819, 1994b.

Sitch, S., Smith, B., Prentice, I. C., Arneth, A., Bondeau, A., Cramer, W., Kaplan, J. O., Levis, S., Lucht, W., Sykes, M. T., Thonicke, K., and Venevsky, S.: Evaluation of ecosystem dynamics, plant geography and terrestrial carbon cycling in the lpj dynamic global vegetation model, Global Change Biology, 9, 161–185, 2003.

Spivakovsky, C., Yevich, R., Logan, J., Wofsy, S., and McElroy, M.: Tropospheric oh in a three-dimensional chemical tracer model: An assessment based on observations of ch3ccl3, J. Geophys. Res., 95, 18 441–18 471, 1990.

Spivakovsky, C. M., Logan, J. A., Montzka, S. A., Balkanski, Y. J., Foreman-Fowler, M., Jones, D. B. A., Horowitz, L. W., Fusco, A. C., Brenninkmeijer, C. A. M., Prather, M. J., Wofsy, S. C., and McElroy, M. B.: Three-dimensional climatological distribution of tropospheric oh: Update and evaluation, J. Geophys. Res.-Atmos., 105, 8931–8980, 2000.

Sprengnether, M., Demerjian, K. L., Donahue, N. M., and Anderson, J. G.: Product analysis of the oh oxidation of isoprene and 1,3-butadiene in the presence of no, J. Geophys. Res.-Atmos., 107(D15), 4268, doi:10.1029/2001JD000716, 2002.

Stockwell, W., Kirchner, F., Kuhn, M., and Seefeld, S.: A new mechanism for regional atmospheric chemistry modeling, J. Geophys. Res., 102, 25 847–25 879, 1997.

Tang, T. and McConnell, J. C.: Autocatalytic release of bromine from arctic snow pack during polar sunrise, Geophys. Res. Lett., 23, 2633–2636, 1996.

Taylor, G. E.: Risk assessment of tropospheric ozone: Human health, natural resources, and ecology, Human and Ecological Risk Assessment, 7, 1183–1193, 2001.

Tiedtke, M.: A comprehensive mass flux scheme for cumulus parameterization in large-scale models, Mon. Wea. Rev., 117, 1779–1800, 1989.

Tsigaridis, K. and Kanakidou, M.: Global modelling of secondary organic aerosol in the troposphere: a sensitivity analysis, Atmos. Chem. Phys., 3, 1849–1869, 2003.

Tyndall, G., Wallington, T., and Ball, J.: FTIR product study of the reactions CH3O2 + CH_3O_2 and CH_3O_2 + O_3, J. Phys. Chem.-A, 102, 2547–2554, 1998.

Tyndall, G. S., Orlando, J. J., and Calvert, J. G.: Upper limit for the rate coefficient for the reaction HO_2 + NO_2 → HONO + O_2, Environ. Sci. Technol., 29, 202–206, 1995.

Van der Werf, G. R., Randerson, J. T., Collatz, G. J., and Giglio, L.: Carbon emissions from fires in tropical and subtropical ecosystems, Global Change Biology, 9, 547–562, 2003.

Van Leer, B.: Towards the ultimate conservative difference scheme. part iv: A new approach to numerical convection, J. Comput. Phys., 23, 276–299, 1977.

von Kuhlmann, R., Lawrence, M. G., Pöschl, U., and Crutzen, P. J.: Sensitivities in global scale modelling of isoprene, Atmos. Chem. Phys., 4, 1–17, 2004.

Walcek, C., Brost, R., Chang, J., and Wesely, M.: SO_2, sulfate and HNO_3 deposition velocities computed using regional land-use and meteorological data, Atmos. Environ., 20, 949–964, 1986.

Walmsley, J. L. and Wesely, M. L.: Modification of coded parametrizations of surface resistances to gaseous dry deposition, Atmos. Environ., 30, 1181–1188, 1996.

Wang, Y. H., Jacob, D. J., and Logan, J. A.: Global simulation of tropospheric O_3-NO_x-hydrocarbon chemistry 1. model formulation, J. Geophys. Res.-Atmos., 103, 10 713–10 725, 1998a.

Wang, Y. H., Logan, J. A., and Jacob, D. J.: Global simulation of tropospheric O_3-NO_x-hydrocarbon chemistry 2. model evaluation and global ozone budget, J. Geophys. Res.-Atmos., 103, 10 727–10 755, 1998b.

Wang, Y. H., Jacob, D. J., and Logan, J. A.: Global simulation of tropospheric O_3-NO_x-hydrocarbon chemistry 3. origin of tropospheric ozone and effects of nonmethane hydrocarbons, J. Geophys. Res.-Atmos., 103, 10 757–10 767, 1998c.

Warneke, C., Karl, T., Judmaier, H., Hansel, A., Jordan, A., Lindinger, W., and Crutzen, P. J.: Acetone, methanol, and other partially oxidized volatile organic emissions from dead plant matter by abiological processes: Significance for atmospheric hox chemistry, Global Biogeochem. Cycles, 13, 9–17, 1999.

Wennberg, P.: Atmospheric chemistry – bromine explosion, Nature, 397, 299pp., 1999.

Wesely, M.: Parameterization of surface resistances to gaseous dry deposition in regional-scale numerical models, Atmos. Environ., 23, 1293–1304, 1989.

Wesely, M. L. and Hicks, B. B.: A review of the current status of knowledge on dry deposition, Atmos. Environ., 34, 2261–2282, 2000.

World Meteorological Organisation: Scientific assessment of ozone depletion: 1998, Rep. 44, Global Ozone Obs. Syst., Geneva, Switzerland, 1998.

Yienger, J. and Levy II, H.: Empirical model of global soil-biogenic nox emissions, J. Geophys. Res., 100, 11 447–11 464, 1995.

Yu, H. and Varandas, A.: Dynamics of H(D) + O_3 reactions on a double many-body expansion potential-energy surface for ground state HO_3, J. Chem. Soc. – Faraday Trans., 93, 2,651–2,656, 1997.